GPCR and G protein mobility in D. discoideum : a single molecule study

Hemert, F. van

Citation

Hemert, F. van. (2009, December 21). *GPCR and G protein mobility in D. discoideum : a single molecule study*. *Casimir PhD Series*. Retrieved from https://hdl.handle.net/1887/14549

Version:	Corrected Publisher’s Version
License:	Licence agreement concerning inclusion of doctoral thesis in the Institutional Repository of the University of Leiden
Downloaded from:	https://hdl.handle.net/1887/14549

Note: To cite this publication please use the final published version (if applicable).

GPCR and G protein mobility in *D. discoideum*
a single molecule study

Proefschrift
ter verkrijging van
de graad van Doctor aan de Universiteit Leiden,
op gezag van Rector Magnificus prof. mr. P. F. van der Heijden,
volgens besluit van het College voor Promoties
te verdedigen op maandag 21 december 2009
klokke 13:45 uur

door

Freek van Hemert
geboren te Oostburg
in 1982

Promotiecommissie:

Promotor:	prof. dr. Thomas Schmidt, Leiden Institute of Physics
Co-Promotor:	dr. B. Ewa Snaar-Jagalska, Leiden Institute of Biology
Overige leden:	prof. dr. Gerhard Schütz, University of Linz
	prof. dr. Theodorus W. J. Gadella, University of Amsterdam
	prof. dr. Peter J. M. van Haastert, University of Groningen
	dr. ir. John van Noort, Leiden Institute of Physics
	prof. dr. Jan M. van Ruitenbeek, Leiden Institute of Physics
	prof. dr. Herman P. Spaink, Leiden Institute of Biology

ISBN 978-90-8593-065-5
Casimir PhD series, Delft-Leiden 2009-20

Contents

1 Chemotaxis: a mechanistic perspective 1

1.1 *Dictyostelium discoideum* 2

1.2 The biochemistry of chemotaxis 3

1.3 Signaling dynamics 5

1.4 Biophysical techniques provide quantitative data 7

1.5 The cAR1 - G protein system 9

1.6 Chemotaxis models 12

1.6.1 Gradient sensing 12

1.6.2 Polarization 14

1.6.3 Biased pseudpods 14

1.7 Conclusion 16

1.8 Thesis outline 16

2 Heterogeneous G protein mobility during chemotaxis 19

2.1 Introduction 20

2.2 Materials and methods 22

2.2.1 Cell culturing and transformation 22

2.2.2 Cell preparation for measurements 22

2.2.3 Developmental test 23

2.2.4 Global cAMP stimulation assay 23

2.2.5 Chemotaxis micropipette assay 23

2.2.6 Latrunculin A treatment 24

2.2.7 Single molecule microscopy 24

2.2.8 Estimation of the expression level of Gα2-YFP and Gβ-YFP 24
2.2.9 Particle image correlation spectroscopy (PICS) 25
2.2.10 Analysis of the cumulative probability functions 25
2.3 Results 26
2.3.1 Heterogeneity in the mobility of Gα2-YFP and Gβ-YFP . . 26
2.3.2 Mobility suggests the existence of a receptor/G protein precoupled complex in the absence of agonist 27
2.3.3 A fraction of Gβ-YFP becomes immobilized upon cAMP-induced receptor activation 34
2.3.4 Stimulation induces confined diffusion of fast Gα2 and G$\beta\gamma$ 34
2.3.5 cAMP-induced membrane domains and Gβ-YFP immobilization are F-actin dependent 35
2.3.6 G$\beta\gamma$ immobilization is leading edge specific 37
2.3.7 cAMP-induced domain formation is PI3K and PLA2 independent 40
2.4 Discussion 40
Supplemental information 48

3 Leading edge specific cortex attenuation leads to higher GPCR mobility 51
3.1 Introduction 52
3.2 Materials and methods 54
3.2.1 Cell culture and transformation 54
3.2.2 Preparation of cells for measurements 54
3.2.3 Global cAMP stimulation assay 55
3.2.4 Applied gradient assay 55
3.2.5 Latrunculin A treatment 55
3.2.6 Single-molecule microscopy 55
3.2.7 Analysis of single molecule data 56
3.2.8 Error estimation 57
3.3 Results 60
3.3.1 In naïve wt cells cAR1 moves slowly and exists in two distinct states 60

3.3.2 cAR1 mobility is increased and polarized during chemotaxis 62
3.3.3 cAR1 mobility is not influenced by Gα2 or G$\beta\gamma$ binding . . 63
3.3.4 Polarized cAR1 mobility is F-actin independent 65
3.4 Discussion 68
Supplemental information 75
Appendix 78

4 cAR1 and G protein mobility in *rasC⁻/rasG⁻* cells 81
4.1 Introduction 82
4.2 Materials and methods 84
4.2.1 Cell culture 84
4.2.2 Preparing naïve cells for measurements 85
4.2.3 Single molecule measurements 85
4.2.4 Global cAMP stimulation assay 85
4.2.5 Applied gradient assay 86
4.2.6 Latrunculin A treatment 86
4.2.7 Data analysis 86
4.3 Results 87
4.3.1 The mobility of cAR1 in *rasC⁻/rasG⁻* cells is increased and reflects the mobility found for F-actin depleted cells 88
4.3.2 The polarized mobility of cAR1 is lost in the *rasC⁻/rasG⁻* knockout 90
4.3.3 G$\beta\gamma$ in the RasC/RasG knockout does not immobilize upon cAMP stimulation 93
4.4 Discussion 95
Supplemental information 102

Bibliography 119

Samenvatting 121

List of publications 127

Curriculum Vitae 129

Chapter 1

Chemotaxis: a mechanistic perspective

Chemotaxis is a complex interplay between numerous molecular species whose coordinated interactions culminate in highly effective directed motion in concentration gradients. Many proteins that play vital, important and minor roles have been identified and biochemically characterized. Several pathways have been recognized to act in parallel each of which contributes to, but is not essential for chemotaxis. Nevertheless a definitive answer as to how cells like *Dictyostelium disciodeum* perform chemotaxis is still unknown. Qualitative descriptions of molecular interactions have proven to be insufficient when trying to understand complex cellular cascades. New techniques such as single molecule microscopy are able to add temporal, spatial and quantitative information to the network of molecular interactions. Biophysics groups are probing the properties of cytoskeleton meshworks and tightly controlled artificial membranes *in vitro* providing information on cellular components relevant to chemotaxis which cannot be investigated in the complex environment of the living cell. Abstract simulations may give insights in the effects of noise in the biological systems and lead to new ways of interpreting old biochemical data. Here we will look at chemotaxis from a biophysicists' view, combining *in vitro*, *in silico* and *in vivo* experiments with a particular emphasis on our own single molecule work.

1.1 *Dictyostelium discoideum*

Dictyostelium discoideum is a single celled organism that can, when environmental conditions deteriorate, aggregate into a multicelled structure called a pseudoplasmodium or a slug. This pseudoplasmodium gains the ability to sense heat and light in order to guide itself towards the soil surface where it transforms into a fruiting body bearing stalk that releases spores. Taken away by the wind or passing animals, these spores are allowed to germinate in more favourable regions.

The first person that became fascinated by these organisms was the German botanist Oskar Brefeld. In 1869 he carefully described the process of cellular aggregation and culmination into a spore containing fruiting body. About 80 years later, in 1946, John Tyler Bonner showed (using axenically growing mutants) that he could manipulate the characteristic aggregation process by creating a flow in the cell medium. His experiments proved the involvement of a chemical substance in the directional movement that leads to cell aggregation. With this discovery Bonner paved the road towards extensive research in the area of chemotaxis. This process, in which cells compute the direction of a concentration gradient and initiate directional movement based on this computation, plays a role in many cellular behaviors critical to the existence of multi-cellular organisms. Examples include: embryogenesis, wound healing and the detection of infection by the immune system. The discovery of cyclic adenosine mono-phosphate (cAMP) as the chemoattractant that Bonner proposed by Konijn and others in 1967 [51] lead to a more systematic way of investigating the phenomenon. Since the advent of molecular biology, a lot has become clear as to how these cells can sense and move directionally towards cAMP sources. The publication of the genome [20] meant that many unknown factors could be easily identified and investigated using knockout techniques. Moreover, the discovery of green fluorescent protein (GFP) technology and its straightforward application in *D. Discoideum* combined with high gene sequence homology to higher eukaryotes has made it an immensely popular model organism for the study of chemotaxis.

1.2 The biochemistry of chemotaxis

The cellular response to cAMP during the aggregation stage can be divided into two facets: 1; the cells produce cAMP using adenylyl cyclase (ACA) and secrete it from their posterior [54]. 2; the cells initiate movement up cAMP concentration gradients using precise modulation of their cytoskeleton. The emergent behavior of these two distinct signaling units (which are biochemically intertwined) is highly effective aggregation through characteristic stream formation. The process is initiated by starvation which induces the expression of cAMP receptor 1 (cAR1), the first expressed and most sensitive cAMP receptor [37]. At the same time, other proteins needed for directional movement and signal relay are also expressed. Being a G protein coupled receptor (GPCR); cAR1 relays the cAMP signal via a G protein. G proteins are membrane localized heterotrimers consisting of a Gα, Gβ and a Gγ subunit. Although it was always assumed that *D. Discoideum* only has a single Gβ subunit, the genome shows that there should be two [20], knocking out only one of them is enough to interrupt chemotaxis [60]. Only a single Gγ subunit is found in the genome [102, 20], consequently, it takes part in every G protein mediated reaction. In contrast, the genome contains 12 Gα subunits [20]. The G protein Gα subunit determines the specificity for downstream effectors. Gα2 is vital to cAMP mediated responses and the principal signaling partner of cAR1 [68]. The binding of cAMP to cAR1 leads to activation of the G protein by the exchange of guanine di-phosphate (GDP) for guanine tri-phosphate (GTP) in the Gα2 subunit. Both the Gα2 and the G$\beta\gamma$ subunits then engage in signaling towards several different pathways that operate in parallel. The best studied of which is the Ras/PI3K pathway. The activation of Ras proteins by the G protein proceeds via Ras guanine exchange factors (RasGEFs). RasGEFs function as on switches for the Ras family of small GTPases, promoting the, as does cAR1 for the Gα2 subunit, exchange of GDP for GTP [7]. For chemotactic responses, RasC and RasG are the most important members of the Ras family [5].

Activated Ras molecules stimulate (among others) phosphatidylinositol-3-kinase (PI3K) which is subsequently recruited to the membrane where it phosphorylates phosphotidylinositol 4,5-bisphosphate (PI(4,5)P_2) to create phosphotidylinositol 3,4,5-trisphosphate (PI(3,4,5)P_3). PI(3,4,5)P_3 functions as a docking site for proteins that contain a pleckstrin homology (PH) domain, these proteins include a multitude of signaling agents that play a role in cellular polarization and cytoskeleton regulation. Phosphatase and tensin homolog on chromosome 10 (PTEN) catalyses the opposite reaction of PI3K (PI(3,4,5)P_3 => PI(4,5)P_2). PTEN binds its own product, PI(4,5)P_2, this creates a feedback loop resulting in PI(4,5)P_2 rich membrane areas [41]. The same holds true for PI3K whose localization is self organising as well [74, 3]. Conspicuously PI3K and PTEN have opposing locations in a polarized cell with PI3K at the leading edge (the anterior) and PTEN lining the lateral sides and trailing edge (also called the posterior). The result of this segregation is a steep amplification of PI(3,4,5)P_3 signaling with respect to the external cAMP gradient. PI(3,4,5)P_3 enriched membrane areas such as the leading edge of a crawling cell, stimulate the generation of pseudopods [3]. For a long time, it was believed that PI3K was the key pathway that leads to cell polarization. PI(3,4,5)P_3 mediated signaling was thought to initiate actin polymerization at the side of the cell facing the highest concentration of cAMP but this view recently changed.

The generation of a mutant which has all five PI3Ks knocked out ended the notion that PI(3,4,5)P_3 signaling is vital to chemotaxis by showing that even in the total absence of PI3K mediated signaling, cells could still polarize and move directionally at near wildtype (wt) efficiencies [38]. A possible parallel pathway that *Dictyostelium* cells can address in this situation is the Phospholipase A2 (PLA2) pathway. It was shown that on inhibition of PI3K, the product of PLA2, arachidonic acid is essential for efficient chemotaxis [11, 35]. A third pathway operating downstream of the small G proteins (among which is RasC) but independent of PI3K is the Tor complex 2 (TorC2) pathway [48]. When TorC2 encounters active membrane associated activators it will phosphorylate protein kinase B R1 (PKBR1) and PKBA before returning to the cytosol. The fact that TalinB is a PKB target provides a direct link to the cytoskeleton. Talin has been shown to be important in cytoskeleton / membrane interactions [64] and cell adhesion [87]. Despite of intensive research, at the moment it is still not clear how all these parallel pathways orchestrate the cytoskeleton resulting in efficient chemotaxis. The current state of the biochemical pathways is depicted in figure 1.1. Many feedback mechanisms are in place to evoke strong, switch-like behavior and to allow cells to polarize in the absence of gradients. As is shown, feedback mechanisms exist that are independent of cAR1 / G protein signaling, they are in place to facilitate random movement in the absence of signaling [80]. The feedback routes that do involve either cAR1 or the G protein are probably involved in the stabilisation of pseudopods, the generation of a persistent front or the regulation of signaling. From this linear, 1 dimensional view on the signaling pathway it is not at all obvious how complex spatial patterns can arise. To explain how cells can sense, amplify, polarize and move directionally in a large variety of cAMP gradients requires knowledge of the mechanics and dynamics of each of the individual molecular players.

1.3 Signaling dynamics

A polarized *Dictyostelium* cell performing chemotaxis is a highly organised but very dynamic entity. To achieve and to maintain polarization places several interesting restrictions on the constituents responsible for the process. Let's focus only on the very first step of chemotaxis, the transduction of the cAMP gradient by the cAR1 - G protein system. At a first glance, just the linear transduction of a signal seems trivial, however in this polarized system several non-trivial constraints apply to the gradient information carriers. The "output" gradient of the receptor, cAR1, is a function of the "input" (cAMP) gradient and (more importantly) several cAR1 specific parameters. If cAR1, once activated, would be allowed to move completely around the cell, the gradient information would be washed out. It is thus of vital importance that cAR1 remains localized upon activation and does not disperse the gradient. The dispersion range, and thus the output gradient of cAR1 is consequently a function of its diffusion constant but also of its signaling off-rate. Apart from maintaining signal localization, cAR1 has to interact with the G protein, whose mobility and activation rates consequently also play a role. Moreover, in a 2D system such as the cell membrane the rate of a reaction involving multiple molecular species is directly proportional to their diffusion constant [4]. This means that high reaction rates can only be achieved at the cost of loosing gradient information by signal dispersal. A possible way around this limitation would be to confine fast moving signaling agents to domains or to a grid, indeed this seems to be a mechanism cells make use of [94]. A more detailed look

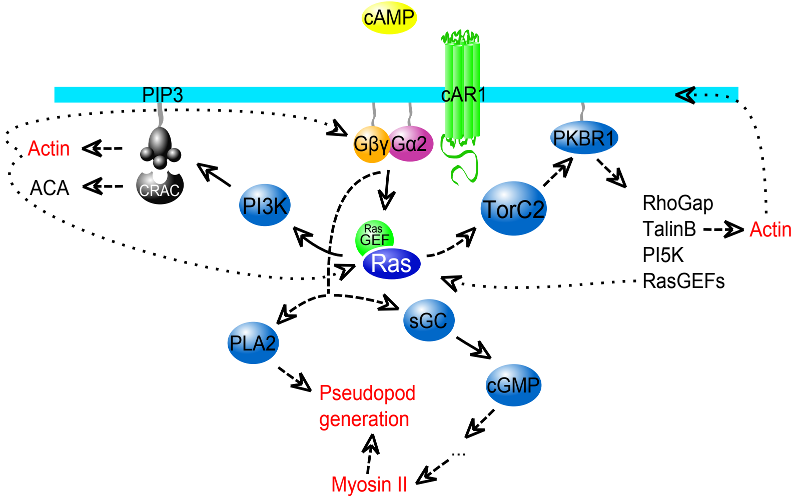

Figure 1.1: A depiction of the *D. Discoideum* chemotaxis pathway. Upon activation of cAR1 by cAMP, the Gα2$\beta\gamma$ heterotrimer dissociates. Both subunits engage in signaling, Gα2 is more important in pathways that lead to pseudopod extension whereas G$\beta\gamma$ is more important for cAMP relay involving cytosolic regulator of ACA (CRAC) and ACA [54]. The PLA2 and soluble guanilyl cyclase (sGC) pathways are activated; these pathways play important roles in the regulation of pseudopod placement [91]. RasGEFs activate Ras proteins [7]. Ras proteins and other small G proteins locally activate TorC2 which via membrane localized PKBR1 subsequently activates a multitude of factors including TalinB [48]. Talin mediates cytoskeleton - membrane interactions [64] and plays a role in cell adhesion [87]. Ras proteins also activate the PI3K pathway [79]. PI3K localizes to the leading edge where it produces PI(3,4,5)P_3 from PI(4,5)P_2. PI(3,4,5)P_3 functions as a docking site for several chemotaxis related proteins like the ACA regulator CRAC [54]. A feedback loop involving F-actin that activates Ras proteins [80] leads to the generation of pseudopods without G protein input facilitating random cell motility. We propose that there is also a feedback from actin acting on the G$\beta\gamma$ subunit specifically at the leading edge. This conceivably leads to a more persistent leading edge or the stabilisation of pseudopods. More generally, actin polymers form fences in the membrane functioning as physical diffusion barriers that influence and maintain localized signaling.

into the requirements of (polarity maintaining) signaling molecules is found elsewhere [75], the authors conlude that molecules moving at diffusion constants up to D = 5 μm^2/s and a high off-rate are most favourable. For a fixed gradient steepness and midconcentration there are certainly optimal values for cAR1 and G protein mobility and signaling off-rates however, *D. Discoideum* cells are known to be able to chemotax in gradients that cover orders of magnitude in steepness and midconcentration. Cells are able to move directionally in gradients that cause only a minute difference in receptor occupancy over the cell body and cope with a noise that is large enough to cause the cell to experience inverted gradients for segments of time [65]. Apparently, the complex molecular mechanics in *D. discoideum* can serve as a temporal averaging filter. On the other end of the spectrum, cells can move in very steep gradients with orders of magnitudes higher mid concentrations. The properties leading to this extreme sensitivity are achieved by the tight regulation of the dynamics of all of the signaling components. signaling pathways are in principal not more than descriptive and qualitative maps of causal relations between molecules involved in the transduction of a signal. They lack the power to describe spatially organised systems such as chemotaxing *Dictyostelium* cells which requires that we take molecular properties such as mobility into account.

1.4 Biophysical techniques provide quantitative data

Fluorescent proteins, such as GFP, were traditionally used as labels in fluorescence (confocal) microscopy. At the moment however, they are also used in a variety of techniques with the ability to quantify signaling dynamics. The mobility of fluorescently tagged molecules can be determined using (among others) FRAP (Fluorescence Recovery After Photobleaching), FCS (Fluorescence Correlation Spectroscopy) and SMM (Single Molecule Microscopy). Each technique has its own set of advantages and shortcomings. FRAP is easy to implement and can report nicely on the mobility of a molecular species. Although it has difficulties dissecting multicomponent diffusion, it is able to report on complex binding/unbinding kinetics [85]. FRAP works for micrometer length scales and is thus not suited for the inspection of finer details of cell membranes. FCS is also able to report on mobility as well as complex dynamics including multi-component systems but the error in the reported mobility depends highly on the accuracy with which one knows the used laser spot dimensions. These dimensions depend on a number of parameters making it basically impossible to estimate. The recently developed Two-focus FCS may solve some of these shortcomings though [18]. SMM, although limited to slow molecules (D = 0-10 $\mu m^2/s$, generally molecules confined to membranes or crowded spaces), is able to report very well on multi component diffusion and can even be used in 3D [39]. The positional accuracy depends only on the signal to background and the number of photons collected and thus can be arbitrarily small, in practice though, a resolution of 30-40 nm is obtained. Moreover, since the movement of molecules directly reflects the structure of their surroundings it can used to probe the underlying organization of, for example, the cell membrane at nm resolutions. Micro domains and crowding effects readily show up and in case a labeled ligand is used, SMM can report on signaling off-rates [90]. None of the before mentioned techniques can however report on molecular interactions. For such details, Förster Resonance Energy Transfer (FRET) is the appropriate technique to use. A FRET signal is extremely sensitive to the distances between a donor and an acceptor fluorophore over a range of $\sim$1-10 nm. As such it can be used to directly report on inter- and intramolecular interactions. FRET can also be used in combination with FCS to see molecular dynamics in solution [52]. When used in combination with TIR (Total Internal Reflection) illumination, FRAP and SMM are able to gain a large boost in signal to noise, TIR fluorescence microscopy is however limited to the basal membrane of a cell because the high signal to noise ratio is a direct result of its very small penetration depth (generally $\sim$100 nm).

To discern subtle changes in molecular behavior that could be key to chemotaxis, one should quantify them in a controlled environment and as a function of e.g. activation state. The tight control that is a prerequisite for precise quantification of molecular properties can be obtained using micro-fluidics. Micro-fluidic devices have been created that can make precise and stable gradient for hours, switch gradient direction very fast and allow for temporal gradient modulation [84, 78]. Nanometric, high time resolution techniques such as those described above in combination with micro-fluidics will be instrumental in solving the "problem of" chemotaxis.

1.5 The cAR1 - G protein system

Due to the existence of parallel pathways which provide considerable signaling redundancy, very few individual components apart from cAR1 and the G protein are truly essential to chemotaxis. This is one of the reasons that our group focuses on these molecules. Although in a highly polarized cell cAR1 is homogeneously distributed around the membrane, its dynamics show clear polarization. At the leading edge, cAR1 has a twofold higher cAMP off-rate [90] and its mobility is increased with respect to the posterior [17]. The first observation was G protein dependent implying that cAR1 spends less time in a G protein bound state at the leading edge, a sign of faster cycling though activation stages. The second observation is probably the result of differential cortex - membrane interactions [64]. We have established that the mobility of cAR1 is dependent on the presence of F-actin and possibly other cortex components (chapter 3). The fact that the cortex is specifically weakened at the leading edge facilitates normal (actin polymerization driven) pseudopod extension by locally reducing the cell structural integrity as well as bleb facilitated leading edge protrusion [101, 58]. The latter type of movement requires decoupling of the membrane from the stiff cortex. A faster mobility means more interactions with targets in the membrane per time unit, in this case leading to higher reaction rates specifically at the leading edge.

The G protein heterotrimer, due to its complex dynamics, lends itself for even more forms of activity modulation [97]. Like cAR1, Gα2 and G$\beta\gamma$ both exist in two mobility states and are homogeneously distributed over the cell with $\sim$70% located on the membrane and $\sim$30% in the cytosol [22]. G protein activation, as determined directly by the separation of the Gα2 and G$\beta\gamma$ subunits using FRET, is a direct reflection of cAR1 activation [44, 22]. In polarized cells, activation follows the external cAMP gradient [100]. The dogmatic view on G protein signaling dictates that upon stimulation of the GPCR, GDP is exchanged for GTP in the Gα subunit. The Gα and G$\beta\gamma$ subunits then dissociate from each other and from the GPCR and engage in signaling. In reality though, it is much less clear and many questions remain unanswered: Does the G protein decouple from the GPCR after stimulation? Are they coupled at all or do they show very transient interactions? Can a single receptor activate multiple G proteins? All these questions (and more) are important if we want to fully understand the impact and regulation of G protein signaling.

For the cAR1 / Gα2$\beta\gamma$ system several new discoveries are starting to answer the questions. Recent experiments have shown that: i; The Gα2 and G$\beta\gamma$ subunit dissociate upon activation [44, 22]. ii; Both Gα2 and G$\beta\gamma$ cycle between the membrane and the cytosol [22]. iii; Gα2 is enriched at the membrane upon stimulation whereas G$\beta\gamma$ is not [22]. iv; a majority portion of both subunits have a diffusion constant $\sim$10 fold higher then cAR1 and a small portion ($\sim$30%) matches cAR1 movement (chapter 2). v; The slow G$\beta\gamma$ immobilize upon activation in an F-actin dependent manner and this fraction increases in size, this effect is restricted to the leading edge of chemotaxing cells. The immobilization results in the loss of any fractions that match receptor diffusion. In the absence of F-actin, only the slow fraction size increase is observed and this fraction maintains a diffusion constant that matches cAR1. vi; Gα2 maintains a diffusion constant which matches cAR1 regardless of its activation state (chapter 2).

From these observations, several conclusions can be drawn. First; the default, resting state of Gα2 and G$\beta\gamma$ is the heterotrimeric form. This is confirmed by our single molecule microscopy (SMM) experiments that show that indeed the two subunits have identical movement and fraction size distributions in the cell membrane in the absence of stimulation (chapter 2). Moreover, the fact that 30% of the Gα2$\beta\gamma$ heterotrimers match the diffusion constant and type of roughly 50% of the receptors is indicative of partial receptor - G protein precoupling. The remaining 70% and the large cytosolic pool of the G protein heterotrimers cannot be coupled to cAR1 leading to the proposition that the majority fraction serves as a pool of ready-to-be-activated G proteins. Such a pool is required for initial amplification of the signal and plays an important role in polarization in shallow gradients according to the diffusion-translocation model [75]. The observation that upon activation only the Gα2 subunit increases the time spent on the membrane but not G$\beta\gamma$, implies that there must be active G$\beta\gamma$ in the cytosol. The increased membrane "on-time" of Gα2 may be the result of membrane binding or cAR1 binding. Our results suggest both take place as the Gα2 subunit's membrane fraction distribution remains unchanged after stimulation implying that both cAR1 and membrane-only associated Gα2 increase equally.

When interpreting the results of the above used techniques we must not forget their respective limitations. Elzie and others use FRAP and FRET in combination with total internal reflection fluorescence (TIRF) microscopy [22] whereas we use epifluorescence SMM. Tirf only visualizes molecules up to ∼100 nm (illumination intensity decreases very fast with distance) from the glass slide; this boosts the signal to noise enormously but puts heavy restrictions on the observed depth. SMM is only able to visualize molecules that are sufficiently slow compare to the illumination time, in practice this means it is limited to membrane localized molecules or molecules that have their mobility restricted otherwise. For our model system this means there are several molecular depots for which each of the two techniques cannot account. Whereas TIRF will not show cytosolic molecules more than ∼100 nm above the glass, Epifluorescence SMM will observe any molecule within a Z range of ∼1 µm but cytosolic (fast moving) molecules only contribute to the background. A very important difference between the two techniques in addition is that TIRF is limited to the basal membrane whereas our SMM measurements were done at the apical membrane. The basal part of the cell may respond differently with respect to the top membrane, especially regarding the F-actin cytoskeleton (data not shown). In the interpretation of the data it is of vital importance to incorporate the fractions that are not observed, specifically for Gβγ which might have an important function in the cytosol [59, 22]. Putting together the results obtained with both techniques we arrive at a model wherein cAMP binds to cAR1 causing Gβγ to dissociate from the cAR1-Gα2βγ complex and (partly) leave the membrane to bind F-actin if present. This F-actin may very well be part of the cell cortex however since this binding is cAMP dependent and restricted to the leading edge in chemotaxing cells it most likely binds force generating F-actin fibers that are part of the Ras/PI3K/actin feedback mechanism [80]. This interaction could mean that F-actin functions as a scaffold for Gβγ signaling or, alternatively F-actin could attenuate the suggested inhibitory function of Gβγ [59] and prevent signaling to ACA. In both cases, restricting such signaling feedback to the leading edge is beneficial to cellular polarization and the stabilization of pseudopods. After activation Gα2 increases its affinity for the membrane and cAR1 leading to an increase in the net time spend at the membrane. Such dynamics are advantageous when Gα2 signaling takes place at the membrane. If the suggested cAR1-Gα2 signaling dimer exists, the fact that cAR1 shows higher mobility at the anterior becomes more relevant to G protein signaling. A graphical representation of cAR1-G protein signaling as we envision it is shown in figure 1.2. Differences between the leading and trailing edge are also indicated.

1.6 Chemotaxis models

A chemotaxing *Dictyostelium* cell is not only complex regarding molecular interactions, dynamics and pathways but also displays intricate spatio-temporal organization of the involved molecules. The ability to organize spatially and to maintain this organization, as we discussed earlier, depends highly on the mobility parameters of those molecules. Within minutes of exposure to a cAMP gradient, cells are able to transform from being roughly symmetric into highly polarized entities.

To understand how this process can function over a very wide range of gradient parameters has been a great challenge for researchers and there have been many models that try to mimic *D. Discoideum in silico*. For the sake of modelling, the process of chemotaxis is often divided into three separate modules being; directional sensing, polarization and movement. Directional sensing is independent of the F-actin cytoskeleton and can be observed in cells which have actin polymerization completely inhibited [26]. Polarization of the cytoskeleton configuration follows the detection and amplification of the gradient and a leading and trailing edge are formed. Movement is realized subsequently by the actin dependent extension of pseudopods at the anterior and the myosin II mediated retraction of the posterior. In this dogma, once a cell has determined the gradient direction, amplified it and assumed a polarized configuration, movement is a trivial step requiring only straightforward signaling to the cytoskeleton. For this reason, models up to now focussed mainly on establishing a stable, amplified intracellular gradient or a completely polarized configuration of signaling molecules.

1.6.1 Gradient sensing

One such a model is the local excitation, global inhibition (LEGI) model [63]. This model is based on the reciprocal actions of PI3K and PTEN and can explain the

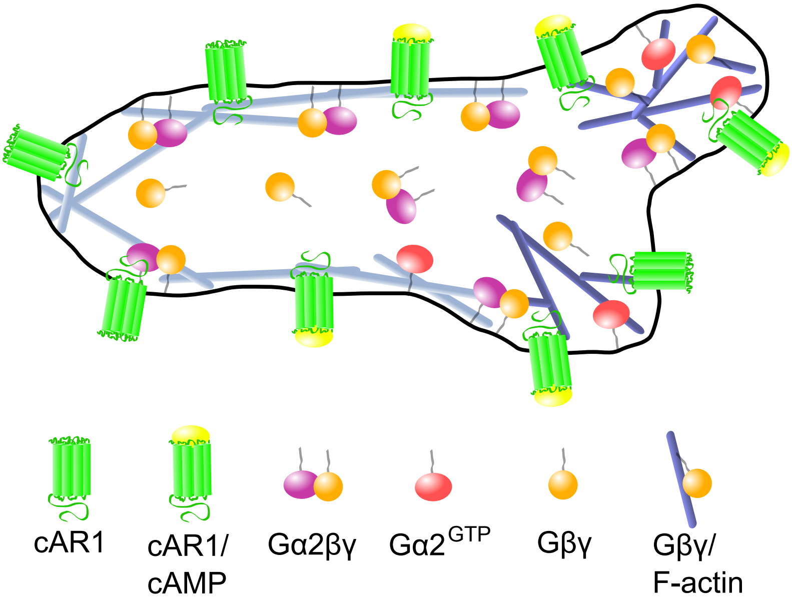

Figure 1.2: A model for cAR1 - G protein signaling during chemotaxis. The membrane is populated with cAR1, complexed cAR1-Gα2$\beta\gamma$ and Gα2$\beta\gamma$; the latter is in equilibrium with a fraction in the cytosol. Upon cAMP binding by cAR1, G$\beta\gamma$ dissociates from cAR1-Gα2$\beta\gamma$. At the leading edge it binds F-actin, either at the membrane or in the cytosol, which immobilizes it. At the posterior, it simply enters the cytosol. Possibly, the immobilisation is part of an F-actin - G protein feedback loop. The function of this loop could be beneficial to the stabilisation of forming pseudopods either by F-actin functioning as a scaffold for G$\beta\gamma$ signaling or by inhibiting suggested "backness" signals [59]. Gα2 increases its affinity for the membrane and for cAR1 upon activation which at the same time makes is available for reactivation and allows it to better activate downstream, membrane localized signaling components. It is possible that activated Gα2 remains coupled to cAR1 in its GTP bound form. The cAR1-Gα2 complex and free cAR1 show a higher mobility at the anterior [17], this is a direct result of the fact that cortex - membrane interactions are less tight there [64]. The local attenuation of the cortex allows for faster pseudopod growth. Since the cortex is a major inhibitor of cAR1 diffusivity this leads to higher reaction rates relevant to chemotaxis at the leading edge.

observed amplification found in PI(3,4,5)P_3 signaling. In this model, upon binding of cAMP, cAR1 quickly activates downstream components (PI3K) but at the same time a slower inhibitory response is initiated (mediated by PTEN) which becomes stronger over time. This eventually results in a situation where the leading edge still overcomes inhibition while trailing edge activation diminishes. This model almost perfectly explains the polarized behavior seen in PH-domains but it lacks the ability for cells to polarize in the absence of a gradient. This is because maintenance of activation is directly dependent on cAR1 signaling however; the same molecules can be used to replicate this observation if positive feedback loops are incorporated [32]. The addition of such feedback would lead to the existence of PI(4,5)P_2 and PI(3,4,5)P_3 enriched patches on the membrane which are indeed observed [74].

1.6.2 Polarization

A more abstract model, not based on the PI3K / PTEN system is the balanced inactivation model [59]. This model is better able to explain the switch like behavior, leading to absence of activation at the anterior that is seen in many signaling components. It does so by adding a component that is fast diffusing in the cytosol ensuring its concentration is equal throughout the cell. This cytosolic component is inhibiting signaling and created at an equal rate as the activating membrane localized component. In a gradient this generates a situation in which at the posterior signaling is completely blocked but at the anterior it is not. The result is a switch like behavior that is also capable of quickly adapting to changing gradients. Interestingly, the required molecules and their characteristics correspond nicely to the cAR1 / G protein system. An important assumption is that G$\beta\gamma$ has an inhibitory function and is able to diffuse in the cytosol, the latter at least, seems to be very well possible [22].

1.6.3 Biased pseudpods

The models listed so far are compass based models. They are based on the proposition that signaling precedes the generation of well placed pseudopods. These models are a natural extension of the prevailing "gradient sensing => polarisation => movement" dogma. Several recent observations however conflict with this proposition: i; chemotaxis at low gradients is best described by a biased random walk. ii; Pseudopods are extended at a constant rate irrespective of the cells orientation in a gradient. iii; Unfavourable pseudopods can be retracted. iv; New pseudopods originate mostly from previous ones [6, 1]. Observations i and ii show that *D. Discoideum* cells move by default and generate pseudpods at a constant speed. In order to move directionally, regulation should take place not on when the pseudopods are generated but on where. This observation agrees with the finding that the Ras/PI3K/F-actin system does not require G protein input [80] but instead facilitates polarization leading to random movement in the absence of cAMP. When a gradient is applied, this autonomous system receives directional input and polarizes in the correct direction. Observation iii and iv suggest that not only do cells show persistence in their trajectories because of the fact that new pseudopods are (mostly) restricted to the current leading edge, a form of temporal sampling also plays a role and the decision to keep a pseudopod is made after its generation. This mechanism is reminiscent of bacterial chemotaxis which functions by a higher persistence in "correct" directions [92]. Taken together this leads to a model where instead of the gradient determining the correct direction for a pseudopod, pseudopods are positioned with a certain probability around the cell. The input parameters that govern pseudopod positioning are gradient steepness, direction and the position of the previous pseudopod. Such a model implies; i; a steeper gradient will lead to a higher directional accuracy due to more pseudopods being placed in the correct direction, ii; deviation of the cells polarity axis with respect to the gradient will lead to a corresponding bias in the probability distribution of pseudopod generation and iii; dependence of pseudopod position on the position of the previous pseudopod will lead to autocorrelation in the cells movement characterized by a certain persistence time. Indeed, the observation of thousands of cells reveals the probabilistic nature of pseudopod generation and persistence of movement nicely [6]. Additionally, it was found that cells retain the ability to generate "*de novo*" pseudopods; these are pseudopods uncorrelated from the previous ones. Because even highly developed cells can still create a *de novo* pseudopod every now and then, the ratio between correlated and *de novo* pseudopods is an important factor in the persistence of directional movement. This new view on chemotaxis, in which molecules important to chemotaxis are seen as factors influencing pseudopod generation frequency, persistency or the probability distribution of their placement is especially good at explaining directional movement at very low gradients. Although the nature of pseudopod placement is probabilistic, it is still governed by cAR1 - G protein signaling combined with various downstream pathways and thus hard limits exist when it comes to noise and detection thresholds. We expect these realisations to generate numerous new models and discoveries which will bring us closer to a full understanding of the phenomenon known as chemotaxis.

1.7 Conclusion

The biochemistry governing chemotaxis is becoming more and more clear. Alternative pathways are being identified and the field is at a stage where it has identified a lot of key components. The recent realisations regarding pseudopod generation at low gradient strength will probably inspire a multitude of new models likely to encapsulate older models as well. Despite of the probabilistic nature, the detection is governed by the properties of signaling molecules. High time and spatial resolution techniques such as FRET, FRAP, FCS and SMM in combination with tightly controlled micro-fluidics will be instrumental in the quantification of the molecular interactions and mobilities. As quantitative information in the form of diffusion constants and reaction rates are added to the pathways, models will be become more realistic and spawn more testable hypothesis which in term will give rise to new insights. This positive feedback between biology and (bio)physics will definitely lead to a more complete and more detailed picture of eukaryotic chemotaxis.

1.8 Thesis outline

In this thesis I will focus on the mobility of the GPCR cAR1 and its associated G protein subunits, Gα2 and G$\beta\gamma$ in *D. discoideum*. Each of these three proteins has been labeled with Yellow Fluorescent Protein (YFP) which allows for the localization of individual molecules with a positional accuracy of $\sim$40 nm at a temporal resolution of 50 ms. Their respective mean squared displacements (MSDs) are measured over timelags of 50 - 400 ms. The slope of the MSD *vs* timelag plots is a proportional to the diffusion constant while the shape reveals details on the underlying structure of the membrane and/or the cytoskeleton. In chapter 2 we focus on the G protein in its resting state, upon global stimulation and in polarized cells. We show that the behavior of G$\beta\gamma$ at the leading edge is radically different from the posterior: where at the posterior G$\beta\gamma$ behaves as in resting cells, in the leading pseudopod a fraction immobilizes in an F-actin dependent fashion and F-actin related domains form. These observations are indicative of feedback mechanisms acting directly on G protein signaling. In resting cells, $\sim$50% of the cAR1 molecules appear to be precoupled to $\sim$30% of the membrane localized G protein heterotrimers. This leaves the majority of G protein heterotrimers free to diffuse and allows cAR1 to amplify its signal. In chapter 3, we examine the mobility of cAR1. As found for the G protein, F-actin restricts cAR1 diffusion however; it appears that the cell cortex is mainly responsible instead of agonist induced actin polymerization. Our findings support the observation that cortex - membrane interactions are weaker at the anterior of a chemotaxing cell. Other factors than F-actin, related to directional sensing, also seem to be able to regulate cAR1 mobility. Chapter 4 focuses on the behavior the cAR1 and G$\beta\gamma$ in a *rasC*$^-$*/rasG*$^-$ background. In the absence of these proteins that are vital to chemotaxis we lose the polarized behavior of both cAR1 and G$\beta\gamma$. The RasC/RasG knockout cells have difficulties regulating their cytoskeleton resulting in loss of G$\beta\gamma$ immobilization and loss of spatial regulation of the actin cortex. Introduction of a functional cAR1 however, seems to restore the reported lack of chemotaxis. This implies that RasC and RasG mediate chemotaxis by induction of cAR1 expression in addition to directly functioning in the signaling pathway. Our data is important to any modelling of the system and leads to new insights on GPCR - G protein signaling.

Chapter 2

Mobility of G proteins is heterogeneous and polarized during chemotaxis

The interaction of G-protein-coupled receptors with G proteins is a key event in transmembrane signal transduction leading to vital decision-taking of the cell. Here we applied single-molecule epifluorescence microscopy to study the mobility of both the $G\beta\gamma$ and the $G\alpha2$ subunits of the G protein heterotrimer in comparison to the cAMP-receptor responsible for chemotactic signaling in *Dictyostelium discoideum*. Our experimental results suggest that $\sim$30% of the G protein heterotrimers exist in receptor pre-coupled complexes. Upon stimulation in a chemotactic gradient this complex dissociates, subsequently leading to a linear diffusion/collision amplification of the external signal. The further observation of partial immobilization and confinement of $G\beta\gamma$ in an agonist, F-actin and $G\alpha2$-dependent fashion led to the hypothesis of functional nanometric domains in the plasma membrane that locally restrict the activation signal and in turn lead to faithful and efficient chemotactic signaling.

2.1 Introduction

G protein mediated signaling is a widely used mechanism for transmembrane signal transduction. It entails a seven-transmembrane receptor, the G protein coupled receptor (GPCR), and a heterotrimeric G protein consisting of a Gα and a heterodimeric G$\beta\gamma$ subunit. Compared to other transmembrane signaling systems, the complex, modular mechanics of G protein linked signaling allows for divergence, convergence and regulation to take place at the level of the GPCR/G protein complex by modulation of their interaction [97]. Mammalian genomes generally encode for > 1000 GPCRs the majority of which does not have a known ligand. Although the atomic structure of three GPCRs have been resolved so-far [69, 77, 43] a mechanism for how ligand induced conformational changes lead to G protein activation is still unknown. Even the simple quest of whether GPCRs and G proteins can exist together in a stable complex or interact dynamically has been solved for only one system [67]. In the dogmatic view the ligand-based activation of the GPCR promotes the exchange of guanosine diphosphate (GDP) for guanosine triphosphate (GTP) in the Gα subunit which subsequently dissociates from the complex allowing both Gα and G$\beta\gamma$ to engage in downstream signaling. Hydrolysis of GTP to GDP in the Gα subunit, either autocatalytically or by effector proteins, leads to re-association of the GPCR/G$\alpha\beta\gamma$ complex.

An intriguing system in which GPCR signaling leads to a dramatic change in cellular behavior is that of eukaryotic chemotaxis. Chemotaxis controls e.g. the developmental cycle in the social amoeba *Dictyostelium discoideum*. Generally, chemotaxis is interpreted as a three-stage process starting with gradient sensing followed by cellular polarization, ultimately resulting in directional movement. *D. discoideum* cells secrete cyclic adenosine mono-phosphate (cAMP) that acts as a chemoattractant leading to cell aggregation. Aggregation is achieved by a chemotactic process being initiated by activation of the cAMP receptor 1 (cAR1) which in turn activates a G protein heterotrimer, consisting of a Gα2 and a G$\beta\gamma$ subunit [49]. Sequencing of the *D. discoideum* genome showed that there are two Gβ and a single Gγ subunit type in *D. discoideum* [60, 102, 20].Consequently these G$\beta\gamma$ heterodimers participates in all GPCR triggered responses. Receptor-mediated activation of heterotrimeric G protein complexes was visualized in *D. discoideum* using Förster Resonance Energy Transfer (FRET) between the Gα2 and Gβ subunits, fused to cyan and yellow fluorescent proteins respectively [44]. These FRET experiments demonstrated that G protein heterotrimers are stable in the absence of agonist and rapidly dissociate upon addition of cAMP. Recently the FRET experiments were complemented with Fluorescence Recovery After Photobleaching (FRAP) data. A new model for G protein signaling was suggested in which the Gα2 increases the time it spends on the membrane or in a cAR1-bound state and the activated G$\beta\gamma$ subunit dissociates into the cytosol. Both processes will lead to a cycling of the G protein heterotrimer between the membrane-bound and a free cytosolic state [22].

Although many molecular details of the pathways are known, a direct connection between gradient sensing and the movement machinery is still to be discovered. At this moment there are several pathways known to act in parallel downstream of G protein activation that mediate the final chemotactic response. The most thoroughly studied pathway involves PI3-kinase (PI3K) and its antagonist, a PI3-phosphatase (PTEN). The coördinated action of both leads to local accumulation of PI(3,4,5)P_3 in the leading edge of the crawling cells [40, 30]. Recently, additional pathways have been discovered to act in parallel; the phospholipase A2 (PLA2) pathway [11] and the TorC2 pathway [48].

In cells placed in a gradient of cAMP, the pathways downstream of G protein signaling trigger actin polymerization selectively in the cell's leading edge, whereas actin polymerization occurs globally upon uniform cAMP stimulation [12]. Unlike the highly polarized localization in actin polymerization and the preceding highly polar translocation of a variety of intracellular signaling molecules like PI(3,4,5)P_3 and PI(4,5)P_2, receptor localization is fully homogeneous. The G$\beta\gamma$ subunit of the G protein is localized in a shallow anterior-posterior gradient, however at a level of polarization impossible to restrict signaling to the leading edge [46]. Recent studies [17] revealed however a spatially restricted increase of receptor mobility in the leading edge of *D. discoideum* cells when exposed to a stable cAMP gradient. Those data suggested an asymmetry in the activation level of the receptor-G protein pathway with a predicted linear amplification of the local activation level of the G proteins.

Here we set out to address this prediction. We analyzed Gα2 and G$\beta\gamma$ mobility in the absence of agonist, upon uniform cAMP stimulation and in a cAMP gradient using single-molecule epifluorescence microscopy [81]. We found that Gα2 and Gβγ occur as a smaller (∼30%) receptor-precoupled fraction, and a larger (∼70%) receptor-uncoupled fraction. Upon global stimulation with cAMP the receptor-coupled fraction disappeared. In terms of the receptor those occupation numbers correspond to about 50% of all available receptors. The activated Gβγ molecules immobilize in an F-actin dependent manner. Concurrently, the formation of F-actin-dependent domains of size ∼600 nm was observed. Strikingly the dramatic changes in mobility were restricted to the leading edge of chemotaxing cells. We propose that Gβγ immobilization is caused by its incorporation into a larger signaling complex, a signalosome for which F-actin functions as a scaffold. Such a mechanism would lead to stabilization of pseudopods and the formation of a persistent leading edge by means of a direct F-actin - G protein feedback loop.

2.2 Materials and methods

2.2.1 Cell culturing and transformation

The axenically growing *D. discoideum* strain Ax2 [93] was used in this study and referred to as wild-type (wt), to discriminate from other genetic backgrounds that were used. The wt, $g\beta^-$ (LW5, [60]), $g\alpha2^-$ (myc2, [13]) and $car1^-$ [9] cells were transformed by electroporation with a plasmid, encoding the Gβ-YFP fusion protein. The same procedure was followed for wt, $g\alpha2^-$ and $car1^-$ cells with the plasmid encoding for the Gα2-YFP fusion protein. G418 (Geneticin, Invitrogen) was used to select for successfully transformed *D. discoideum*. Cells were grown as a monolayer on plastic dishes in axenic culture medium, HL5-C (Formedium), containing 10 µg/ml penicillin/streptomycin (1:1) (Invitrogen) and 20 µg/ml G418, at 22 °C.

2.2.2 Cell preparation for measurements

To assess chemotactic competence, *D. discoideum* cells from axenic exponentially growing cultures were cultured in a plastic dish overnight in low fluorescence medium (Formedium). The physiological state of the cells treated in this way was comparable to 1-2 hr starved cells. After that the cells were detached from the plate, washed three times with developmental buffer [24], centrifuged for 3 min at 400×g RCF, and resuspended in 5 ml developmental buffer at a concentration of $\sim10^7$cells/ml in a 100 ml Erlenmeyer flask. After 1 hr of shaking at 100 rpm the cells were pulsed with a peristaltic pump (Gilson, Minipulse 2) with 150 nM cAMP at 6 min intervals, for 4 hr for the transformants in wt, and overnight for the transformants in knock-out backgrounds [21]. After pulsing, the cells were shaken for an additional 30 min and finally diluted in developmental buffer to a concentration of 10^6 cells/ml. Cells were transferred into 2-well chambered cover glasses (1.5 Borosilicate Sterile, Lab Tek II) where they were allowed to adhere.

2.2.3 Developmental test

Gα2-YFP/$g\alpha2^-$ and Gβ-YFP/$g\beta^-$ transformants, as well as $g\alpha2^-$ and $g\beta^-$ cells were pulsed overnight with 150 nM cAMP per pulse and subsequently plated on non-nutrient 1.5% agar plates at a concentration of 3-4 $\cdot$ 10^7 cells/cm^2. After 24 hr the developmental state was assessed.

2.2.4 Global cAMP stimulation assay

The developmental buffer, covering the developed cells in the chambered cover-glasses was supplemented with cAMP to a final concentration of 10 µM. Experiments were performed within 20 min after addition of cAMP.

2.2.5 Chemotaxis micropipette assay

Cells were placed at a distance of $\sim$75 µm from the opening (r = 0.25 µm) of a pipette (Eppendorf femtotip) filled with 10 µM cAMP. The internal pressure in the pipette was set to 40 KPa by means of a FemtoJet injector (Eppendorf). This setup created a stable, shallow gradient estimated at 0.4 nM/µm cAMP over the cell body at a mid concentration of $\sim$60 nM. The gradient caused polarization of the developed *D. discoideum* cells towards the micropipette tip. The region-of-interest was set to the leading and trailing edge (20% of the cell body) of a polarized cell, respectively.

2.2.6 Latrunculin A treatment

The developmental buffer, covering the developed cells in the chambered coverglasses was supplemented with 0.5 µM latrunculin A. After 10 min, single-molecule measurements were performed for 10 min. To observe the effect of latrunculin A on the cell's response to cAMP, 10 min after addition of the latrunculin A, cAMP was added to the buffer at final concentration of 10 µM, measurements were taken within 10 min of cAMP addition [28].

2.2.7 Single molecule microscopy

The experimental setup for single-molecule imaging has been described in detail previously [81]. The samples were mounted onto an inverted microscope (Axiovert100, Zeiss) equipped with a 100× objective (NA=1.4, Zeiss). The region-of-interest was set to 50 × 50 pixels. The apparent pixelsize was 220 nm. Measurements were performed by illumination of the samples for 5 ms at 514 nm (Argon-ion laser, Spectra Physics) at an intensity of 2 kW/cm^2. The cells were photobleached for a period of 2-5 s and sequences of 500 images with a timelag of 50 ms were taken. Use of an appropriate filter combination (Chroma) permitted the detection of the fluorescence signal on a liquid nitrogen-cooled CCD-camera (Princeton Instruments). The setup allowed imaging of individual fluorophores at a signal-to-background-noise ratio of $\sim$30 leading to a positional accuracy of σ_0 = $\sim$40nm.

2.2.8 Estimation of the expression level of Gα2-YFP and Gβ-YFP

The expression level of Gα2-YFP in $g\alpha 2^-$, and Gβ-YFP in $g\beta^-$ cells was calculated in the following manner. The image of a single fluorescent molecule was given by an intensity distribution characterized by a full-width-at-half-maximum of w_0 = 1.7 pxl = 0.37 µm. The average signal for a single YFP molecule was S_1 = 220 cnts when illuminated with 2 kW/cm^2 for 5 ms at 514 nm [36]. The fluorescence of Gβ-YFP at the apical membrane at identical conditions was $S_{G\beta}$ = 4300 cnts/pxl, and for Gα2-YFP $S_{G\alpha 2}$ = 4000 cnts/pxl. The surface of the membrane for a whole cell (approximated by a spheroid with a short axis of r_1= 5 µm and long axis r_2= 10 µm) is about 540 µm^2. The fluorescence data were used in the estimation of the expression level yielding $S_{G\beta}$ / $S_1 \cdot A/w_0^2$ = $7.7 \cdot 10^4$ Gβ-YFP and $7.2 \cdot 10^4$ Gα2-YFP molecules per cell. A similar estimation has been done for the receptor yielding $4 \cdot 10^4$ cAR1 per cell [17].

2.2.9 Particle image correlation spectroscopy (PICS)

The reconstruction of trajectories from molecule positions is severely hampered by blinking and photobleaching of eYFP [36]. Therefore we used an alternative analysis method, particle-image-correlation-spectroscopy (PICS), described in detail elsewhere [83]. In short, the cross-correlation between single-molecule positions at two different time lags is calculated. Subsequently, the linear contribution from uncorrelated molecules in close proximity is subtracted. This results in the cumulative distribution function $cdf(r^2, t_{lag})$ which yields the distribution of squared jump widths between within the given time lag t_{lag}. For each time lag $cdf(r^2, t_{lag})$ is fitted to a two fraction model (eq.2.2).

2.2.10 Analysis of the cumulative probability functions

From the jump width distributions the diffusion characteristics of all molecules is extracted. Given that the population of particles is homogeneous, the diffusion equation is solved for $cdf(r^2, t_{lag})$ given by:

$$cdf(r^2, t_{lag}) = \alpha \cdot \exp\left(-\frac{r^2}{MSD_1}\right) \tag{2.1}$$

where $MSD(t_{lag})$ is the mean square displacement at time lag t_{lag}. Given the exponential distribution in r^2 data are represented on $\log(r^2)$-scale. Our experimental data could not be fitted with this one fraction model, however (fig.2.2A). Therefore the data were fit to a two-fraction model described by:

$$cdf(r^2, t_{lag}) = 1 - \left(\alpha \cdot \exp\left(-\frac{r^2}{MSD_1}\right) + (1-\alpha)\exp\left(-\frac{r^2}{MSD_2}\right)\right) \tag{2.2}$$

where $MSD_1(t_{lag})$ is the characteristic mean squared displacement for the fast fraction of size α, and $MSD_2(t_{lag})$ the characteristic mean squared displacement for the slow fraction of size 1-α. The bi-exponential fit properly describes the experimental results (fig.2.2A). This showed that there are two fractions of Gβ-YFP and of Gα2-YFP molecules that differ in their mobility on the membrane. Molecules were defined immobile when their MSD for the largest time lag (0.4 sec) was smaller than twice the positional accuracy. Together with equation 2.3 this leads to an upper estimate for their diffusion constant of $D_{immobile} < 0.001\ \mu m^2/s$.

2.3 Results

2.3.1 Heterogeneity in the mobility of Gα2-YFP and Gβ-YFP in the absence of agonist

D. discoideum cells were transformed stably with Gα2-YFP or Gβ-YFP constructs to analyze the mobility of individual Gα2 and G$\beta\gamma$ molecules, respectively. The fluorescent fusion proteins were functional as they rescued the developmental and chemotactic defects of $g\alpha2^-$ and $g\beta^-$ cells. In contrast to $g\alpha2^-$ and $g\beta^-$ cells that both are fully deficient in cAMP-induced responses, the Gα2-YFP/$g\alpha2^-$ and Gβ-YFP/$g\beta^-$ transformants faithfully crawl towards a cAMP source and rescue the developmental cycle started upon starvation [46, 44].

Single-molecule microscopy, a combination of regular wide-field microscopy with laser excitation and ultra-sensitive CCD camera detection [81], was used to observe the diffusion of Gα2-YFP and Gβ-YFP on the apical cellular membrane of *D. discoideum*. Measurements on the apical membrane eliminate any potential influence of the substrate surface on mobility. Fluorescence images were taken consecutively for up to 500 images per sequence at an imaging rate of 20 Hz. Diffraction-limited fluorescent signals with signal strengths comparable to that reported for individual monomeric YFP molecules [36] were observed and followed over time (fig.2.1B&C). Given the signal-to-noise ratio achieved the position of each molecule was determined to an accuracy of $\sim$40 nm. Statistical significance of all results was assured by the analysis of > 40 cells for each experimental condition. In total our analysis is based on 1-4 $\cdot 10^4$ observed molecules per condition.

Particle image correlation spectroscopy (PICS) [83] was subsequently applied to construct the cumulative probability (cumulative density function, cdf) of the squared displacements for time-lags of 0.05-0.4 sec (fig.2.1D, fig.2.2A&B). To our surprise it became obvious for all cdfs that G protein mobility was not homogeneous and was best described by a two-fraction model (fig.2.2A) which, after fitting, yielded a fraction size and two mean squared displacements per time-lag (see section 2.2). The result of a final analysis is shown in figure 2.2C&D for the fast and slow fraction of Gβ-YFP in non-stimulated aggregation competent cells, respectively (supplemental fig.2.8 for results on Gα2-YFP). For both fractions the mean squared displacement, MSD, increased linearly with time-lag, indicative of free Brownian motion of the proteins within the membrane characterized by diffusion constant D,

$$MSD(t_{lag}) = 4Dt_{lag} + s_0 \tag{2.3}$$

where the offset, s_0, accounts for the limited positional accuracy, σ, in the experiment ($s_0 = 4\sigma^2 = 0.0064\ \mu m^2$ with σ = 40 nm). Because the Gγ subunit has been shown to be essential for the membrane localization of Gβ [102] we assume, in what follows, that Gβγ is in heterodimeric form and all information obtained for Gβ reflects in an identical manner the behavior of Gγ. For Gβγ-YFP in unstimulated cells the fast fraction was characterized by a diffusion constant $D_1 = 0.15 \pm 0.01\ \mu m^2/s$, and the slow fraction, consisting of $32 \pm 3\%$ of all molecules, was characterized by $D_2 = 0.011 \pm 0.001\ \mu m^2/s$. For the membrane-bound Gα2-YFP in unstimulated cells the respective diffusion constants of the fast and the slow fraction were $D_1 = 0.14 \pm 0.01\ \mu m^2/s$ and $D_2 = 0.015 \pm 0.001\ \mu m^2/s$, with the slow fraction constituting $32 \pm 4\%$ of the total pool of molecules (supplemental fig.2.8). Identical results for the mobility and fraction size of Gα2 and Gβγ were obtained in $g\alpha2^-$ and $g\beta^-$ cells that expressed Gα2-YFP and Gβ-YFP respectively at endogenous levels (supplemental fig.2.9). The latter findings proved that the predominant fast fraction was not an artifact caused by the over-expression of the constructs in a wt background.

2.3.2 Mobility suggests the existence of a receptor/G protein precoupled complex in the absence of agonist

The strong similarity of the diffusion constants of both fractions for Gα2 and Gβγ further suggests that all membrane-bound G proteins in unstimulated cells were Gα2βγ

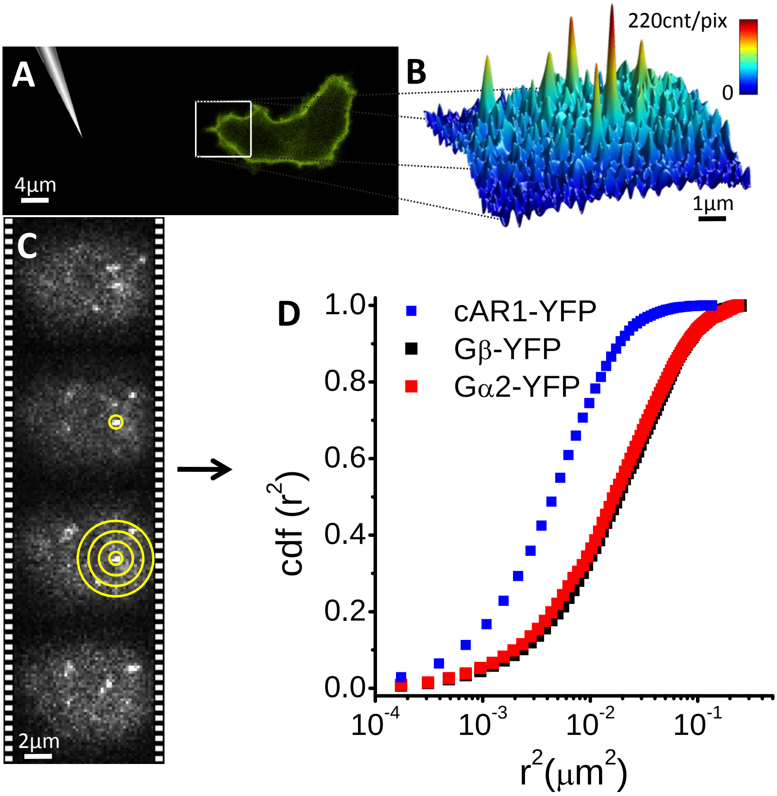

Figure 2.1: Experimental setup. **(A)** A micropipette containing 10 µM cAMP created a stable concentration gradient around its opening. *D. discoideum* cells in the vicinity of the pipette opening polarized within minutes and moved up the cAMP concentration gradient. The anterior and posterior of a cell were defined as the part closest and farthest away from the pipette, respectively. **(B)** A 514 nm laser beam was focused on the apical cell membrane where signals originating from individual Gβ-YFP or Gα2-YFP proteins were observed with a signal-to-noise ration of ∼30. **(C)** Single-molecule positions were determined to an accuracy of ∼40 nm by fitting to a 2D-Gaussian profile. Image-stacks were analyzed using PICS (see section 2.2.9), yielding the cumulative density functions of squared displacements ($cdf(r^2)$) for each time lag. **(D)** Cdfs at time lag of 50 ms are compared for cAR1-YFP (blue), Gβ-YFP (black) and Gα2-YFP (red).

heterotrimers. It is tempting to associate the slow mobility fractions of Gα2 and Gβγ to a receptor/G protein precoupled complex. The G protein diffusion constants (D_2= 0.015 µm^2/s for Gα2 and D_2= 0.011 µm^2/s for Gβγ) were similar to that found for the fast fraction of the receptor cAR1 ($MSD_{(44ms)}$ = 0.034 µm^2 [17]; D = 0.015 µm^2/s, see chapter 3). On the other hand, the diffusion constants of the fast fractions of the G protein subunits in unstimulated, aggregation competent cells were one order of magnitude higher than that found for cAR1, demonstrating that the fast fraction cannot be associated with a receptor-precoupled complex.

The association of the slow G protein fractions with a receptor/G protein precoupled complex was further supported by the analysis of Gβ-YFP mobility in *car1*$^-$and in $g\alpha 2^-$ cells (fig.2.3). Both, Gβ-YFP/*car1*$^-$and Gβ-YFP/$g\alpha 2^-$ cells were fully deficient in chemotactic signaling and unable to aggregate. For both cell types mobility was best described by a two-fraction model, with decreased slow fraction size of 18 ± 3% and 27 ± 4% for Gβ-YFP/*car1*$^-$ and Gβ-YFP/$g\alpha 2^-$, respectively (fig.2.3A). In addition, the diffusion constants of the slow fraction of Gβ-YFP in both knock-out cells was found to be D_2 = 0.020 ± 0.001 µm^2/s in $g\alpha 2^-$ and D_2 = 0.023 ± 0.001 µ^2/s in *car1*$^-$, respectively (fig.2.3B, left), higher as compared to the diffusion constants in wild-type (wt) cells, and in particular the diffusion constant of cAR1. In comparison, the mobility of the fast fractions, D_1 = 0.16 ± 0.01 µm^2/s in $g\alpha 2^-$ and D_1 = 0.19 ± 0.01 µm^2/s in *car1*$^-$, were found unchanged as compared to wt cells (fig.2.3C, left). Within experimental uncertainty Gα2 mobility was unchanged in *car1*$^-$ and gβ$^-$ cells (supplemental fig.2.8B&C, left).

Additional support for our hypothesis on association of the slow fraction with a receptor/G protein precoupled complex was obtained from the estimated expression levels of all components in wt and knock-out cells. We used the membrane-localized fluorescence signal to estimate the density of Gβ-YFP and Gα2-YFP (see 2.2). Approximately 7.7 $\cdot$ 10^4 Gβ-YFP were expressed, which is at the lower end of the expression level of reported endogenous Gβγ molecules of 8-40 $\cdot$ 10^4 molecules [46]. It was reported earlier that 4 $\cdot$ 10^4 receptors were expressed in wt as well as in transformed cells [34, 17], the active fraction of which, 2 $\cdot$ 10^4 ($\sim$50% of 4 $\cdot$ 10^4 [17]) corresponds very well to the number of slow Gβγ molecules, 2.5 $\cdot$ 10^4 ($\sim$32% of 7.7 $\cdot$ 10^4).

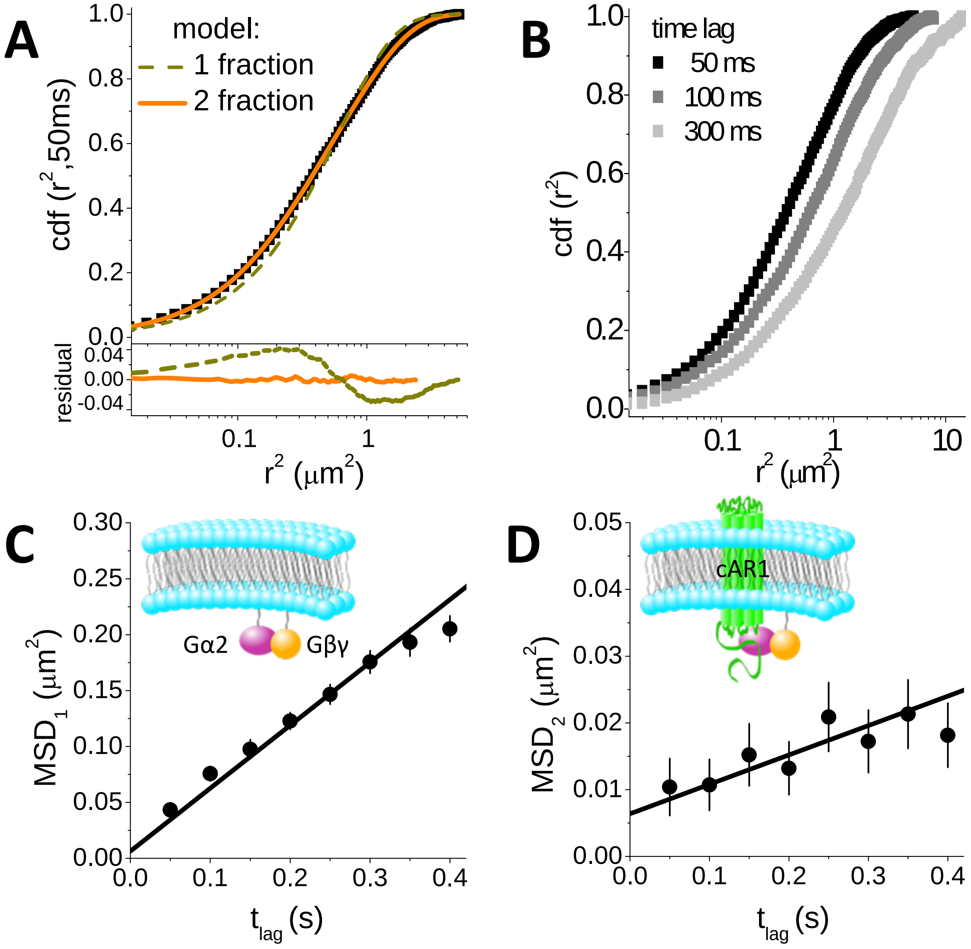
A
model:
1 fraction
2 fraction
cdf (r^2,50ms)
1.0
0.8
0.6
0.4
0.2
0.0
residual
0.04
0.00
-0.04
0.1
1
r^2 (μm^2)
B
time lag
50 ms
100 ms
300 ms
cdf (r^2)
1.0
0.8
0.6
0.4
0.2
0.0
0.1
1
10
r^2 (μm^2)
C
Gα2
Gβγ
MSD_1 (μm^2)
0.30
0.25
0.20
0.15
0.10
0.05
0.00
0.0
0.1
0.2
0.3
0.4
t_{lag} (s)
D
cAR1
MSD_2 (μm^2)
0.05
0.04
0.03
0.02
0.01
0.00
0.0
0.1
0.2
0.3
0.4
t_{lag} (s)

Figure 2.2: Mobility of Gβ-YFP. **(A)** Cumulative probability distribution of the square displacements $cdf(r^2)$ of Gβ-YFP on the apical membrane of developed Gβ-YFP/wt, recorded with a time interval of 50 ms between subsequent images. Data were fitted to a two component model (eq.2.2) (orange solid line; residuals are displayed in the lower part of the figure), resulting in a fraction (α) of slow Gβ subunits, and a fraction ($1-\alpha$) of fast Gβ subunits. The two fraction model describes the experimental results well in all the experimental conditions described. For comparison, a one-fraction model fit (eq.2.1) is shown (dark yellow dashed line). **(B)** Cumulative probability distributions of the square displacements on the apical membrane of developed Gβ-YFP/wt cells after 50 (black), 100 (gray), and 300 ms (light gray) time lag. As expected the data shifts with time lag towards higher squared displacements, r^2. **(C)** The characteristic mean squared displacements (MSD_1) were plotted versus time lag for the first ten time lags (50-500 ms) for the fast fraction of Gβ-YFP in wt cells. The data was fit with a free-diffusion model (eq.2.3), yielding a diffusion constant of $D_1 = 0.15 \pm 0.01$ μm^2/s. **(D)** Mean squared displacements (MSD_2) versus time lag for the slow fraction of GβYFP in wt cells. The free-diffusion model (eq.2.3) yielded a diffusion constant of $D_2 = 0.011 \pm 0.001$ μm^2/s. The offset at zero time lag, s_0, in (C) and (D) is given by the limited positional accuracy, $s_0 = 4\sigma^2 = 0.0064$ μm^2 with $\sigma = 40$ nm. The mobility of the slow fraction is equivalent to that of the cAMP receptor $D_{\mathrm{cAR1}} = 0.015$ μm^2/s (see chapter 3).

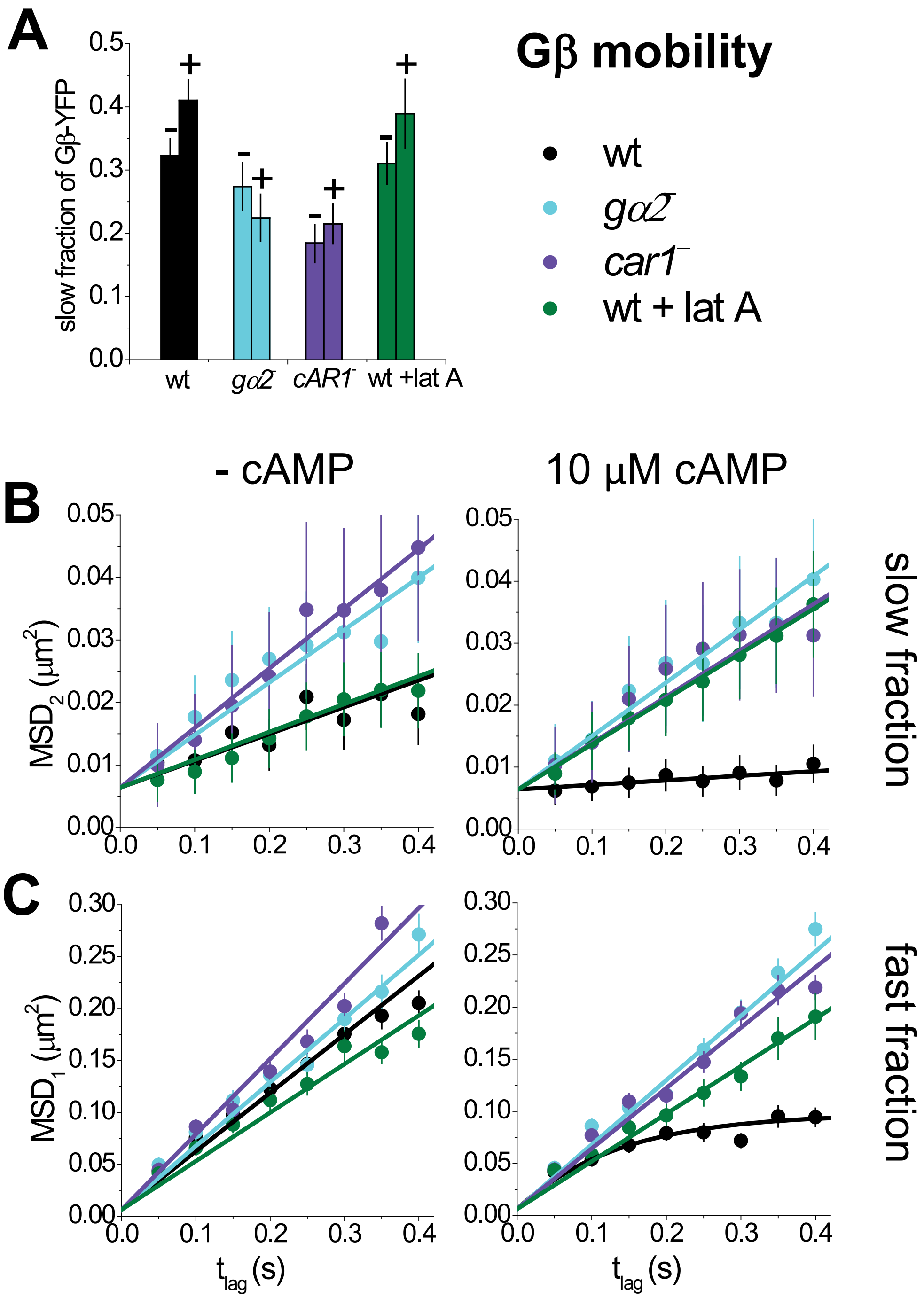
A
Gβ mobility
slow fraction of Gβ-YFP
0.0
0.1
0.2
0.3
0.4
0.5
-
+
wt
gα2⁻
cAR1⁻
wt +lat A
● wt
● gα2⁻
● car1⁻
● wt + lat A
- cAMP
10 μM cAMP
B
MSD2 (μm2)
0.00
0.01
0.02
0.03
0.04
0.05
0.0
0.1
0.2
0.3
0.4
slow fraction
C
MSD1 (μm2)
0.00
0.05
0.10
0.15
0.20
0.25
0.30
fast fraction
tlag (s)

Figure 2.3: Mobility of Gβ-YFP upon stimulation. (For the mobility of Gα2-YFP see supplemental fig.2.8) **(A)** Size of the slow fraction for Gβ-YFP in wt (black), *gα2*- (light blue), *car1*$^{-}$ (violet), and wt cells treated with 0.5 µM lat A (green), before and after global stimulation with 10 µM cAMP (indicated by - and +, respectively). The slowly diffusing population of Gβ-YFP in wt cells increased after cAMP stimulation. The slow fractions of Gβ-YFP in $g\alpha 2^{-}$ and *car1*$^{-}$ were smaller and did not change significantly upon cAMP addition. In lat A treated cells the slow fraction was the same when compared to untreated cells. After stimulation, however, there was an increase similar to that found for cells with intact actin cytoskeleton. **(B)** MSD$_2$ versus time lag plot of the slow fraction of Gβ-YFP in wt (black), $g\alpha 2^{-}$ (light blue), *car1*$^{-}$ (violet), and wt cells after treatment with 0.5 µM lat A (green) before (left) and after (right) stimulation with 10 µM cAMP. In wt cells the slow fraction was fully immobilized after cAMP stimulation. Gβ-YFP in $g\alpha 2^{-}$ and *car1*$^{-}$ cells was diffusing nearly two times faster than Gβ-YFP in wt cells. In the knock-out strains cAMP addition did not influence the diffusion constants, suggesting that immobilization of the slow population of Gβ-YFP in wt cells was due to signaling events. Lat A treated wt cells did not show any immobilization suggesting that immobilization is caused by interaction of the Gβ subunit with F-actin structures. **(C)** MSD$_1$ versus time lag of the fast fraction of Gβ-YFP in wt (black), *gα2*- (light blue), *car1*$^{-}$ (violet), and wt cells treated with 0.5 µM lat A (green) before (left) and after (right) stimulation with 10 µM cAMP. The diffusion behavior of Gβ-YFP in wt cells changed from free (eq.2.3) to confined (eq.2.4) upon cAMP stimulation. This was not observed in lat A treated, $g\alpha 2^{-}$, and *car1*$^{-}$ cells, where G protein signaling was impaired.

2.3.3 A fraction of Gβ-YFP becomes immobilized upon cAMP-induced receptor activation

To study the effect of cAMP-induced activation on Gα2 and Gβγ mobility, cells were uniformly stimulated with 10 μM cAMP. Single-molecule data were taken between 1 and 20 min after addition of cAMP (see section 2.2.4). A redistribution of the fraction sizes and mobilities was observed. The slow fraction of Gβ-YFP increased to 41 ± 3% upon stimulation (fig.2.3A), and became immobile ($D_2 \leq 0.001$ μm^2/s; fig.2.3B, right).

Neither immobilization nor change in fraction size was observed for Gα2-YFP fig.2.8. As Gα2 cycles rapidly between the membrane and the cytosol upon stimulation of cAR1 [22] this latter finding suggests that a receptor/Gα2 complex is formed prior to the full receptor/G protein heterotrimer complex.

The increase of the Gβ-YFP slow fraction and concomitant immobilization was not observed in Gβ-YFP/*car1*$^-$and Gβ-YFP/*gα2*$^-$ cells, where the slow fraction was 22 ± 4% and 21 ± 3% after stimulation, respectively (fig.2.3A and fig.2.3B right). This remaining slow fraction may be bound to other Gα subunits that are related to signaling via other G protein coupled receptors. Whereas the result on Gβ-YFP/*car1*$^-$ was predicted, the lack of Gβ-YFP response in Gβ-YFP/*gα2*$^-$ cells supports the notion that coupling to and activation by cAR1 requires Gα2. These observations together were taken as further support for the hypothesis that the slow Gα2-YFP and Gβ-YFP population reflected a receptor/G protein precoupled complex which dissociates upon ligand binding and receptor activation.

2.3.4 cAMP stimulation induces confined diffusion of fast Gα2-YFP and Gβ-YFP fractions into 600 nm membrane domains

Upon global cAMP stimulation, the fast fractions of both Gα2-YFP and Gβ-YFP changed their behavior from free diffusion (eq.2.3) to confined diffusion (fig.2.4, eq.2.4). Confined diffusion is a process in which a molecule is free to diffuse in a restricted domain surrounded by impermeable fences. The corresponding relation between MSD and timelag is:

$$MSD(t_{lag}) = \frac{l^2}{3}\left(1 - exp\left(\frac{-12D_{init}t_{lag}}{L^2}\right)\right) + s_0 \tag{2.4}$$

where D_{init} is the initial diffusion coefficient for small time-lags, and L represents the side-length of a square domain [57]. From figure 2.4B the domain size was determined to be 600 ± 100 nm for both Gα2-YFP and Gβ-YFP, and the initial diffusion constants $D_{init,1}$= 0.19 ± 0.02 and $D_{init,1}$ = 0.16 ± 0.02 $\mu m^2/s$ for the two constructs, respectively.

2.3.5 cAMP-induced membrane domains and Gβ-YFP immobilization are F-actin dependent

To determine whether there is a relation between actin polymerization, the 600 nm membrane domains, and the cAMP-induced immobilization of the Gβγ slow fraction, aggregation-competent Gβ-YFP/wt cells were incubated with 0.5 µM latrunculin A (lat A) for 10 min. The diffusion behavior of Gα2-YFP and Gβ-YFP was unchanged after lat A treatment in unstimulated cells (fig.2.3B&C, left; fig.2.8). However, upon global stimulation with 10 µM cAMP a significant change in the diffusion behavior was observed. The slow fraction size of Gβ-YFP increased slightly to 39 ± 5%, and the immobilization seen for untreated cells disappeared (D_2= 0.016 ± 0.001 $\mu m^2/s$; fig.2.3B, right). Further, the confinement observed in the fast fractions of Gα2-YFP and Gβ-YFP vanished and both constructs diffused freely with D_1 = 0.15 ± 0.01 $\mu m^2/s$ (fig.2.3C right; fig.2.8C). These results led us to conclude that the membrane domains observed were F-actin dependent, and that immobilization of Gβ-YFP required either a direct or an indirect interaction of Gβ-YFP with the F-actin meshwork. It should be noted however, that the increase of the slow fraction upon global cAMP stimulation was undisturbed by lat A. In contrast, the immobilization of the slow Gβ-YFP fraction was clearly regulated by F-actin and is presumably involved in maintaining cell polarity during chemotaxis.

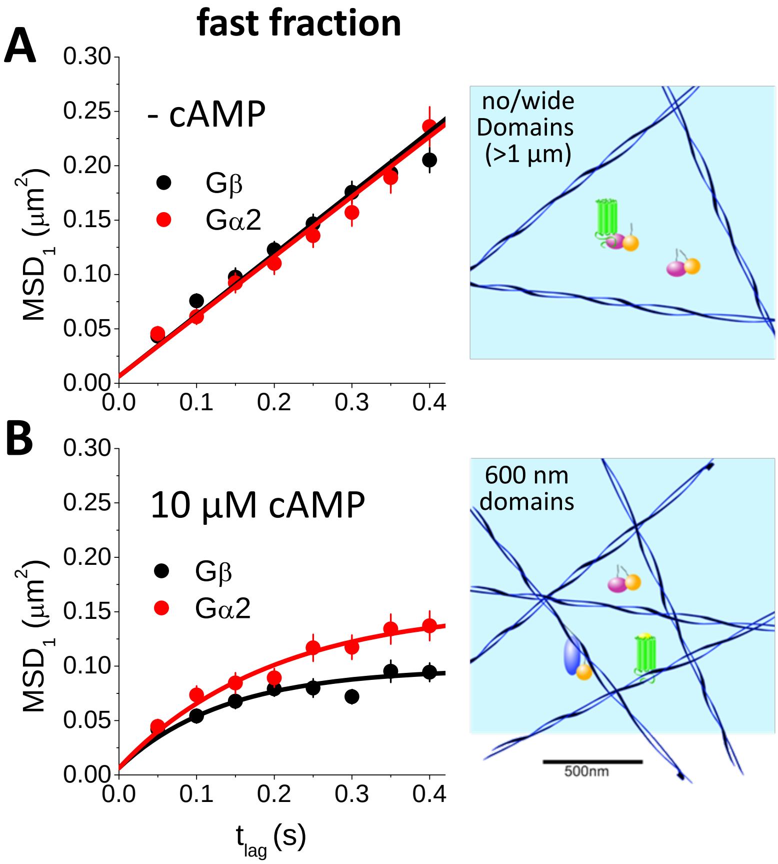

Figure 2.4: Comparison of the mobility of the fast fractions of Gβ-YFP and Gα2-YFP. The behavior of the fast Gβ-YFP (black) and Gα2-YFP (red) on the apical membrane of wt *D. discoideum* **(A)** before, and **(B)** after uniform stimulation with 10 µM cAMP changes from free to confined diffusion respectively. The formed domains have an average side length of 600 nm.

2.3.6 The increase of the slow fraction and $G\beta\gamma$ immobilization occur selectively in the leading edge

Whether the increase of the slow fraction and immobilization of Gβ-YFP upon global stimulation with 10 µM cAMP reflects a differential G protein behavior in the chemotaxis process was subsequently tested in a micropipette assay. The opening of a micropipette, filled with 10 µM cAMP, was placed at a distance of ~75 µm from the cells generating a shallow cAMP gradient of ~0.4 nM/µm at the cell position. After 13 min cells became highly polarized and oriented towards the micropipette (fig.2.1A). The size of the slow fraction of Gβ-YFP differed significantly when comparing leading to trailing edge and was found to be 38 ± 4% and 23 ± 3%, respectively (fig.2.5A). Strikingly we found that the diffusion constants of the slow fraction were different at the anterior as compared to the posterior: at the anterior the slow Gβ-YFP fraction was immobilized ($D_2 < 0.001$ µm^2/s; fig.2.5C, left) exactly as observed upon global stimulation whereas at the posterior the diffusion constant was comparable to the one found for unstimulated cells ($D_2 = 0.012 \pm 0.001$ µm^2/s). We also found that the formation of the characteristic 600 nm domains was restricted to the anterior (fig.2.5B). All together, the behavior of $G\beta\gamma$ in the absence of agonist matches the behavior in the posterior whereas $G\beta\gamma$ behavior at the anterior matches the situation observed after global agonist stimulation. Micropipette experiments on lat A treated cells confirmed that F-actin, in part, controls G protein mobility in an activation dependent manner. As lat A pretreated cells did not evolve any morphological polarity we defined the part nearest to the micropipette as the anterior. The posterior part of the cell was defined accordingly. The difference in slow fraction size between the anterior and the posterior cell regions was found to be the same as that found in polarized cells with intact cytoskeleton (fig.2.4A, right). This finding could have been predicted given that gradient-sensing is an actin-independent process. Like in the case of uniform cAMP stimulation, the immobilization of Gβ-YFP at the anterior, as well as the confined diffusion behavior of the fast fraction disappeared upon F-actin disruption.

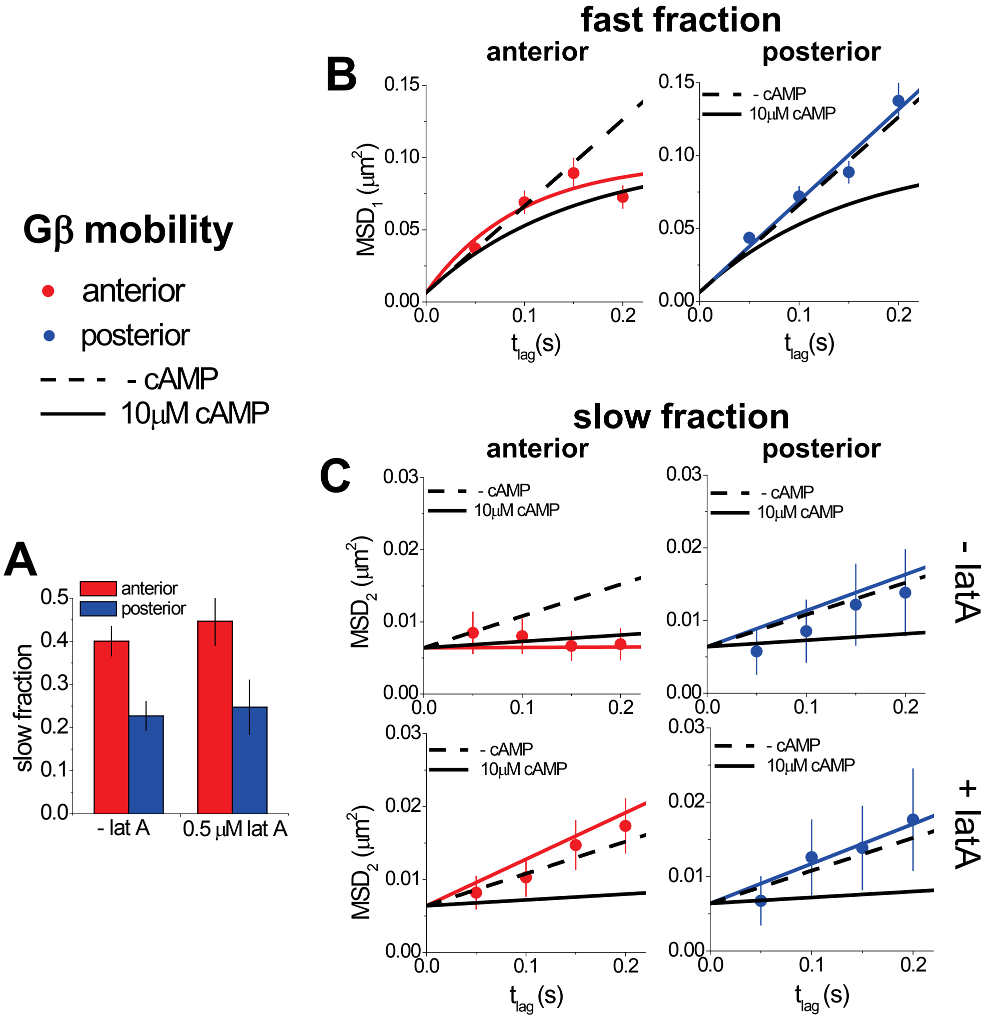
Gβ mobility
● anterior
● posterior
- - - - cAMP
—— 10μM cAMP
A
anterior
posterior
slow fraction
0.0
0.1
0.2
0.3
0.4
0.5
- lat A
0.5 μM lat A
fast fraction
B
anterior
posterior
MSD$_1$ (μm^2)
0.00
0.05
0.10
0.15
0.0
0.1
0.2
t_{lag}(s)
- cAMP
10μM cAMP
slow fraction
C
anterior
posterior
MSD$_2$ (μm^2)
0.00
0.01
0.02
0.03
- cAMP
10μM cAMP
- latA
+ latA
t_{lag} (s)

Figure 2.5: Gβ-YFP mobility is highly polarized. The diffusion of Gβ-YFP in the anterior (red) and the posterior (blue) apical membrane of wt *D. discoideum* crawling in a shallow (0.4 nM/ µm) cAMP gradient shows distinct differences. The black lines show the results obtained for cells before (dashed line; fig.2.2, left) and after global stimulation with 10 µM cAMP (solid line, fig.2.2, right). **(A)** Slow fraction size of Gβ-YFP in the leading (red) and trailing (blue) edge of wt cells (left) and cells treated with lat A. **(B)** MSD_1 versus time lag for the fast fraction in the leading (red) and trailing edge (blue). Both showed confinement as observed for the fast fraction upon uniform stimulation with cAMP. **(C)** MSD versus time plot for the slow fraction in the leading (red) and trailing edge (blue) in wt cells (left) and cells treated with lat A (right). In the wt cells the slow fraction was immobilized in the front ($D < 0.001$ µm^2/s). Immobilization was not observed in lat A treated cells.

2.3.7 cAMP-induced domain formation is PI3K and PLA2 independent

To investigate whether the observed cAMP-induced changes in the mobility of the Gβ subunits are the consequence of the activity of the PI3K pathway, we treated the cells with the PI3K inhibitor LY294002. At a concentration of 60 µM and incubation times of 15 min PI3K activity is reduced by > 95% [11]. In the absence of agonist, the inhibitor did not influence the mobility of Gβ subunits. Uniform stimulation with 10 µM cAMP also resulted in diffusion parameters similar to the control situation of wt cells when stimulated with cAMP. The fast fraction was confined, revealing the presence of ∼600 nm domains (fig.2.6C). The slow fraction in LY294002-treated cells was significantly slowed ($D_2 = 0.006 \pm 0.001$ µm^2/s) but mobile (fig.2.6B). As in the control experiments on global cAMP stimulation, the size of the slow fraction grew by 17% (fig.2.6A).

The observed results suggested that the F-actin-dependent domain formation was PI3K activity independent. Although the PI3K/PTEN pathway is known to be important for ligand-induced actin polymerization probably the latter finding is justified by the presence of parallel pathways. Therefore in addition to LY294002 we also used the PLA2 inhibitor bromoenol lactone (BEL) at a saturating concentration of 5 µM [11]. Cells were incubated with both inhibitors and subsequently stimulated with 10 µM cAMP. Treatment with both inhibitors did not result in any significant change in the mobility as compared to treatment with LY294002 alone (fig.2.6B). This result further proved the notion that additional pathways act in parallel to PI3K and PLA2 pathways and that they are sufficient for actin reorganization albeit at a reduced efficient as compared to when all pathways are active.

2.4 Discussion

The spatiotemporal behavior and interaction of activated GPCRs with G proteins constitutes a key event in chemotaxis. Using single-molecule epifluorescence microscopy we measured G protein diffusion in the absence and presence of agonist and in cells in an agonist gradient. By analysis of the mobility in various signaling states we developed a mechanistic model of the early steps in chemotactic signaling (fig.2.7). In the inactive state (fig.2.7, top) G proteins at the membrane are in either of two fractions, a highly mobile $G\alpha 2\beta\gamma$ heterotrimer or a low-mobility receptor/$G\alpha 2\beta\gamma$ precoupled complex. The receptor/$G\alpha 2\beta\gamma$ complex, which accounts for 32% of the membrane-bound $G\alpha 2$, 32% of the $G\beta\gamma$, and 50% of the activateable receptor population was identified by comparison of their mobility. Binding of the G protein to the receptor leads to a slow-down in its mobility by one order of magnitude. This latter finding is in line with recent FRAP and TIRM experiments [22] in which an increase in membrane-bound G protein fraction on receptor activation has been found and attributed to G protein / receptor interaction. Given that fast cytosolic proteins [76] are not visible with our technique and only lead to an increased background signal our results provide a detailed view on the membrane-bound fraction and the processes that play a role within the membrane.

Receptor activation by stimulation with cAMP (fig.2.7), bottom) disrupts the equilibrium between the $G\alpha 2\beta\gamma$ heterotrimer and the receptor/$G\alpha 2\beta\gamma$ precoupled complex by allowing the latter to form an activated receptor/$G\alpha 2\beta\gamma$ complex. This intermediate complex subsequently dissociates into a free activated receptor, and into free $G\beta\gamma$ and $G\alpha 2^{GTP}$ subunits. As argued by de Keijzer et al. [17], in turn the activated cAMP-receptor is able to interact with and activate further $G\alpha 2\beta\gamma$ heterotrimers (68% of the initial $G\beta\gamma$ and the membrane-bound $G\alpha 2$ population) (fig.2.7 bottom, red arrows) resulting in a local increase of G protein activation until cAMP dissociates from cAR1 at a rate of 0.4-1 s^{-1} [45]. It was predicted earlier [17] that such local amplification step, governed by the simultaneous increase in receptor mobility, will lead to a final 5-fold linear amplification of the external cAMP gradient to an intracellular gradient in active $G\beta\gamma$ proteins. The current experiments confirmed this prediction.

In parallel to the increase in fraction size, we observed a slow-down of $G\beta\gamma$ mobility upon stimulation. Since measurements were performed within 20 min after stimulation, a time after which adaptive processes have been initiated [19, 96], we conclude that the immobilization is not transient but persists as long as cells are stimulated. The observation confirms the previously observed dose-dependent steady-state loss-of-FRET which was explained by the dissociation of the $G\alpha 2\beta\gamma$ complex into its subunits [44].

Following G protein activation and further downstream signaling the actin cy-

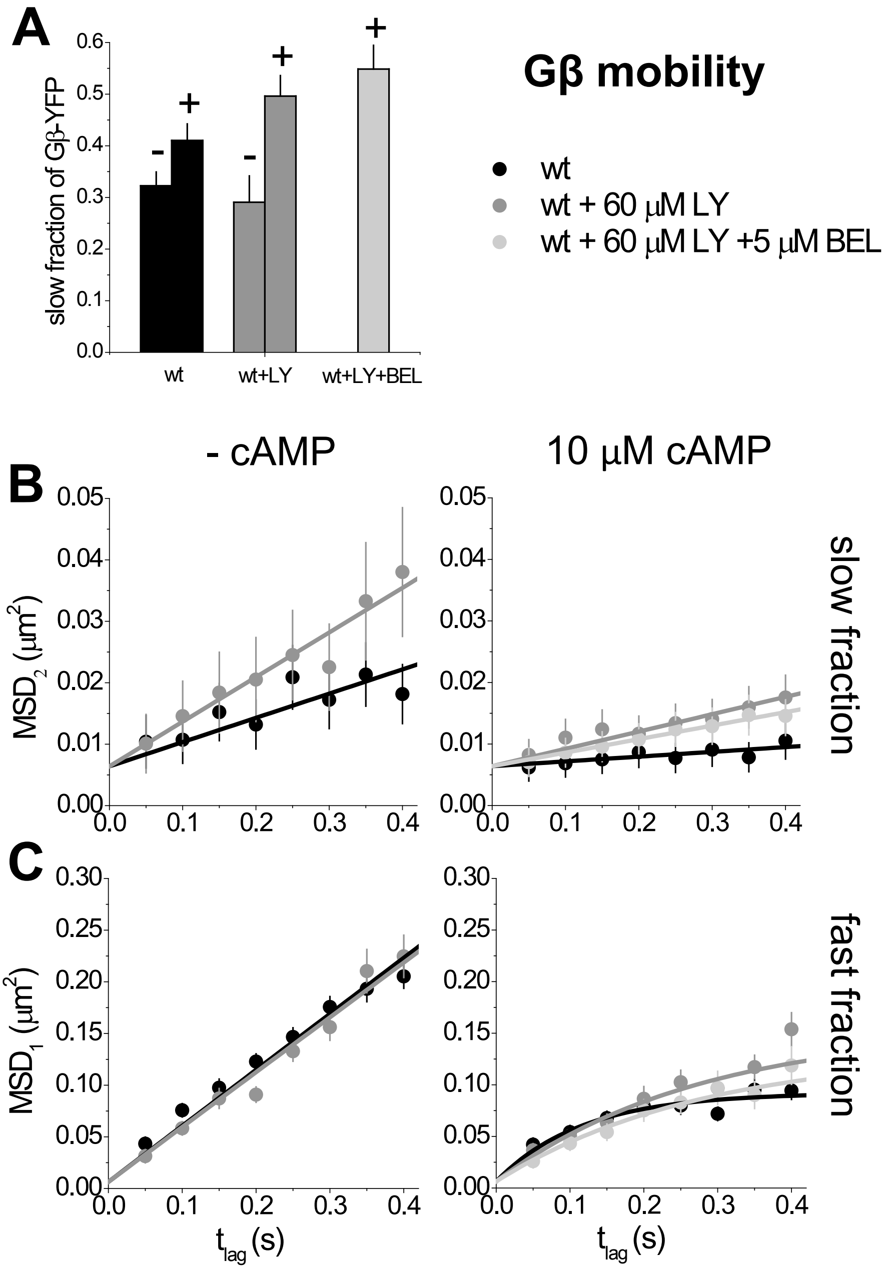
A
Gβ mobility
slow fraction of Gβ-YFP
0.0
0.1
0.2
0.3
0.4
0.5
0.6
-
+
-
+
+
wt
wt+LY
wt+LY+BEL
● wt
● wt + 60 μM LY
● wt + 60 μM LY +5 μM BEL
- cAMP
10 μM cAMP
B
MSD₂ (μm²)
0.00
0.01
0.02
0.03
0.04
0.05
0.0
0.1
0.2
0.3
0.4
slow fraction
C
MSD₁ (μm²)
0.00
0.05
0.10
0.15
0.20
0.25
0.30
t_lag (s)
fast fraction

Figure 2.6: Mobility of Gβ-YFP on inhibition of PI3K and PLA2. Diffusion of Gβ-YFP on the apical membrane of wt *D. discoideum* treated with the PI3K inhibitor LY294002, and the PLA2 inhibitor Bromoenol Lactone (BEL). **(A)** Size of the slow fraction of Gβ-YFP before and after uniform stimulation with 10 µM cAMP in wt cells (black), cells treated with LY294002 (grey), and cells treated with both LY294002 and BEL (light grey). **(B)** MSD_2 versus time lag of the slow fraction of Gβ-YFP in wt cells (black), cells treated with LY204002 (grey), and cells treated with both LY294002 and BEL (light grey) before (left) and after (right) uniform stimulation with 10 µM cAMP. cAMP stimulation caused a dramatic slowdown of the diffusion of the slow fraction in wt cells. This slowdown was impaired after treatment with both inhibitors. **(C)** MSD_2 versus time plot of the fast fraction of Gβ-YFP in wt cells (black), cells treated with LY294002 (grey), and cells treated with both LY294002 and BEL (light grey) before (left) and after (right) uniform stimulation with 10 µM cAMP. Confinement upon cAMP stimulation was observed even in presence of both LY294002 and BEL. These findings suggest that a third parallel pathway, which was not inhibited (most likely the TorC2 pathway [48]) is acting in gradient sensing.

toskeleton is reorganized [27]. Reorganization leads to a tightening of the membrane associated F-actin, apparent in Gα2 and G$\beta\gamma$ mobility which shows confinement to F-actin dependent domains of $\sim$600 nm in size. At this point it is still unclear whether F-actin is sufficient for G$\beta\gamma$ immobilization or whether associated proteins are needed to allow for the immobilization to occur. Inhibition of downstream PI3K (with 60 µM LY294002) and PLA2 (with 5 µM bel-inhibitor) however revealed that the G$\beta\gamma$ slow down was PI3K and PLA2 dependent only to a certain degree. Complete immobilization, as in the control experiment, was not observed. This might indicate either immobilization of only a part of the G$\beta\gamma$ subunits or binding to less rigid F-actin fibers. The formation of the 600 nm F-actin dependent domains, in contrast, was undisturbed. The restriction of activated signaling molecules to a small part of the membrane by inhibiting them from moving across the cell leads to a suggestive biological role for F-actin mediated confinement. Indeed the leading edge of moving fish epidermal keratocytes has been described as a diffusion barrier, even for lipids [94].

Clustering signaling components in a multicomponent signaling complex via a scaffold and/or anchoring proteins to the cytoskeleton was found for various signaling cascades [71] and seems ubiquitous. After initial G protein activation and respective activation of downstream signaling leading to enhanced actin polymerization at the front, activated G$\beta\gamma$ subunits are constrained to actin-dependent scaffolds at the leading edge. This process which spatially restricts G$\beta\gamma$ signaling may in turn lead to a further enhancement of the related signaling cascade at the anterior of the cell in an F-actin dependent positive feedback loop. This process may facilitate chemotactic signaling by spatially restricting the activated signaling components in a larger protein complex; a signalosome. Our data show that, if domains are present before stimulation, they must have a side-length of $L > 1$ µm (fig.2.2C, left). Upon stimulation such domains shrink to $L = 600$ nm (fig.2.2C, right). Assuming a homogeneous distribution of receptors and G proteins in the cell membrane (surface area = 540 µm^2, see section 2.2.8) before stimulation we estimate that such domains on average contain $4 \cdot 10^4$ receptors / 540 µm^2 $\cdot$ (600 nm)^2 = $\sim$27 receptors, $\sim$48 Gα2 subunits and $\sim$52 G$\beta\gamma$ subunits. Experiments performed on F-actin depleted cells have revealed that gradient sensing, the mere detection of the chemical gradient, was not impaired [70]. Hence, the role of Gβγ immobilization is likely related to the stabilization of pseudopods and perhaps, at a later stage, to the development of an innate cell polarity as is observed after prolonged directional stimulation of *D. discoideum* [27].

A variety of studies have clearly demonstrated that gradient sensing is reflected as a remarkable relocation of signaling components shortly after application of the chemical gradient [70, 15, 100]. Phosphatidylinositol-3,4,5-trisphosphate (PI(3,4,5)P_3) and its related kinase (PI3K) are largely localized at the leading edge whereas their related phosphatase (PTEN) is excluded from the anterior [40]. Despite extensive research relocation of neither the receptor nor the G protein has ever been observed. Protein behavior and activation can be different at different locations due to local variations in membrane curvature [25], activated signaling cascades [90], and the presence of signaling scaffolds [71]. Our experiments here show, as for the cAMP receptor, that cell polarization is reflected in a dynamical property of the G proteins, namely their mobiliy, rather than in their localization. It is noteworthy that the polarized distribution of Gβγ mobility was found to be independent on the presence of F-actin: an identical distribution between fast (inactive) and slow (active) fractions was observed in cells treated with 0.5 µM lat A. Hence, the increase in G protein activity is related to gradient sensing and not to processes responsible for subsequent pseudopod stabilization or amplification and persistent cell polarity.

We and other groups have shown before that polarization in chemotaxing *D. discoideum* cells is present at the level of the GPCR [90, 17]. Here we extended our model and show an F-actin dependent, leading edge specific immobilization of the Gβγ heterodimer, an important mediator of chemotactic responses. We show that this immobilization is due to activation of the chemotactic pathway and hypothesize that F-actin functions either directly or indirectly as a signaling enhancing scaffold, suggesting a function for this mechanism in the stabilization of pseudopods and/or the onset of a persistent leading edge. Likewise, in terms of a balanced inactivation model [59] which suggests a possible inhibitory function for Gβγ, binding Gβγ to F-actin would prevent its inhibitory function specifically at the leading edge, finally leading to the steep amplification of the activation signal observed in experiments.

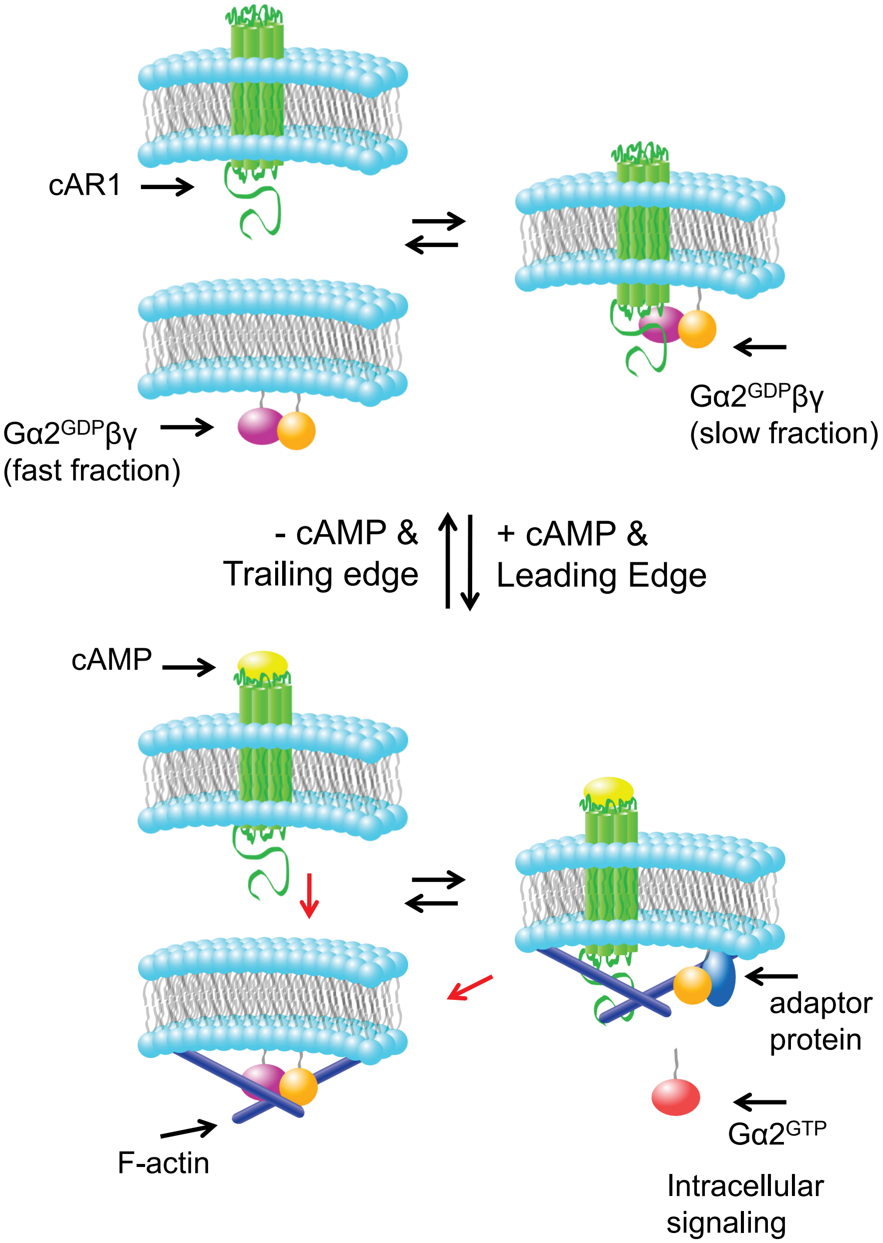
cAR1
Gα2GDPβγ
(fast fraction)
Gα2GDPβγ
(slow fraction)
- cAMP &
Trailing edge
+ cAMP &
Leading Edge
cAMP
adaptor
protein
Gα2GTP
F-actin
Intracellular
signaling

Figure 2.7: Model describing the dynamic cAR1 / G protein interaction at the leading and trailing edge. Before cAMP stimulation (top) the G protein's fast fraction is diffusing freely on the membrane with diffusion constant D = 0.15 $\mu m^2/s$. The slow fraction (D = 0.011 $\mu m^2/s$) exists as a complex which is precoupled to cAR1. 30% of the G protein and about 45% of the receptor population exist in this fraction. Upon binding of cAMP to the receptor (bottom) the G protein heterotrimer is dissociated: the Gα2 subunit exchanges GDP for GTP and diffuses into the cytosol where it is free to activate downstream signaling molecules. The previously precoupled cAR1 fraction is engaged in catalytic activation of the large G protein heterotrimer pool (indicated by red arrows). The G$\beta\gamma$ heterodimeric subunit is immobilized by interaction with F-actin associated structures which potentially serve to locally enhance chemotactic signaling. Tightening of the membrane-associated F-actin restricts the diffusion of the G proteins to $\sim$600 nm domains.

Supplemental information

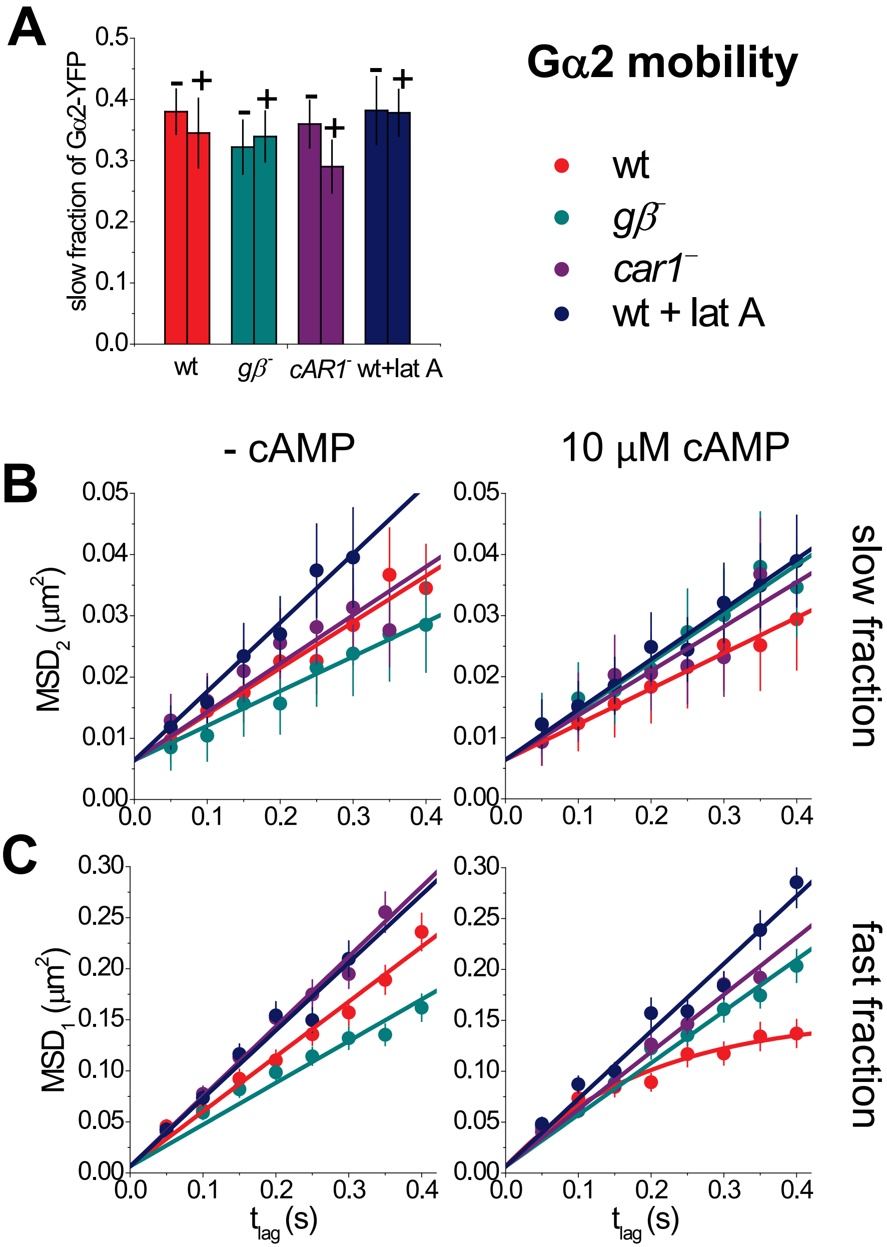

Figure 2.8: Mobility of Gα2-YFP upon stimulation. **(A)** Size of the slow fraction of Gα2-YFP in wt (red), $g\beta^-$ (cyan), $car1^-$ (purple), and cells treated with 0.5 µM lat A (blue), before (-) and after (+) global stimulation with 10 µM cAMP. **(B)** MSD$_2$ versus time lag of the slow fraction of Gα2-YFP in wt (red), $g\alpha2^-$ (cyan), $car1^-$ (purple), and cells treated with 0.5 µM lat A (blue) before (left) and after (right) uniform stimulation with 10 µM cAMP. The diffusion of the slow fraction of Gα2-YFP was not influenced by stimulation with cAMP, knockout of $g\beta$, or disruption of the F-actin cytoskeleton. **(C)** MSD$_1$ versus time lag of the fast fraction of Gα2-YFP in wt (red), $g\beta^-$ (cyan), $car1^-$ (purple), and cells treated with 0.5 µM lat A (blue) before (left) and after (right) uniform stimulation with 10 µM cAMP. The diffusion behavior of Gα2-YFP in wt changed from free (eq.2.3) to confined (eq.2.4) upon cAMP stimulation. This was not observed for lat A treated, $g\beta^-$ nor $car1^-$ cells.

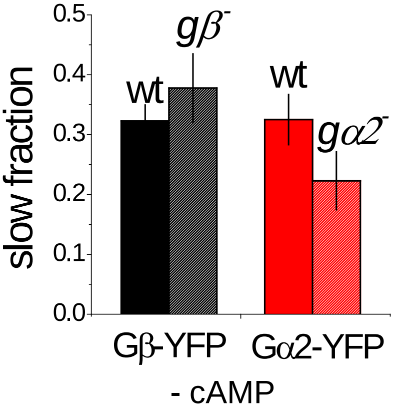

Figure 2.9: Comparison of slow fraction sizes between wt and knockout backgrounds. The slow fraction size of Gβ-YFP in non-stimulated wt and $g\beta^-$ cells (left) is compared to the fraction size of Gα2-YFP in non-stimulated wt and $g\alpha2^-$ cells (right). Both the wt cells and the respective knock-out cells showed a similar size of the slow fraction, assuring that the predominant fast fraction was not an artifact caused by the overexpression of the constructs in wt background.

Chapter 3

Leading edge specific attenuation of cortex / membrane interactions leads to polarized GPCR mobility

Single Molecule Microscopy (SMM) was used to investigate the diffusion of the G Protein Coupled Receptor cAR1 which is responsible for gradient sensing in *Dictyostelium discoideum*. We show that the mobility of cAR1 is globally increased $\sim$twofold during chemotaxis with respect to naïve (not exposed to cAMP) cells, higher at the leading than at the trailing edge and that this effect requires an intact G protein. Upon disruption of the F-actin cytoskeleton network by latrunculin A (lat A) the mobility of cAR1 also increases twofold indicating either a direct or an indirect interaction with actin filaments and implicating them as a likely regulator of cAR1 mobility. Surprisingly, in lat A treated cells in a cAMP gradient the overall mobility is even higher than in naïve lat A treated cells and cAR1 mobility is still increased at the anterior with respect to the posterior. We propose that F-actin restricts diffusion of cAR1 and that G protein dependent attenuation of F-actin or its interaction with the membrane leads to the polarized cAR1 mobility but clearly other factors involved in gradient sensing are also playing a part.

3.1 Introduction

Tight regulation of the cytoskeleton is vital to a multitude of cellular functions. Proteins that fulfill this task are important in cytokinesis, maintaining cell shape, stabilization of cell-cell and cell-substrate interactions, and regulation of cell motility. The cytoskeleton interactions however do not go one way, signaling molecules, even lipids, can be spatially confined by filamentous actin (F-actin) [94]. Such interactions presumably serve as a feedback between F-actin and its activating molecules and play an important role during directed as well as random cell movement of multiple cell types [80, 42].

In *Dictyostelium discoideum* more than 50% of the obstruction experienced by cytosolic signaling molecules is caused by F-actin [76]. Regarding cell polarization, the relevance of the mobility of signaling molecules on their function was predicted by a diffusion-translocation model [75] and recently confirmed by us in an initial study of receptor mobility [17]. The model concludes that "the capacity of a second messenger to establish and maintain localized signals, is mainly determined by its dispersion range". It is clear that the dispersion range is a function of the messenger's "off-rate" and its diffusion constant. Moreover in the cell membrane in which diffusion is restricted to two dimensions the rate of a reaction involving multiple molecular species is proportional to their concentration and speed [4]. In short, the mobility of signaling components in a polarized system, and any polarity regarding the latter, determines how well such a system can maintain and amplify that polarity. The only way to circumvent signal delocalization of highly mobile signaling molecules while preserving a high reaction rate is compartmentalization. The F-actin cytoskeleton has been suggested numerous times before as candidate to provide for micro-compartments [57, 94, 2].

The social single cell eukaryote *D. discoideum* is a widely used model organism for studying directed cell movement and cytoskeleton dynamics. *D. discoideum* is easily accessible to microscopy, easy to culture, its genome is completely sequenced, and the biochemical networks leading to chemotactic behavior have been extensively characterized. In addition, reliable methods have been developed to observe individual, fluorescence-tagged molecules during chemotaxis [90, 17].

In order to detect a gradient, *D. discoideum* relies on a G protein coupled receptor system making it an interesting model from a physiological perspective as well. The binding of cyclic adenosine mono-phosphate (cAMP) to the *D. discoideum* cAMP receptor 1 (cAR1) promotes the exchange of guanine di-phosphate (GDP) for guanine tri-phosphate (GTP) in the Gα2 subunit of the Gα2βγ heterotrimer. In the dogmatic view the trimer subsequently dissociates into a Gα2 and a Gβγ subunit. Recently, it has been shown that both G protein subunits continuously cycle between the membrane and the cytosol. Upon stimulation of cAR1, the Gα2 subunit decouples from Gβγ [44, 22] and increases its affinity for the membrane and potentially cAR1 [22]. The Gβγ subunit immobilizes in an F-actin dependent manner (chapter 2) and decouples from cAR1 presumably entering the cytosol [22]. In a cAMP gradient, G protein activation is proportional to the activation of cAR1 [44, 100] along the cell membrane. In addition, Gβγ immobilizes specifically at the leading edge in an F-actin dependent manner (chapter 2). It is known that both G protein subunits have specific downstream targets of which the most important ones for chemotaxis are probably Ras guanine exchange factors (RasGEFs). RasGEFs activate small G proteins of the Ras subfamily in a specific manner. For chemotaxis and cAMP relay, RasC and RasG are the most important proteins of the Ras subfamily [5]. Activation of Ras proteins is the earliest polarized response downstream of G proteins [103] and leads to the polarized activation of PI3K [40, 30], PLA2 [11], TorC2 and subsequently 2 PKB homologues (PKBA and PKBR1) [48]. How exactly the coordinated action of these pathways leads to the spatial regulation of the cytoskeleton that finally results in cell motility still has to be revealed.

In this paper we investigate the role of the F-actin cytoskeleton on the mobility of cAR1. We show that the mobility of cAR1 is decreased in the presence of F-actin. When *D. discoideum* cells chemotax, cAR1 mobility increases globally and likewise in a polarized leading edge *vs* trailing edge manner.

The result of finding a higher receptor mobility at the leading edge, where the abundance of F-actin was shown to be increased, lead us to propose to differentiate between two F-actin types. F-actin that lines the membrane making up the membrane cortex or membrane cytoskeleton, and the F-actin that generates force required for leading edge propulsion. The first type inhibits cAR1 diffusivity. Cortex - membrane interactions are less tight at the leading edge of chemotaxing *D. discoideum* [64], probably to facilitate the formation of blebs which result in faster cellular movement [101, 58]. The fact that lat A treated cells can still modulate cAR1 mobility in a cAMP gradient suggests that other factors involved in gradient sensing also influence the dynamics of membrane localized signaling molecules.

3.2 Materials and methods

3.2.1 Cell culture and transformation

The axenically growing *D. discoideum* strain Ax2 will be referred to as wildtype (wt). All cells were cultured at 22°C. Wt, $g\alpha2^-$ (myc2, [13]) and $g\beta^-$ (LW5, [60]) cells were transformed using electroporation with a cAR1-eYFP containing plasmid. We used G418 (Geneticin, Invitrogen) to select for successfully transformed cells, Cells were grown as a monolayer on plastic dishes in axenic culture medium, HL5-C (Formedium), containing 10 µg/ml penicillin/streptomycin (1:1) (Invitrogen) suitably supplemented with 10-20 µg/ml G418.

3.2.2 Preparation of cells for measurements

A confluent 10 cm petridish was incubated overnight in loflo medium (Formedium) to reduce cellular autofluorescence. In the morning, cells were washed once by collecting all cells in 5 ml development buffer (DB, [24]) and spinning down for 4 min at 400× g RCF. Cells were then resuspended in 5 ml DB and shaken gently at $\sim$100 rpm After 1 hr the cells were pulsed with 150 nM cAMP per pulse every 6 min using a timer and a peristaltic pump for 4 hr. Subsequently the cells were washed again with fresh DB as before and left to shake for 40 min After settling for 20 min on a chambered coverglass (labtek), measurements commenced. All measurements took place in DB at room temperature for a maximum of 2 hr (15-60 sec/cell). The term "naïve" is used for cells that have undergone this treatment but were not further subjected to cAMP (not by global stimulation and not by the application of a cAMP gradient) or lat A.

3.2.3 Global cAMP stimulation assay

The developmental buffer, covering naïve cells in the chambered cover-glasses was supplemented with cAMP to a final concentration of 100 nM or 10 µM. Experiments were performed within either 6 or 20 min after addition of cAMP.

3.2.4 Applied gradient assay

After settling on the coverglass, a micropipette (Eppendorf femtotip) attached to an Eppendorf Femtojet was suspended just above the glass coverslide on which the cells reside. The internal pressure of the Femtojet was set to 40 KPa. This created a stable cAMP gradient of about 10% over the cell body at a mid-concentration of 60 nM as verified experimentally and by simulation. Wt cells polarized within a minute and moved accurately towards the needle. Measurements at the anterior and posterior of polarized cells were taken at a distance of $\sim$70 µm from the pipette tip. The region of interest was set up such that we measured approximately 20% of the cell length at the anterior and posterior (fig.3.1A).

3.2.5 Latrunculin A treatment

The DB in which the cells have settled on the coverglass was supplemented to a final concentration of 0.5 µM lat A. After 10 min of incubation measurements were performed for a maximum of 10 min.

3.2.6 Single-molecule microscopy

The experimental setup for single-molecule imaging has been described in detail previously [81]. The samples were mounted onto an inverted microscope (Axiovert100, Zeiss) equipped with a 100× objective (NA=1.4, Zeiss) and a sensitive CCD camera. The region-of-interest was set to 50 × 50 pixels. The apparent pixel size was 220 nm. Measurements were performed by illumination of the samples for 5 ms at 514 nm (Argon-ion laser, Spectra Physics) at an intensity of 2 kW/cm^2. The cells were photobleached for a period of 2-5 sec and sequences of 500 images with a timelag of 50 ms were taken. Use of an appropriate filter combination (Chroma) permitted the detection of the fluorescence signals on a liquid nitrogen-cooled CCD-camera (Princeton Instruments). The setup allowed us to image individual fluorophores at a signal-to-background-noise ratio of $\sim$30 leading to a positional accuracy of σ_0 = 40 nm (fig.3.1B).

3.2.7 Analysis of single molecule data

The positions of individual molecules were determined within each image stack by fitting the intensity profiles to a 2D Gaussian using Matlab (Mathworks Inc). The center-of-mass of the Gaussian fit corresponds within $\sim$40 nm to the position of the molecule. Typically image stacks on 50-200 cells were taken that lead to 2-6 $\cdot$ 10^4 individual molecule positions in each of the experiments shown. The position data were subsequently used to perform particle image correlation spectroscopy (PICS, [83]). PICS calculates the cross-correlation between individual molecule positions at two different points in time (fig.3.1C) from which the cumulative density function ($cdf(r^2, t_{lag})$) of squared displacements was constructed for each timelag (t_{lag}) between 50 and 400 ms (fig.3.1D). At least 2 $\cdot$ 10^4 individual molecules were used to construct the cdfs. The cdfs are subsequently fitted to a two fraction diffusion model:

$$cdf(r^2, t_{lag}) = 1 - \left(\alpha \cdot \exp\left(-\frac{r^2}{MSD_1}\right) + (1-\alpha)\exp\left(-\frac{r^2}{MSD_2}\right)\right) \tag{3.1}$$

The fast fraction size, α, was globally fitted for all timelags in a given data set. This yielded 2 mean squared displacements (MSD_1, MSD_2) per timelag and one fast fraction size for each data set (fig.3.1D). Subsequently the MSDs were plotted versus t_{lag} resulting in a representation of the diffusion behavior. To determine the diffusion constant we fitted each of the MSDs *vs* time datasets to a free diffusion model:

$$MSD = 4Dt_{lag} \tag{3.2}$$

This final analysis yielded two diffusion constants (D_1, D_2) and two offsets (s_0) (fig.3.1E). In the case that two dataset were compared (for example anterior *vs* posterior), MSD_1 and MSD_2 were kept equal per timelag for the two datasets, the fast fraction size (α) was kept constant per dataset but varied between the two data sets resulting in 2 diffusion constants and two fraction sizes per fit. In this analysis, the fast fraction size α was the only parameter signifying the difference between the two experimental conditions.

The offset s_0 is a representation of the accuracy by which the position of the molecules, σ was determined in each dimension. The positional accuracy leads to the offset in equation 3.2 of $s_0 = 4\sigma^2$ in two dimensions. Given that σ scales with the signal-to-noise ratio ($\sigma = \frac{\frac{\lambda}{2}}{\sqrt{SNR}}$, λ = wavelength of detected light) and since every observation of an individual molecule is achieved at different signal-to-noise ratios, a distribution in σ must be taken into account. For the data presented here $\sigma = 40 \pm 20$ nm. As outlined in the Appendix this distribution in positional accuracies renders the simple expression in the squared displacement analysis of equation 3.1 inaccurate. This becomes important in the case that MSD_1 and MSD_2 are close to σ^2, as presented here. Subsequently the data treatment leads to two different offset values $s_{0,1}$ and $s_{0,2}$ for the fast and slow fraction, respectively. It should be noted that independent of this inaccuracy, the diffusion constants as determined from the slopes of the MSD with timelag were unchanged.

3.2.8 Error estimation

To determine the correct error in the diffusion constants and the fraction size distributions we used bootstrapping. Each dataset was build up from all the observed molecules found in 40-200 individual cells. From the total dataset 30 random sub-sets were chosen. These resampled sub-sets were subsequently analyzed as describe before, yielding 60 different diffusion constants (2 for each dataset) and 30 fast fraction sizes. The standard deviation of these distributions was taken as an accurate representation of the biological variance among cells and as error estimates for the data obtained on the full data set.

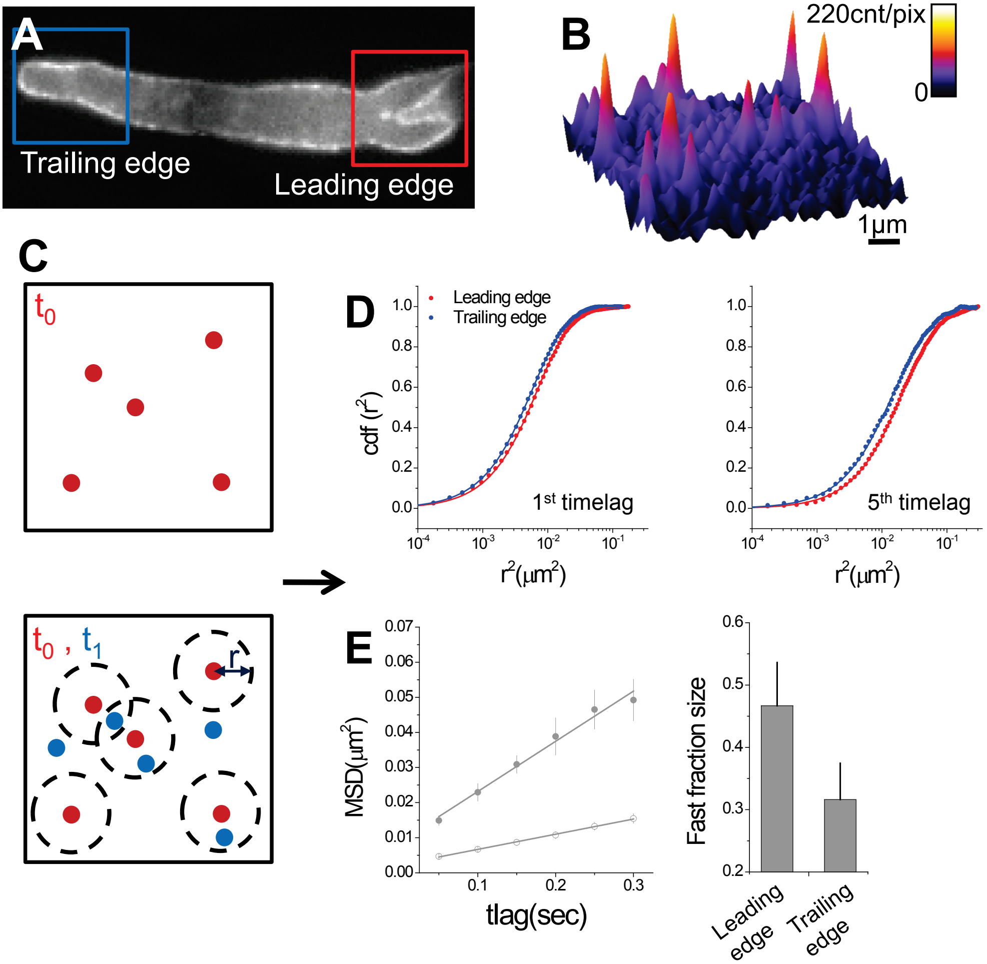
A
Trailing edge
Leading edge
B
220cnt/pix
0
1μm
C
t_0
t_0 , t_1
r
D
Leading edge
Trailing edge
cdf (r^2)
1.0
0.8
0.6
0.4
0.2
0.0
1st timelag
5th timelag
10^{-4}
10^{-3}
10^{-2}
10^{-1}
r^2(μm^2)
E
MSD(μm^2)
0.07
0.06
0.05
0.04
0.03
0.02
0.01
0.00
0.1
0.2
0.3
tlag(sec)
Fast fraction size
0.6
0.5
0.4
0.3
0.2
Leading edge
Trailing edge

Figure 3.1: Experimental setup. **(A)** A needle containing 10 µM cAMP is placed at a distance of $\sim$70 µm from the region in which the measurements are taken creating a gradient estimated at 4nM/µm over the cells. As soon as the needle is placed, the cells start to change their morphologies from amorphous to highly stretched. **(B)** A 514 nm laser is focused on the apical membrane of the leading and trailing edge where we observe individual eYFP tagged molecules with a positional accuracy of around 40 nm, after low pass fast Fourier transform filtering. **(C)** The correlation between the images in a stack, typically 500 images / cell with a time lag of 50 ms is calculated using PICS (see section 3.2.7) which yields **(D)** cumulative density plots (cdfs) for each time lag, typically up to 400 ms. Fitting of these plots (eq.2.2) results in two MSDs and a fraction size for each of the fractions which is fitted globally. **(E)** When plotted the slope of the MSD *vs* time lag plots represents the diffusion constant ($D = \frac{4t_{lag}}{MSD}$). By assuming the diffusion to be the same between two datasets, the fraction size, α (eq.3.1), becomes the sole parameter that measures the difference between them.

3.3 Results

3.3.1 In naïve wt cells cAR1 moves slowly and exists in two distinct states

Naïve Ax2 (wt) *Dictyostelium discoideum* cells after having been starved for 6 hr. and challenged by cAMP pulsing were very amorphous in shape and spread out readily on the coverglass. Pseudpods seemed to be generated at random as the cells probed their environment (fig.3.2A). Cells initially moved at random.

The mobility of cAR1-eYFP in these cells was investigated on long timescales (up to 400 ms) to get an idea of cAR1 mobility and possible membrane structures or domains that could influence diffusivity. This data will serve as a control for the data presented in what follows. The mean square displacements for given time lags between 50 and 400 ms were determined by PICS that yielded the distribution of square displacements (fig.3.1D). Fitting of those distributions to a diffusion model (eq.3.1) confirmed the existence of two distinct, slow and fast, cAR1 fractions as has been reported earlier [17]. Taking into account the difference in positional accuracy, the mean squared displacements (MSDs) for a timelag of 50 ms MSD_1 = 0.017 ± 0.002 μm^2 and MSD_2 = 0.005 ± 0.004μm^2 matched the values reported by de Keijzer and others for a time lag of 44 ms [17]. The linear relation between both MSDs and timelag (fig.3.2B) showed that cAR1 mobility was random, and was characterized by the diffusion constants D_1 = 0.015 ± 0.002 $\mu m^2/s$ (α = 0.45 ± 0.06) and D_2 = 0.007 ± 0.001 $\mu m^2/s$ (1-α = 0.55 ± 0.06), respectively. The diffusion constant of the fast fraction, D_1, reported here differs significantly from the earlier estimate [17] as obtained from one MSD value at 44 ms only. The latter overestimation was due to the underestimation of the effect of a wide distribution in the positional accuracies by which individual molecules were detected (see also section 3.2.7 and the Appendix). The diffusion constants we found by the more elaborate study here are in line with typical values found for GPCRs [90, 2] in cell membranes. It should be noted that the diffusion of the fast fraction (D=0.015 ± 0.002 $\mu m^2/s$) closely resembles that of the slow fraction of the G protein heterotrimer (chapter 2). Hence, we suggest that the fast fraction reflects receptors that are pre-coupled to their respective G protein.

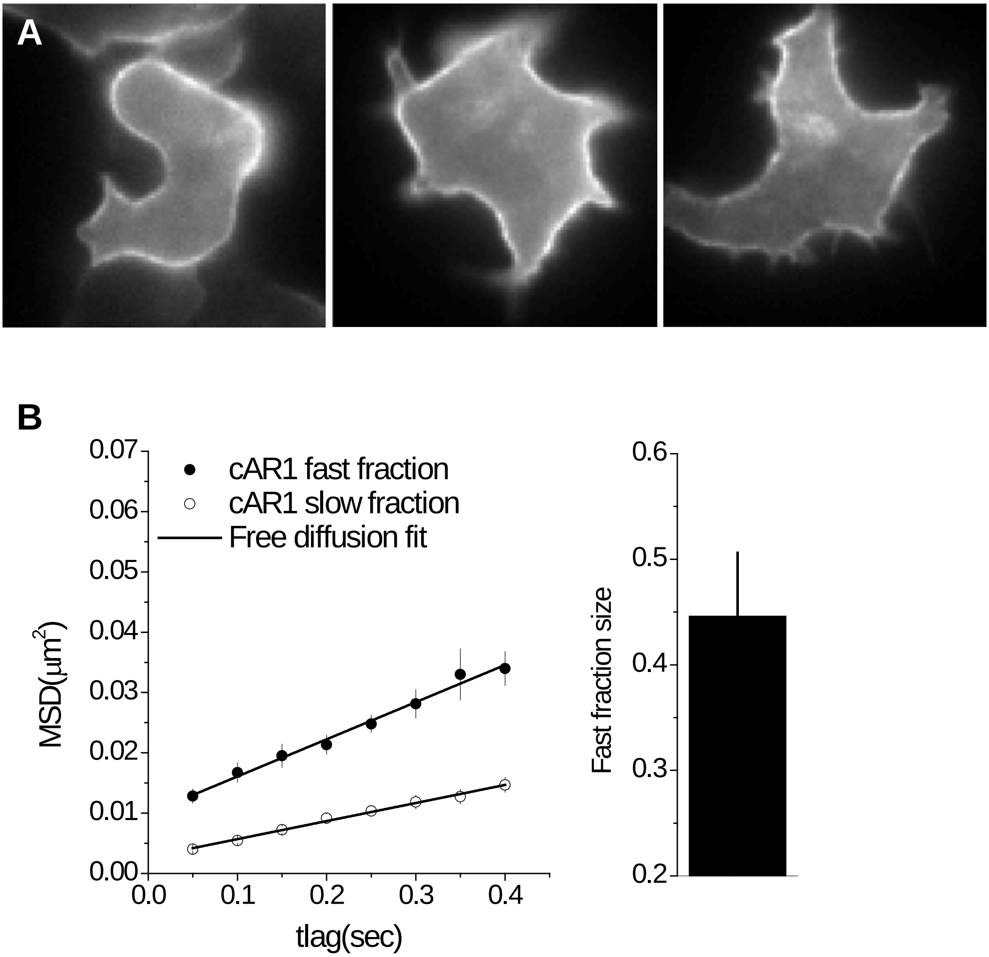

Figure 3.2: Diffusion of cAR1 in naïve wt cells. (A) After settling on the coverglass, cells flatten out and extend pseudopods as if exploring their surroundings. **(B)** cAR1 exists in two states with one diffusion constant ~twofold higher compared to the slower one. The offset difference is explained by a wide distribution of the positional accuracy with which individual molecules are located.

3.3.2 The mobility of cAR1 is polarized and increased in chemotaxing cells

We have previously shown that the mobility of cAR1, as characterized by the MSD after a time lag of 44 ms, was polarized [17]. 23% more fast moving receptors were found at the leading edge of cells as compared to the posterior when cells underwent chemotaxis. In the current paper we set out to characterize the diffusion of cAR1 on longer timescales from 50 up to 400 ms. In this way we intended to retrieve additional details on receptor mobility that in turn is taken as indicator for the local structure of the plasma membrane and its potential restructuring following gradient detection.

Upon application of the cAMP gradient the cells attain a highly stretched morphology (fig.3.3A). We measured > 200 cells and constructed the anterior and posterior cdfs for 6 timelags between 50 and 300 ms. Clearly, the receptor mobility at the anterior was increased with respect to that at the posterior (fig.3.7). Furthermore, we confirmed that the two-fraction model was sufficient to interpret the data. We assumed that the mobility per fraction was identical at the anterior as compared to the posterior. The latter assumption was confirmed by independent fit of the anterior/posterior displacement data that yielded equivalent diffusion constants for both fractions (data not shown). The final result of this advanced analysis confirmed our previous results [17]: cAR1 mobility was higher at the anterior as compared to the posterior. We interpret this higher mobility as an increase in fast fraction size (α in eq.3.1). In this two-fraction interpretation the fast fraction was $\alpha = 0.47 \pm 0.05$ at the anterior as compared to $\alpha = 0.32 \pm 0.05$ at the posterior, hence higher by a factor of $\sim$1.5. As compared to naïve cells the diffusion constants of both fractions were also increased twofold to $D_1 = 0.036 \pm 0.005$ µm^2/s, and $D_2 = 0.011 \pm 0.001$ µm^2/s, respectively. In comparison to studies on the G proteins (chapter 2), receptor diffusion did not show confinement, at least up to a length scale of 0.05 µm^2, not even upon activation (data not show). That finding might not be surprising given our earlier finding that confinement in G protein mobility was observed at a length scale of 0.6 µm^2.

Cell movements did not influence the values we report here. A cell crawls at a speed of $v \sim 5$ µm/min equivalent to $\sim$4 nm/50 ms, which is significantly lower than positional accuracy at which we detected individual molecules. Clearly, at much longer timelags ($t_{lag} > \frac{4D}{v^2}$ = 23 sec) the linear displacement of the cell would be comparable to that of the molecules (the MSD quadratically increases with time for linear movement). Such timescales were outside of our experimental reach. In addition, the squared displacements parallel to the direction of cell motility was identical to that in the perpendicular direction (data not shown) yet another strong indicator for random cAR1 movement.

3.3.3 cAR1 mobility is not influenced by Gα2 or G$\beta\gamma$ binding

When comparing the mobility of cAR1 between front and back of wt cells performing chemotaxis, the anterior mobile fraction was increased by 15% (fig.3.3, gray bars). In our previous paper we suggested that this anterior cAR1 mobility shift was directly related to Gα2 uncoupling following receptor stimulation. We further suggested that Gα2 by itself was bound to some (potentially) cytoskeleton, structure in order to explain the difference in anterior/posterior mobility [17]. In a follow-up study we characterized the molecular movement of both the Gα2 and the G$\beta\gamma$ subunits of the G protein heterotrimer by which we were able to confirm the coupling of Gα2 to cAR1. It should be noted however that the majority of the G protein heterotrimers ($\sim$70%) was with high certainty uncoupled from cAR1 (chapter 2).

Upon establishment of the full MSD *vs* time curve of cAR1 in the $g\alpha2^-$ cell line, we found no statistically relevant difference (fig.3.4A) in comparison to wt cells. Within experimental uncertainty the diffusion constants were identical for both cell types (fig.3.4A; $D_1 = 0.019 \pm 0.003$ µm^2/s, $D_2 = 0.007 \pm 0.001$ µm^2/s). The same holds true for cAR1 mobility in $g\beta^-$ cells (fig.3.4C; $D_1 = 0.014 \pm 0.003$ µm^2/s, $D_2 = 0.007 \pm 0.001$ µm^2/s, $\alpha = 0.39 \pm 0.05$). Both findings were in contrast to what we predicted from our earlier studies [17]. Our new, more detailed study shows that the diffusion of cAR1 in $g\alpha2^-$ cells deviates only slightly from that in wt cells, but it does not resemble the diffusion in the leading edge of chemotaxing cells. The loss of polarized cAR1 mobility in $g\alpha2^-$ cells, as reported earlier at the 44 ms timescale [17] however was clearly confirmed here on timescales up to 300 ms. The anterior/posterior mobility difference as seen in the squared displacement distribution in wt cells (fig.3.7) was lost in $g\alpha2^-$ (fig.3.8). A detailed analysis of the mobility showed that the mobile fraction difference for the anterior/posterior cAR1 mobility

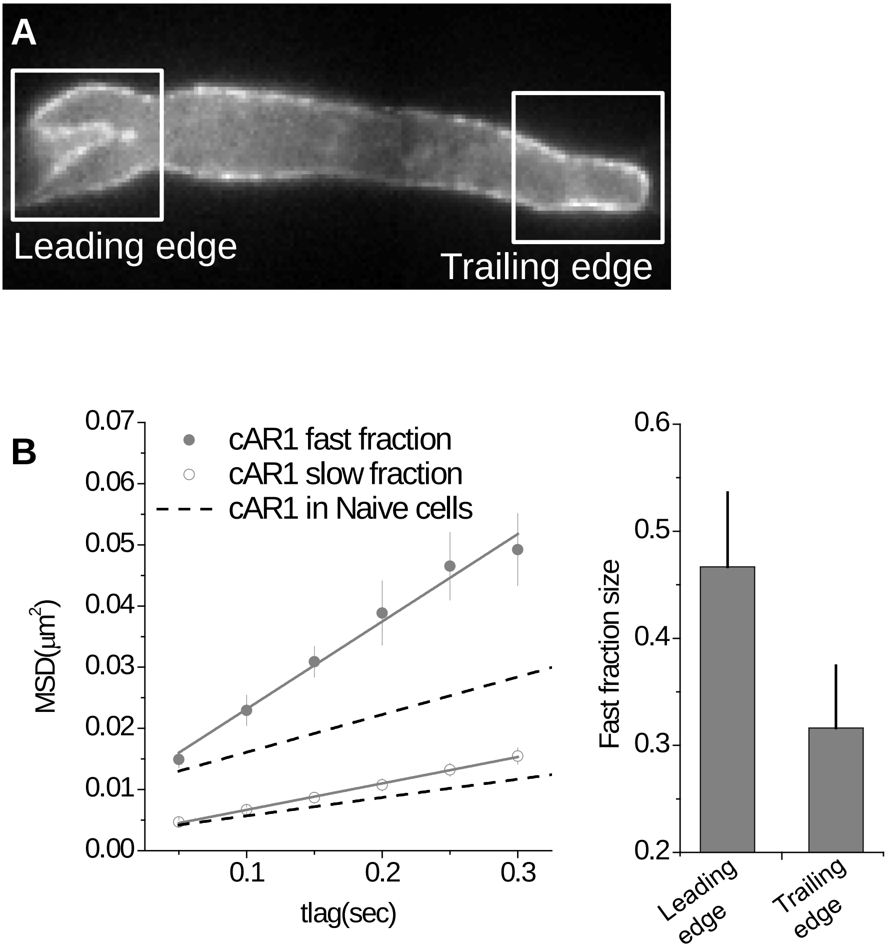

Figure 3.3: Diffusion of cAR1 is polarized and increased in chemotaxing cells. (A) In a gradient, cells attain a highly polarized morphology with a clearly distinguishable leading and trailing edge. **(B)** We fitted the data using a model which assumed the diffusion of both cAR1 fractions to be the same for the leading and trailing edge of a cell (gray dots) and left the fast fraction size (α in eq.3.1, see section 3.2) as the only free parameter which defines the front back difference (gray bars). The overall mobility of cAR1 is significantly higher when compared to the mobility in naïve wt cells (black dashed line). The mobility is higher at the leading edge.

was reduced to 7% (α = 0.36 ± 0.04 *vs* 0.29 ± 0.04) as compared to $\Delta\alpha$ = 0.15 (15%) in wt cells (fig.3.4B, compare blue and grey bars; fig.3.8). Interestingly, also the increase in diffusion constants found for wt cells placed into a gradient disappeared for cAR1 in $g\alpha2^-$ cells. The diffusion constants found for $g\alpha2^-$ cells in a gradient were indistinguishable to those found in naïve cells (fig.3.4B); D_1 = 0.016 ± 0.002 $\mu m^2/s$, D_2 = 0.006 ± 0.001 $\mu m^2/s$). Together those findings suggest that cytoskeleton rearrangements, which are at the base of the change in cAR1 mobility in polarized wt cells, were impaired in the Gα2 knockout.

3.3.4 Polarized cAR1 mobility is F-actin independent

We investigated whether cAR1 mobility and the mobility shift observed in a gradient was the result of F-actin cytoskeleton rearrangements. Using 0.5 µM lat A F-actin polymerization was inhibited. Wt cells incubated for 10 min with 0.5 µM lat A changed their morphology from amorphous to nearly circular (fig.3.5A). The cells were still able to move albeit at a greatly reduced speed and by extending very small and few pseudopods. It might be interesting to note that at the bottom membrane intact cytoskeleton structures were still present (fig.3.5B). That latter observation further ensured us to pursue experiments on the apical membrane of the cell, as compared to experiments performed by many other groups that only address the basal membrane by total-internal reflection microscopy.

After lat A treatment, the diffusion constants of both cAR1 fractions increased twofold to D_1= 0.028 ± 0.006 $\mu m^2/s$ and D_2= 0.015 ± 0.002 $\mu m^2/s$ (fig.3.5C, green dots), when compared to naïve wt cells, whereas the mobile fraction slightly decreased to α = 0.38 ± 0.05 (fig.3.5C, green bar). Both findings were nearly identical to values obtained for wt cells in a cAMP gradient (fig.3.5C, gray dashed line). These results indicate that indeed cAR1 mobility is modulated by F-actin interactions.

To see if absence of the F-actin polymerization also abolished the polarity of cAR1 mobility in a gradient, we applied a cAMP gradient to lat A treated cells. In the gradient cells were not able to take on the elongated shape but were morphologically indistinguishable from lat A treated cells without the challenge (fig.3.5A). The mobility shift that was observed in untreated cells prevailed. We found a difference in fast fraction size in lat A treated cells of 14±7% between anterior (43 ± 6%) and

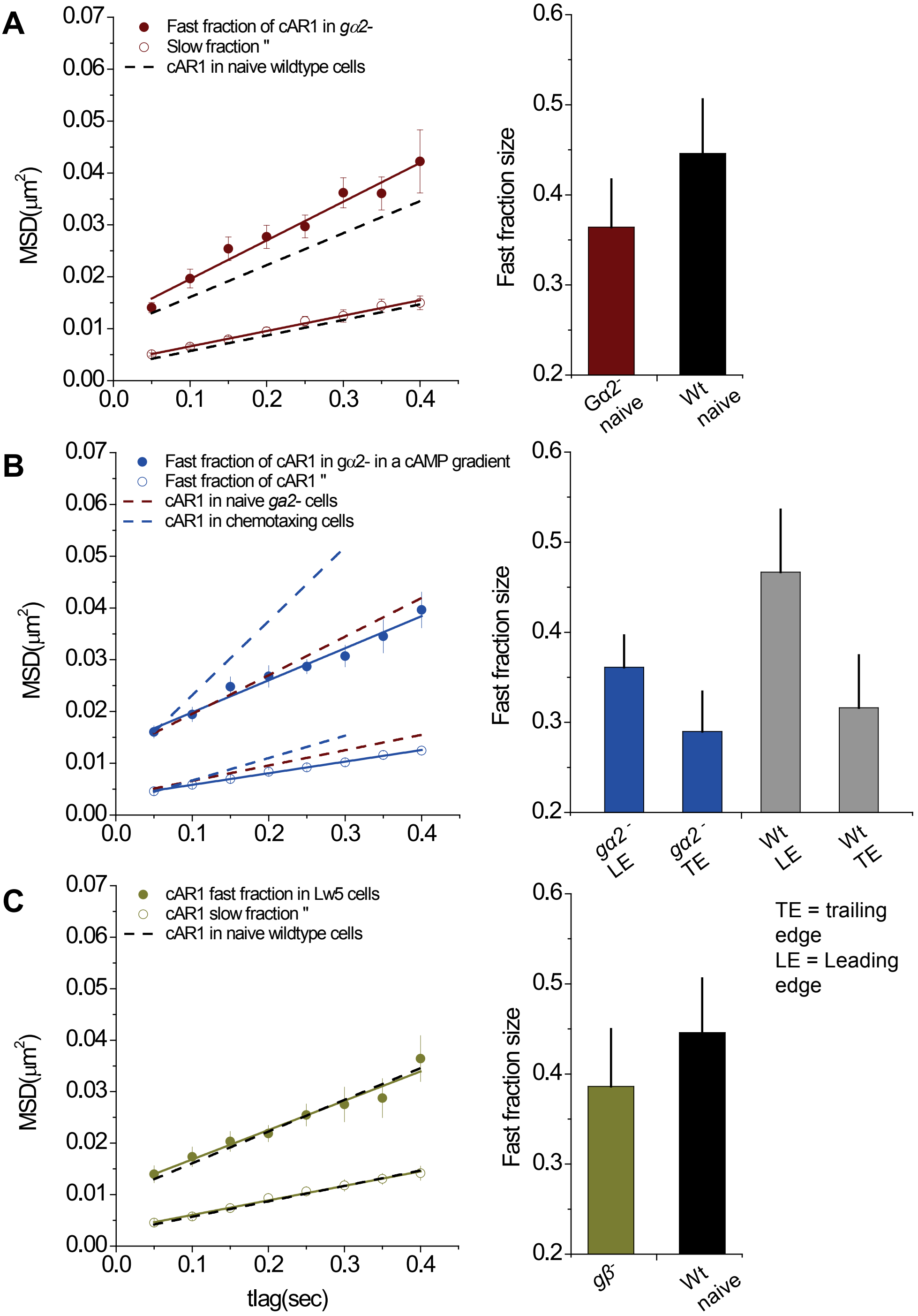
A
Fast fraction of cAR1 in gα2-
Slow fraction "
cAR1 in naive wildtype cells
MSD(μm²)
0.00
0.01
0.02
0.03
0.04
0.05
0.06
0.07
0.0
0.1
0.2
0.3
0.4
Fast fraction size
0.2
0.3
0.4
0.5
0.6
Gα2- naive
Wt naive
B
Fast fraction of cAR1 in gα2- in a cAMP gradient
Fast fraction of cAR1 "
cAR1 in naive ga2- cells
cAR1 in chemotaxing cells
gα2 - LE
gα2 - TE
Wt LE
Wt TE
C
cAR1 fast fraction in Lw5 cells
cAR1 slow fraction "
cAR1 in naive wildtype cells
tlag(sec)
TE = trailing edge
LE = Leading edge
gβ-
Wt naive

Figure 3.4: The G-protein does not affect cAR1 mobility but is needed for the mobility increase during chemotaxis. Comparison of the mobility of cAR1 in wt (black dashed line, black bar) with the mobility in the absence of Gα2 (wine dots, wine bar) does not reveal any difference. **(B)** When the $g\alpha 2^{-}$ cells are placed in gradient, cAR1 does not increase its mobility (blue dots) compared to wt cells in a gradient (black dashed line) but remains the same as in naïve $g\alpha 2^{-}$ cells (wine dashed line), the fraction size difference between front/back decreases to $\sim 8\%$ **(C)** knocking out Gβ also has no effect on the movement of cAR1 (yellow dots, yellow bar) when compared to its movement in wt cells (black dashed line, black bar).

posterior (29 ± 8%) (fig.3.5D, compare red bars, fig.3.9). Likewise the diffusion constants increased to D_1 = 0.058 ± 0.012 µm^2/s and D_2 = 0.013 ± 0.001 µm^2/s.

Hence, the increase in mobility that was found in untreated wt cells on stimulation in a cAMP gradient (fig.3.3) was governed by actin-related cell-cortex components that presumably hinder free cAR1 movement in the cell membrane however; F-actin appears not to be the only cortex/membrane component to attenuate cAR1 mobility. As expected, treatment of $g\alpha 2^-$ cells with lat A gives an identical result as in wt cells indicating that an intact G protein is important for cortex remodeling, required for chemotaxis, but not for basic cortex functioning, as suggested before [80].

3.4 Discussion

As reported earlier [17], in naïve *D. discoideum* cells two fractions of the cAMP receptor cAR1 can be distinguished that differ in their mobility characterized by the diffusion constants of D_1 = 0.015 ± 0.002 µm^2/s for the fast, and D_2 = 0.007 ± 0.001 µm^2/s for the slow fraction, respectively. Those values are in line with previously reported diffusion constants for cAR1 [90], and more generally on G protein coupled receptors [2].

When naïve wt cells were subjected to a cAMP gradient they attained a polarized morphology, and the overall mobility of cAR1 increases about twofold with a clear polarized increase when leading and trailing edge were compared. Our data showed that the mobility of cAR1 and its polarized nature is largely controlled by the cytoskeleton, specifically by F-actin but most likely also other membrane components. The mobility of cAR1 appeared to be a measure for the strength of the underlying cortex-membrane interactions. These interactions were weaker at the anterior of cells crawling in a cAMP gradient than at the posterior which is reflected by the higher cAR1 mobility at the leading edge. It has been reported earlier that the cell cortex is heavily remodeled during chemotaxis [33], and that interactions between GPCRs and F-actin play a role in signaling [86, 2]. Actin cortex - membrane interactions were found to be largely polarized in chemotaxing *D. discoideum* cells [64, 17] and evidence for direct binding of a cAMP receptor to F-actin in *D. discoideum* has been reported [31].

To test whether F-actin was influencing the mobility of cAR1 we incubated the naïve cells with lat A. Indeed, after this treatment the mobility of both receptor fractions increased twofold, reminiscent of the mobility increase in chemotaxing cells. Hence, the modulation of cAR1 mobility was clearly F-actin dependent and must rely on some direct or indirect receptor-actin interaction. The exact nature of the interaction remains elusive though. Several scenarios can be thought of that explain our data. First, fast, transient binding of cAR1 either directly or indirectly to F-actin bundles that line the membrane may explain the relatively low mobility in naïve cells. If these interactions proceed at much faster timescales than the time lag in our measurements (50 ms) the binding/unbinding kinetics will be observed as slower diffusion. Second, cAR1 might be confined to very small F-actin related domains also called corrals [56] (visualized by Morone and others [66]). Hence, the actual diffusion we observed was rather the macroscopic diffusion of cAR1, a result of the fast microscopic diffusion within small corals and a given probability of hopping from coral to coral. If the corals are small and the microscopic diffusion fast, such corals cannot be resolved by our slow (50 ms) technique [98]. Actually, we found evidence of corrals in the diffusion of the G protein subunits (chapter 2) however the average size was $\sim$600 nm, too large to hinder the diffusion of cAR1 in a way that we could observe. A third explanation could be that one fraction of cAR1 was directly bound to F-actin and its movement was thereby determined by the movement of F-actin fibers. This latter possibility appears unlikely as we have shown that the Gβ subunit of the G protein immobilizes completely via F-actin and as such was characterized by a diffusion constant of < 0.002 $\mu m^2/s$, 3 times slower than that of the slow fraction of cAR1.

From these results however, a paradox arises. Although F-actin decreased the mobility of cAR1, we measured a mobility increase in the F-actin rich leading edge of chemotaxing cells. One would expect the mobility to decrease in the presence of high F-actin abundance. This apparent paradox may be explained by differential F-actin membrane interactions though. The fact that F-actin accumulates at the leading edge does not imply that it lines the membrane or that it interacts with membrane molecules. In fact, Merkel and others showed that there is a significant weakening of the cortex-membrane interactions at the anterior during chemotaxis. It was reported that in a *talin* knock-out cell line the posterior of the cell shows the same low level

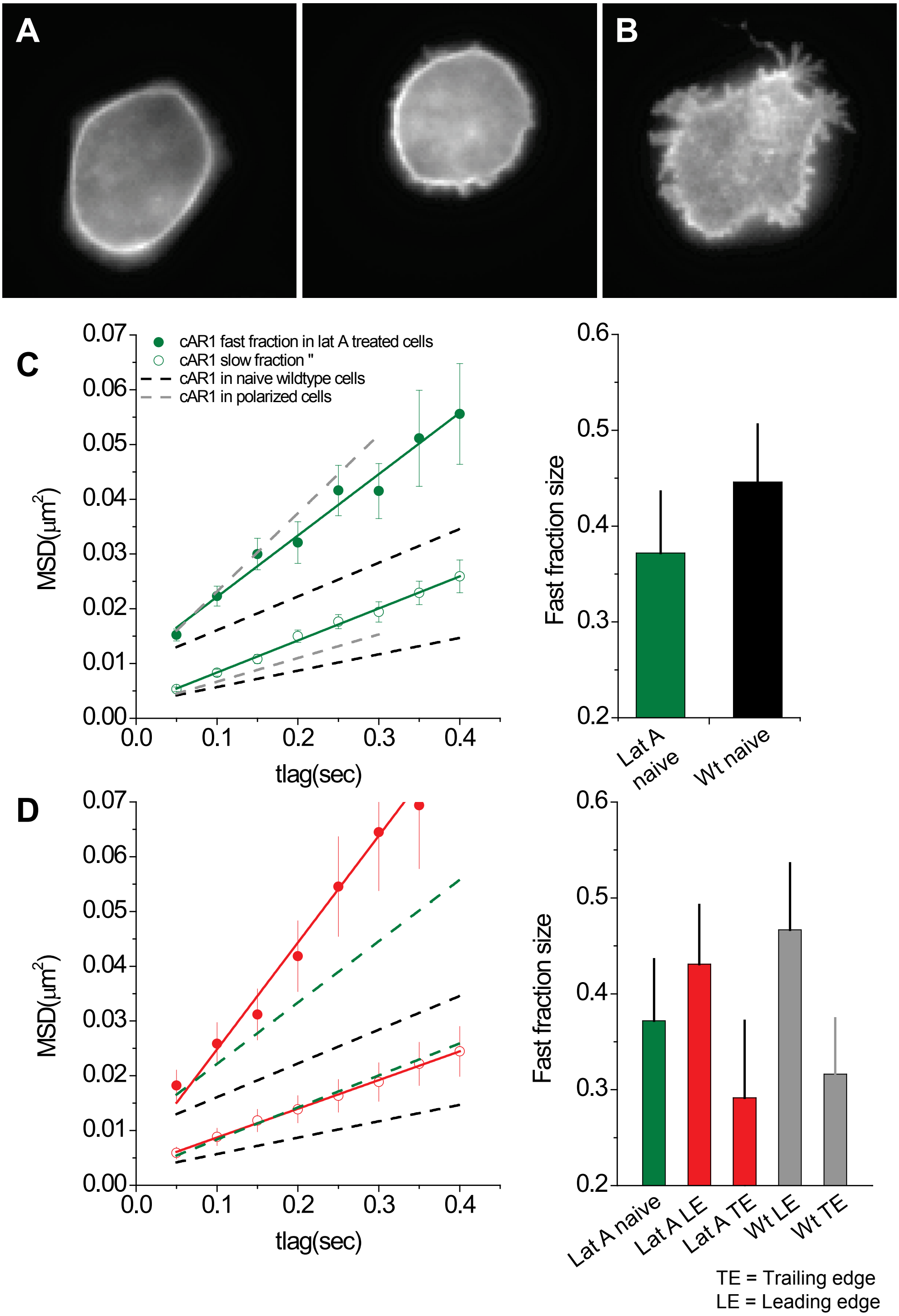
A
B
C
cAR1 fast fraction in lat A treated cells
cAR1 slow fraction "
cAR1 in naive wildtype cells
cAR1 in polarized cells
MSD(μm²)
tlag(sec)
0.00
0.01
0.02
0.03
0.04
0.05
0.06
0.07
0.0
0.1
0.2
0.3
0.4
Fast fraction size
0.2
0.3
0.4
0.5
0.6
Lat A naive
Wt naive
D
MSD(μm²)
tlag(sec)
Fast fraction size
Lat A naive
Lat A LE
Lat A TE
Wt LE
Wt TE
TE = Trailing edge
LE = Leading edge

Figure 3.5: Inhibition of F-actin polymerization leads to higher cAR1 mobility but not the loss of polarized mobility. **(A)** Lat A treated cells lose their amorphous shapes and become nearly round, **(B)** at the bottom membrane however, intact cytoskeleton structures can still be observed. **(C)** Naïve lat A treated wt cells show a higher cAR1 mobility for both fractions (green dots) then naïve cells with an intact cytoskeleton (black dashed line). **(D)** When placing lat A treated cells in a cAMP gradient the overall mobility goes up (red dots) with respect to naïve lat A treated cells (green dashed line). Assuming diffusion between leading edge and trailing edge to be equal, the mobility polarization (red bars) is of the same magnitude as that found in untreated cells in a gradient (black bars), the fast fraction size of naïve lat A treated cell is plotted for comparison (green bar).

of actin-membrane coupling as the anterior [64]. The tighter interaction between the cytoskeleton and the membrane at the posterior probably has a function in myosin mediated trailing edge-retraction [64]. The attenuation of the membrane-cortex interaction at the leading edge may thereby facilitate the production of blebs, a mechanism for amoeboids to obtain high crawling speeds [101]. In addition two types of F-actin have been observed at the leading edge of lung epithelial cells and kidney epithelial cells [73]. Likely, both types are abundant in chemotaxing *Dictyostelium* cells. The actin that is responsible for the protrusion of the membrane and is more abundant at the anterior does not lead to tight actin-membrane interactions, whereas the actin that is responsible for the structure of the membrane cortex is weakened there. In light of these results we can understand how the mobility of cAR1 can be polarized; due to the differential cortex-membrane interactions and the decoupling of the cytoskeleton from the membrane specifically at the leading edge. Such interpretation is further supported by our surprising finding that polarized cAR1 mobility was also found in F-actin-depleted cells. Probably the cortex filaments other than F-actin also influence cAR1 mobility. It was shown that removing F-actin (treatment with 7.5 µM latrunculin B) still leaves cells with an actively regulated cortex [33].

We further found that the polarization in cAR1 mobility was Gα2 dependent, as the anterior/posterior mobility shift disappeared in $g\alpha2^{-}$ cells. Moreover, the overall mobility of cAR1 did not increase upon gradient application. Both results indicate that the restructuring of the cytoskeleton required for chemotaxis does not take place in this knockout, not surprising since chemotactic signaling is abolished. An intact G protein does not seem to be a prerequisite for the formation of pseudopods and random cell movement. For polarization and directional movement though, a fully functional G protein is required [99, 80]. The fact that cAR1 mobility in lat A treated $g\alpha2^{2}$ cells reflects lat A treated wt cells supports that indeed, these cells seem to have normal basal cortex functionality (data not shown).

In conclusion we have shown that cortical F-actin restricts cAR1 movement but it is probably not the only cortex component responsible. Naïve wt as well as $g\alpha2^{-}$ cells exhibit a relatively tight membrane - cortex interaction resulting in low cAR1 mobility. We have shown before (chapter 2) that in naïve cells a large portion of the receptors ($\sim$45%) were coupled to their heterotrimeric G protein (fig.3.6A). When the cells polarize and form a leading edge, a tight cortex-membrane interaction at the anterior would be counter-productive, first because the cortex itself is a major substrate for force generation, and second a less tight membrane - cortex interaction facilitates blebbing mediated motility [101, 58]. It is known that the cortex is weakened at the anterior [64] and that a direct link between cAR1 and cortex components is likely [31]. On the other hand, cortex - membrane connections should be favored at the posterior to allow for myosin II mediated contraction of the uropod [89]. We propose a model in which the mobility of the receptor is governed by F-actin interactions (fig.3.6A). In chemotaxing cells cAR1 mobility is polarized due to the polarized configuration of the cortical F-actin cytoskeleton that interacts with the membrane (fig.3.6B). The anterior and the lateral sides of the cell are lined with an F-actin cortex. This cortex is broken down specifically at the leading edge to facilitate bleb formation and F-actin force generation.

We characterized the molecular motion of cAR1 and showed that this motion is a direct reflection of the underlying cortex - membrane structure. Potentially regulation of the F-actin cytoskeleton goes two ways. Initially the actin polymerization is stimulated by the receptor - G protein system and subsequently F-actin regulates the mobility of both molecules which facilitates their localization and could increase their local concentration. This might help cells to define their direction with respect to an external chemical gradient.

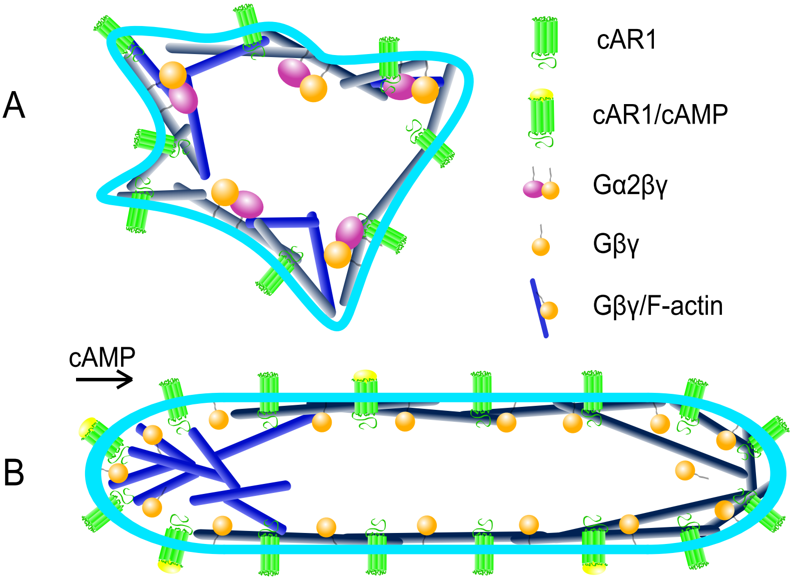

Figure 3.6: A model explaining the results. **(A)** Naïve cells are amorphous; they move randomly and have tight cytoskeleton - membrane interactions. Pseudopods are extended at random but don't persist for very long, as if the cells probe the environment. The cAR1 molecules are restricted in their diffusion by the membrane cytoskeleton. A minority ($\sim$30%) of the membrane associated G protein $\alpha 2$ and $\beta\gamma$ subunits appear to move together with a portion of the cAR1 molecules. **(B)** Upon application of a cAMP gradient, the cells polarize and attain highly elongated shapes. The increase of the overall mobility is explained by F-actin cortex rearrangements which take place in chemotaxing cells. The polarized mobility is explained by the polarized configuration of the cortex. At the leading edge the cortex is broken down or restructured, possibly mediated by talin [64]. This allows for the formation of blebs driven by hydrostatic forces and facilitates growth of the F-actin cytoskeleton [101, 58]. At the leading edge a tight cortex - membrane interaction would obstruct movement whereas at the trailing edge these interactions are needed for the retraction of the uropod. G$\beta\gamma$ as well as Gα2 knock out cells remain as in **(A)** upon exposure to a stable cAMP gradient.

Supplemental information

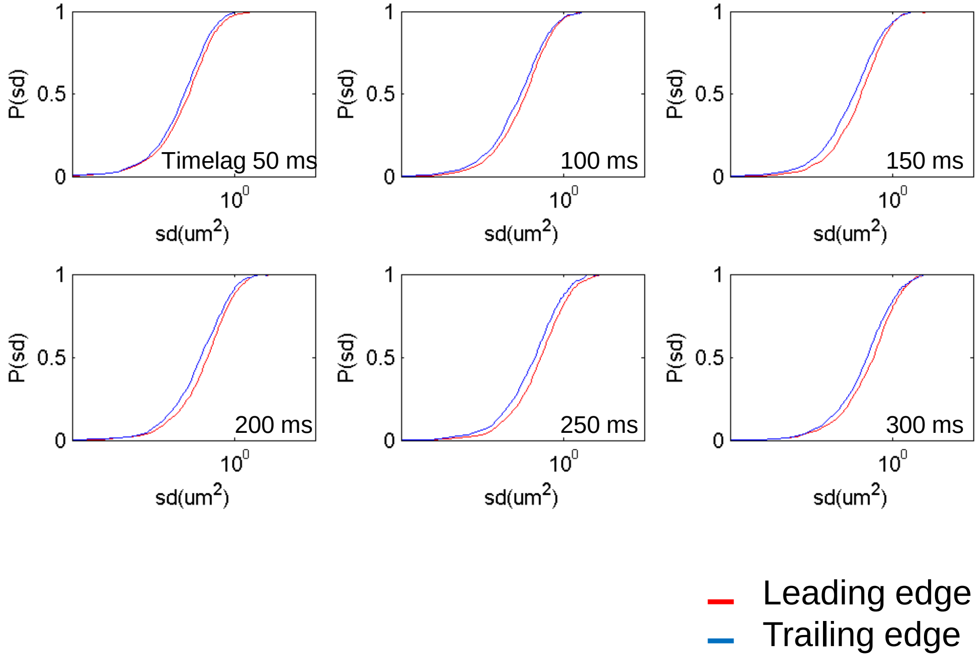

Figure 3.7: Mobility polarization without applying a model. The raw P(sd) plots (cdfs) clearly show the mobility polarization between the anterior and posterior of wt cells in a cAMP gradient. These cdfs are interpreted as showing the same two diffusion constants but differ in their fraction size distribution by fitting with the biexponential function as described in section 3.2.

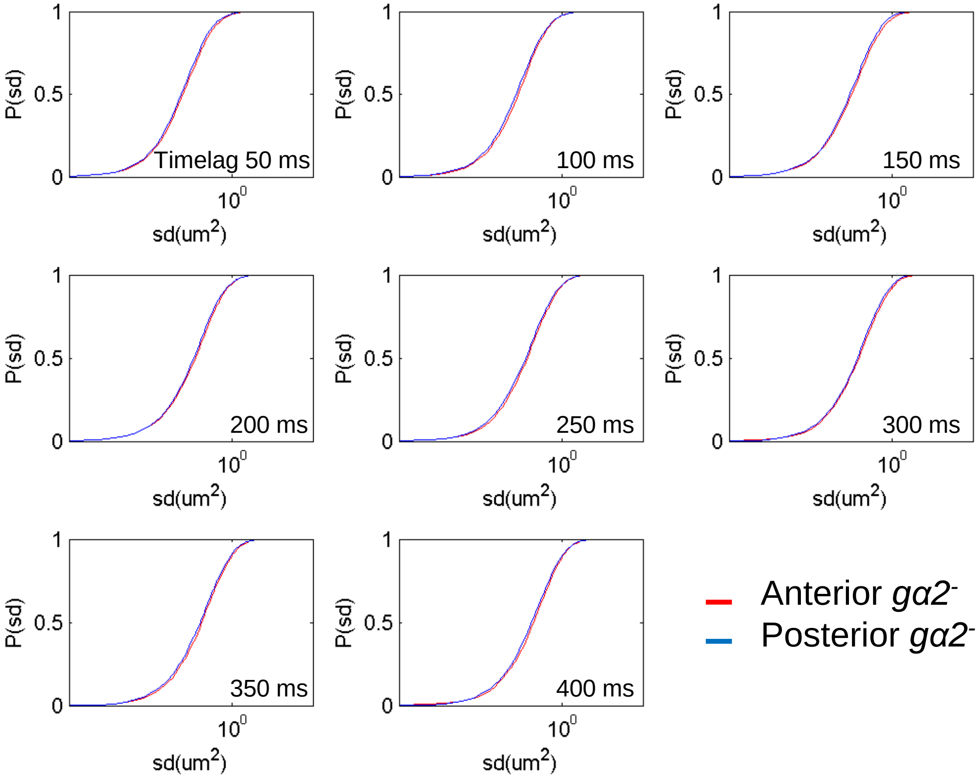

Figure 3.8: Gα2 knockout cells lose polarized cAR1 mobility. The cAR1 mobility difference between the part of the $g\alpha2^{-}$ cells closest to and that furthest away from the needle is negligable.

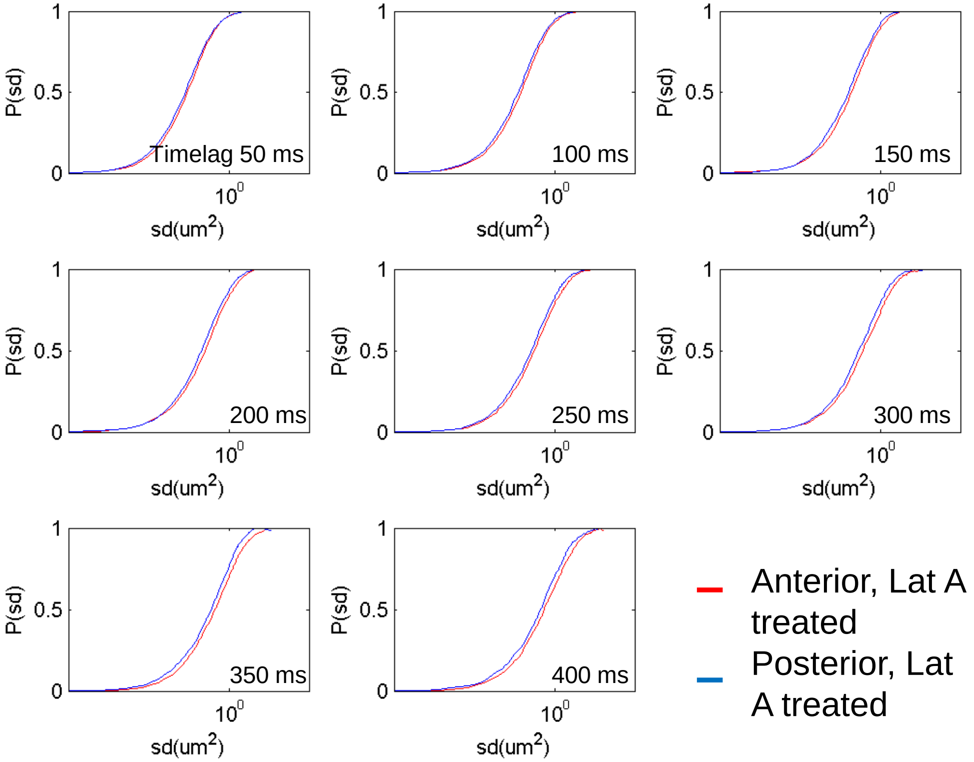

Figure 3.9: Mobility is still polarized after lat A treatment. Despite inhibition of actin polymerization using lat A, a significant mobility shift is still observed between the anterior and posterior of the cells.

Appendix

The distribution of squared displacements, sd, characterized by a mean squared displacement, MSD, and positional accuracy, σ, assuming a random walk in two dimensions is given by [82, 10]:

$$p(sd) = \frac{1}{\sqrt{\pi(MSD + 4\sigma^2)}} \frac{1}{\sqrt{sd}} \exp\left(- \frac{sd^2}{MSD + 4\sigma^2} \right) \tag{3.3}$$

Integration of equation 3.3 from the origin to r^2 leads to the expression of the cumulative distribution function $cdf(r^2)$ found in equation 2.1. In the derivation of eqations 3.1, 3.2& 3.3 it was assumed that the accuracy by which the position of the molecules, σ is determined in each dimension is a constant. However, given that σ scales with the signal-to-noise ratio ($\sigma = \frac{\lambda}{2\sqrt{SNR}}$, λ wavelength of light), and since every observation of an individual molecule is achieved at different signal-to-noise ratio, a distribution in σ must be taken into account. The experimental data show that the distribution in σ is sufficiently represented by a Gaussian of mean σ_0 = 40 nm and width δ_σ = 20 nm (fig.3.10A):

$$p(\sigma) = \frac{1}{\sqrt{2\pi}\delta_\sigma} \exp\left(- \frac{(\sigma - \sigma_0)^2}{2\delta_\sigma^2} \right) \tag{3.4}$$

Hence for a proper treatment of the problem the distribution in positional accuracy must be taken into account as a convolution of equation 3.3 and 3.4. For the cumulative distribution function convolution results in:

$$cdf(r^2) = \frac{1}{\sqrt{2\pi}\delta_\sigma} \int_0^\infty d\sigma \exp\left(- \frac{(\sigma - \sigma_0)^2}{2\delta_\sigma^2} \right) \left(1 - \exp\left(- \frac{r^2}{MSD + 4\sigma^2} \right) \right) \tag{3.5}$$

Equation 3.5 approaches for a narrow distribution in positional accuracy ($\delta_\sigma \ll \sigma$) or for large MSDs (MSD $\gg 4\sigma^2$), $cdf(r^2) = 1 - \exp \frac{-r^2}{MSD+4\sigma^2}$, the solution found in equation 2.1. In both cases the positional offset is given by $s_0 = 4\sigma_0^2$. In all other cases, as those discussed in the current paper, treatment of the data using equation 3.1 results in values of s_0 that depend on MSD, and hence leads to two different offsets $s_{0,1}$ and $s_{0,2}$ for the two mobile fractions, respectively.

The analysis has been verified by simulation. PICS analysis has been performed on simulated data of single-molecule diffusion assuming a fast and a slow fraction and in which the width in positional accuracy, σ_σ, was varied. The results are summarized in figure 3.10B. The dependence of s_0 on δ_σ is clearly revealed.

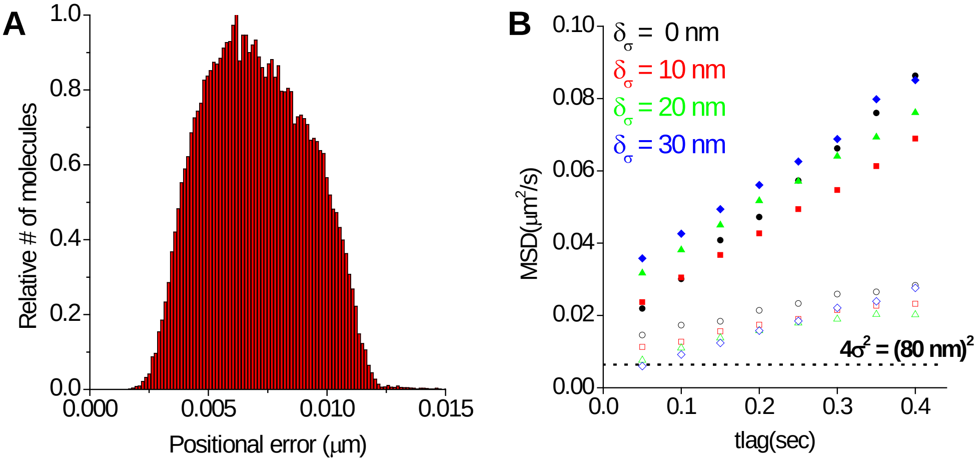

Figure 3.10: The distribution of positional accuracies leads to an offset difference in the two diffusing fractions .

Chapter 4

RasC and RasG regulate membrane / cytoskeleton interactions which organize the polarized behavior of cAR1 and Gβγ in *D. discoideum*

D. discoideum expresses several Ras proteins of which 6 have been characterized. The proteins play roles in cytokinesis, growth, endocytosis en cell polarization. RasC and RasG are the best characterized Ras family-members and are the most important for motility and chemotaxis. The knockout phenotypes of both proteins include reduced random motility, loss of polarization, loss of cAMP relay, aberrant cytokinesis and chemotaxis. Nearly all effects except the defective cAMP-relay are a consequence of abnormal cytoskeleton structure and distribution. We showed before that the cytoskeleton plays a key role in several processes related to the dynamics of the GPCR / G-protein signaling cascade. The mobility of cAR1 is hindered by F-actin and the Gβγ subunit of the G protein immobilizes in a cAMP and leading edge specific manner. Here we report that in *rasC*$^{-}$/*rasG*$^{-}$ double knockout cells we don't observe effects of actin on cAR1 diffusion. Moreover, there is no cAMP dependent immobilization of the Gβ subunit of the G-protein and no domains are formed. We conclude that RasC and RasG regulate F-actin / membrane interactions and membrane organization that are needed for proper cAR1 and Gβγ signaling in directional sensing.

4.1 Introduction

Dictyostelium discoideum is a widely used model organism for studying directed cell motility in chemical concentration gradients, a process called chemotaxis. Chemotaxis is part of more complex processes such as cytokinesis, wound healing and metastasis. *D. discoideum* shares considerable gene sequence homology with higher eukaryotes and many pathways are conserved both in protein homology and function between this amoeba and humans. Because of this fact and the modest culture requirements, its completely sequenced genome, and its accessibility to sensitive (single molecule) microscopy, *D. discoideum* is the organism of choice for many studies.

Chemotaxis is part of the *D. discoideum* lifecycle: upon starvation the cells change the expression of a number of genes resulting in the secretion of, and increased sensitivity to, cyclic adenosine mono-phosphate (cAMP). Within 24 hours the cells go through several stages of development including aggregation and the formation of a pseodoplasmodium (capable of phototaxis) which eventually culminates in a fruiting body used to disperse spores. In order to detect cAMP during the first stage of development, the cells use a G protein coupled receptor (GPCR) called cAMP receptor 1 (cAR1). The GPCR cAR1, upon binding of cAMP, promotes the exchange of guanine di-phosphate (GDP) for guanine tri-phosphate (GTP) in the Gα2 subunit of the Gα2βγ heterotrimer. Currently, evidence suggests that the activated Gα2 subunit (which has been shown to cycle between the cytosol and the membrane) shifts the balance in favor of the membrane and/or cAR1 bound state [22]. The Gβγ subunit detaches from the cAR1-Gα2 complex and immobilizes upon activation in an F-actin dependent manner, possibly as part of a feedback mechanism [22]. Among the most important downstream effectors of the G proteins are the Ras guanine exchange factors (RasGEFs). These proteins function as on switches for the

Ras family of small GTPases. Currently some of the putative RasGEFs have been investigated, for example *Aimless* which, when disrupted shows a phenotype combining the phenotypes of several Ras knockout lines [53]. Ras proteins are small, monomeric GTPases that can be toggled on or off. Just like the Gα subunits of heterotrimeric G proteins they cycle between an active GTP and an inactive GDP bound state [7]. While they are activated by RasGEFs, they are deactivated by Ras GTPase activating proteins (RasGAPs) [14]. Ras proteins are among the earliest molecules to show polarized activation [47, 79, 103]. In a cAMP gradient Ras stimulation leads to the polarized activation of PI3K [40, 30], phospholipase A2 (PLA2) [11], TorC2 and subsequently 2 PKB homologues (PKBA and PKBR1) [48]. Ultimately, the combined actions of these pathways result in orchestrated actin regulation that is required for efficient chemotaxis. *D. discoideum* has several Ras proteins of which RasC and RasG are the most important for chemotaxis [5].

Vegetative *rasC-* cells show reduced random motility, less polarization, altered F-actin distribution and are larger than wildtype (wt) cells [23]. These cells do not aggregate if left unattended. When pulsed with cAMP, or when mixed with wt cells they readily develop and move directionally towards a cAMP secreting micropipette suggesting a cAMP relay deficiency [61]. Major defects in the localization of myosin II, of F-actin organization, and a more general loss of cell polarity have been reported [95]. Although RasC and RasG have been shown to have overlapping functions, RasC is more important for adenylyl cyclase (ACA) activation whereas RasG is more important for directional movement [5].

The F-actin cytoskeleton in *D. discoideum* has a multitude of functions. It is used to maintain cell shape and to achieve polarity essential for development. Both processes require F-actin, but are different regarding their function and regulation. The F-actin in the cell cortex, important for the structural integrity of the cells, necessitates dynamic cross linking and active remodeling. At the leading edge of a highly mobile cell actin polymerizes at high rate and the growing polymers branch to prevent buckling [72]. Regulation does not go one way however. There are countless of examples in which F-actin or other cytoskeleton components regulate signaling [8, 94], and often there is a feedback between actin polymerization and the signaling controlling it [80, 42]. These feedback mechanisms may involve direct binding of signaling proteins to actin [16] or may involve the physical mechanism of inhibition of protein mobility [94]. Thereby regulation of the interaction between actin and the cell membrane is of vital importance. The establishment of a differential cortex - membrane interaction in chemotacting cells may finally lead to amoeboid motion as pointed out by others [101, 58].

Previously we have shown that the mobility of cAR1 varies considerably upon latrunculin A (lat A) treatment and upon polarization of the cell, both indicative that cell cortex arrangement could be important for cAR1 function [17]. Moreover, the cortex - membrane interaction is polarized in chemtacting cells, as experimentally found in the reduced force that is required to aspirate the leading edge membrane compared to the trailing edge [64], and as an increase in cAR1 mobility specifically at the leading edge (chapter 3, [17]). In this paper we focus on the mobility of cAR1 and G$\beta\gamma$, both upstream regulators of Ras-signaling. Given that we have shown before that these two proteins interact with F-actin and the knowledge that RasC and RasG are major regulators of the F-actin cytoskeleton, we investigate here an internal feedback loop in signaling that is mediated by the polarized mobility of its components. Using a *rasC*$^-$/*rasG*$^-$ *D. discoideum* cell line, we probe the effects of disturbing this feedback loop on cAR1 and G$\beta\gamma$ mobility and activation.

4.2 Materials and methods

4.2.1 Cell culture

The JH10/*rasC*$^-$/*rasG*$^-$ cell line was kindly provided by Parvin Bolourani and created by transforming a *rasC-thy1* disruption vector into JH10 cells. Transformants were selected in the absence of thymidine [5]. Subsequently, the *rasC* disruption vector, pJLW26 [62] which carries a blasticidin resistance marker was transformed into the JH10/*rasG*$^-$ cells which were subsequently screened and selected [5]. We transformed these JH10/*rasC*$^-$/*rasG*$^-$ cells with a plasmid containing cAR1-eYFP or Gβ-eYFP and a G418 resistance marker using electroporation. The JH10/*rasC*$^-$/*rasG*$^-$ × cAR1-eYFP or Gβ-eYFP cells were cultured in 6 well plates containing HL-5c medium (Formedium) complemented with 10 µg/ml penicillin/streptomycin (1:1), 10 µg/ml blasticidin and 20 µg/ml G418 (Geneticin, Invitrogen).

4.2.2 Preparing naïve cells for measurements

A confluent 10 cm petridish was incubated overnight in low fluorescent medium (loflo, Formedium). In the morning, the cells were collected in 5 ml development buffer (DB, [24]) and washed by centrifugation for 4 min at a RCF of 400× g and then re-suspending in 5 ml fresh DB. The cells were subsequently incubated on the shaker (100 rpm) for 1 hr and then pulsed every 6 min with 150 nM final [cAMP] per pulse for 4 hr The cells were washed again and suspended in 5 ml fresh DB, shaken for another 40 min and left to settle for 20 min on the bottom of a 2-well chambered coverglass (Labtek). Cells that have not received any additional treatment are defined in the following as naïve.

4.2.3 Single molecule measurements

The experimental setup for single-molecule imaging has been described in detail previously [81]. The samples were mounted on an inverted microscope (Axiovert100, Zeiss) equipped with a 100× objective (NA=1.4, Zeiss). The region-of-interest on an ultrasensitive CCD camera coupled to the microscope was set to 50 × 50 pixels. The apparent pixelsize was 220 nm. Measurements were performed by illumination of the samples for 5 ms at 514 nm (Argon-ion laser, Spectra Physics) at an intensity of 2 kW/cm^2. The cells were photobleached for a period of 2-5 sec and sequences of 200-500 images with a timelag of 50 ms were taken. Use of an appropriate filter combination (Chroma) permitted the detection of the fluorescence signal on a liquid nitrogen-cooled CCD-camera (Princeton Instruments). The setup allowed us to image individual fluorophores at a signal-to-background-noise ratio of $\sim$30 leading to a positional accuracy of σ_0 = 40 nm. The measurements always focused on the apical cell membrane and never lasted longer than 15 - 60 sec per cell and 2 hr in total.

4.2.4 Global cAMP stimulation assay

After settling on the coverglass, the 1 ml DB that covered the cells was supplemented with cAMP to final concentration of 10 μM. Measurements commenced immediately and ended after 20 min involving $\sim$10-15 cells per experiment batch.

4.2.5 Applied gradient assay

By suspending a micropipette (Eppendorf femtotip) containing 10 µM cAMP just above the coverglass and applying a pressure of 40 KPa (pressure set by means of an Eppendorf Femtojet), a stable concentration gradient was created. The micropipette was placed at a distance of $\sim$70 µm from the cells creating a putative gradient of 4 nM/µm over the cells. This gradient was experimentally verified using a fluorescent dye in the pipette. The region of interest was 11 µm^2 which during measurement of the anterior and posterior of the cell body means that we observe $\sim$20% of the cell length.

4.2.6 Latrunculin A treatment

The cells were incubated in DB supplemented with 0.5 µM latrunculin A (Cayman Europe) for 10 min before the measurements began. Measurements were taken within 10 min.

4.2.7 Data analysis

Individual molecule positions were determined within each image in an image stack by fitting the signal intensity profiles to a 2D Gaussian function using Matlab (Mathworks Inc). The center of mass of the Gaussian fit corresponds within $\sim$40 nm to the single molecule positions. The latter were subsequently used to perform particle image correlation spectroscopy [83]. PICS calculates the 2-point correlation between individual molecule positions at two different times from which the cumulative distribution function of squared displacements ($cdf(r^2, tlag)$) for each timelag (t_{lag}) from 50-400 ms was constructed. The cdf's were fitted to a two fraction model:

$$cdf(r^2, t_{lag}) = 1 - \left(\alpha \cdot \exp\left(-\frac{r^2}{MSD_1}\right) + (1-\alpha)\exp\left(-\frac{r^2}{MSD_2}\right)\right) \qquad (4.1)$$

The fast fraction size, α, was globally fitted over all timelags in each data set. This yielded 2 mean squared displacements (MSDs) per timelag and one fast fraction size for each data set. Subsequently the 2 MSDs are plotted versus t_{lag} resulting in a representation of the mobility largely following that expected for diffusion. To determine the diffusion constant we fit each of the MSD *vs* time data to a free diffusion model:

$$MSD(t_{lag}) = 4Dt_{lag} + s_0 \tag{4.2}$$

This gives us the two diffusion constants (D_1 & D_2) and offsets (s_0) for each dataset. In the case that two dataset are compared (for example anterior *vs* posterior), MSD_1 and MSD_2 are kept equal per timelag for the two datasets and the fast fraction size, α, is kept constant per dataset resulting in 2 diffusion constants and two fraction sizes per fit. In this analysis, α is the only parameter left that characterizes the difference between two experimental conditions or two locations along the cell membrane.

The offset (s_0) is a representation of the accuracy by which the position of the molecules is determined. s_0 scales with the signal-to-noise-ratio of the single-molecule signal ($s_0 = 4\sigma^2 = 0.0064$ μm^2 with $\sigma = 40$ nm). It should be noted that not every observation yields the same signal-to-noise ratio, leading to a distribution of positional accuracies in each dataset. If s_0 approaches the mean-squared displacement of both fractions (as is the case for cAR1) and the appropriate fit of the data to (eq.4.1) fails. We have shown by simulation that this can be corrected for by allowing s_0 to be different for the two fractions in equation 4.2 (see Appendix chapter 3).

4.3 Results

Using wide-field single-molecule fluorescence microscopy (fig.4.1, bottom left), individual cAR1-eYFP and Gβγ-eYFP molecules diffusing in the membrane of living *D. discoideum* cells are visualized (fig.4.1, bottom right). The data consists of image stacks (typical 500 images) from which the positions of molecules at specific time points are determined by Gaussian fitting to an accuracy of 40 nm. Typically 2-6 $\cdot 10^4$ positions obtained from the observation of 40-100 cells are used for analysis. Particle image correlation-spectroscopy (PICS [83]) is applied to calculate the correlation between the positions of the molecules in two images at each timelag which results in the cumulative probability of the squared displacements (cdf) for the timelag between the images (typically 50-400 ms). All cdfs related to the current work are found in the supplemetal materials. The cdfs are subsequently fit to two distinct mobility fractions characterized by the mean squared displacement of a fast (MSD_1) and a slow (MSD_2) component, and a fraction size of the fast component, α. The slope of the MSDs *vs* time lag represents the diffusion constant that characterizes protein mobility in the membrane (fig.4.1, bottom right). The result of such detailed mobility analysis of cAR1 in naïve wt cells is shown in figure 4.1 (bottom right). As predicted for free diffusion the MSDs of both fractions scale linearly with timelag characterized by diffusion constants of $D_1 = 0.015 \pm 0.002$ µm^2/s and $D_2 = 0.007 \pm 0.001$ µm^2/s for the fast and slow fraction, respectively. Thereby $\alpha = 0.45 \pm 0.06$ of the population is contained in the fast fraction. In the subsequent figures this result on naïve cells is indicated as dotted black line.

4.3.1 The mobility of cAR1 in *rasC*$^-$/*rasG*$^-$ cells is increased and reflects the mobility found for F-actin depleted cells

We have shown before that the mobility of cAR1 depends on the presence of an intact cell cortex. Disruption of the cell cytoskeleton by lat A treatment resulted in an increased cAR1 mobility (chapter 3). Presumably membrane localized molecules are hindered in their mobility due to the presence of F-actin filaments directly (fence model), or by trans-membrane proteins that are attached to the filaments (picket fence model [29, 86]). We studied cAR1 mobility in a *rasC*$^-$/*rasG*$^-$ double knockout background (JH10/*rasC*$^-$/*rasG*$^-$). These cells were reported to show disregulation of their cytoskeleton meshwork [5].

In a *rasC*$^-$/*rasG*$^-$ cells we found the mobility of cAR1 to be increased with respect to naïve wt cells (fig.4.1, bottom right and fig.4.2, black dotted line). The overall cAR1 mobility matched that of cAR1 in cells that are treated with 0.5 µM latrunculin A (fig.4.2, green dotted line), indicative of reduced cortex strength or less tight cortex - membrane interactions. In comparison to wt naïve cells the diffusion constant of the fast fraction increased twofold to $D_1 = 0.029 \pm 0.002$ µm^2/s and that of the slow fraction to $D_2 = 0.012 \pm 0.002$ µm^2/s. Simultaneously the size of the fast fraction dropped to $\alpha = 0.30 \pm 0.10$. All three parameters representing cAR1 mobility are comparable to those found for lat A treated naïve wt cells ($D_1 = 0.028$

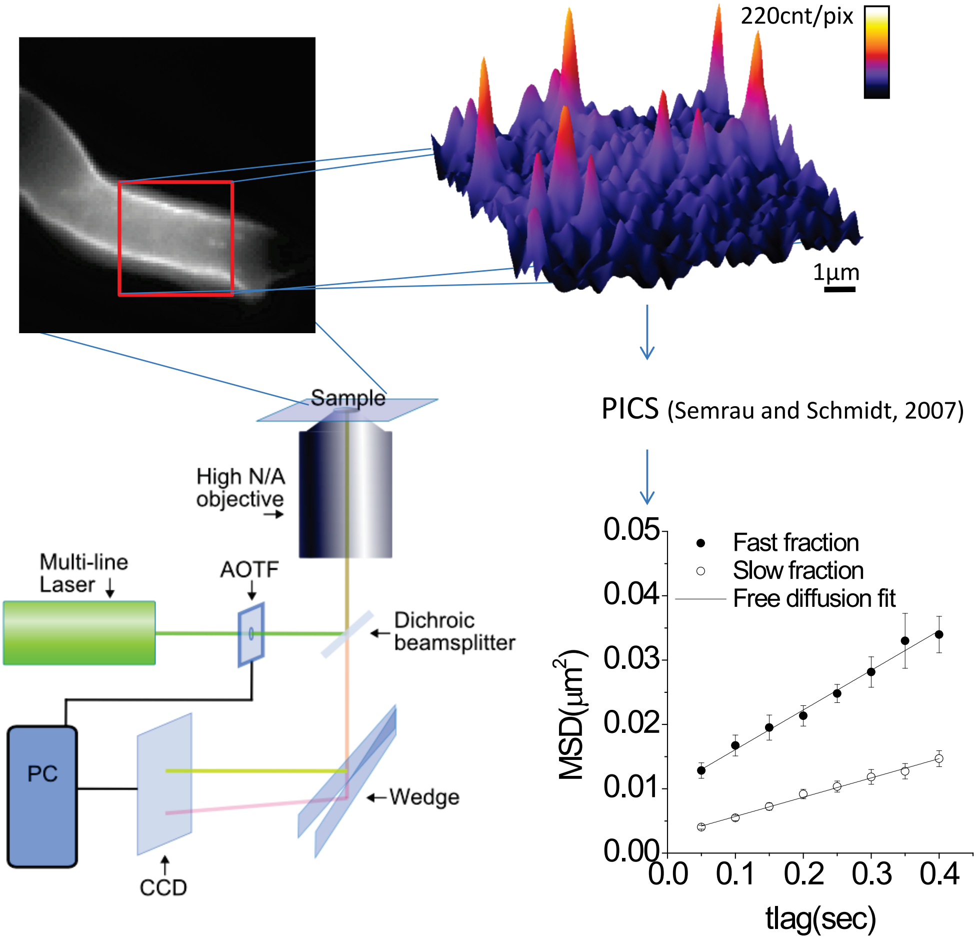
220cnt/pix
1µm
PICS (Semrau and Schmidt, 2007)
Sample
High N/A objective
Multi-line Laser
AOTF
Dichroic beamsplitter
PC
Wedge
CCD
● Fast fraction
○ Slow fraction
Free diffusion fit
MSD(µm²)
0.05
0.04
0.03
0.02
0.01
0.00
0.0
0.1
0.2
0.3
0.4
tlag(sec)

Figure 4.1: Description of the technique and data acquisition. Images of individual cAR1-eYFP and Gβ-eYFP molecules at the apical membrane of *D.discoideum* cells are taken at a rate of 20 Hz on an inverted microscope (bottom left). Individual molecule signals are identified and their position determined with an accuracy of ∼40 nm (top right). The position information is used in particle image correlation-spectroscopy to construct the cumulative density functions (cdfs) of squared displacements (see supplemental figures) over timelags ranging from 50 to 400 ms. Fitting of a bi-exponential and a global fraction size (eq.4.1, section 4.2) results in two diffusion constants and a fraction size of the fast component. For the mobility of cAR1 in naive wt cells $D_1 = 0.015 \pm 0.002$ µm^2/s, $D_2 = 0.007 \pm 0.001$ µm^2/s, and $\alpha = 0.45 \pm 0.06$ (bottom right).

± 0.006 μm^2/s, D_2 = 0.015 ± 0.002 μm^2/s, and α = 0.37 ± 0.06 (chapter 3)).

Whether the increased mobility of cAR1 in the *rasC*$^-$/*rasG*$^-$ cells is due to aberrant regulation of the F-actin cytoskeleton or to direct interaction between cAR1 and Ras was investigated by additional treatment of the cells with latrunculin A (lat A). In the first case lat A treatment should not affect the cAR1 mobility whereas in the latter lat A treatment should lead to a further increase of cAR1 mobility.

The mobility of cAR1 was unchanged after treatment of *rasC*$^-$/*rasG*$^-$ cells with lat A (see the cdfs in supplemental figure 4.7) for *rasC*$^-$/*rasG*$^-$, in contrast to wt cells receiving the same treatment (fig.4.8). For this reason we analyze the data assuming the mobility for both fractions is equal and leave the fraction size (α) as the only free parameter across the datasets (fig.4.3). This analysis yields D_1 = 0.029 ± 0.002 μm^2/s and D_2 = 0.012 ± 0.002 μm^2/s for the fast and slow fractions, respectively. The size of the fast fraction after lat A treatment is α = 0.35 ± 0.11, equivalent to that of untreated *rasC*$^-$/*rasG*$^-$ cells (where α = 0.30 ± 0.10). As an internal check we also analyzed wt cells before and after lat A treatment in the same way, which leads to a difference in fraction size of $\Delta\alpha$ = 0.37 (data not shown).

4.3.2 The polarized mobility of cAR1 is lost in the *rasC*$^-$/*rasG*$^-$ knockout

It was reported before [5] that naïve *rasC*$^-$/*rasG*$^-$ double knockout cells do not move directionally. After transformation with cAR1-eYFP however the *rasC*$^-$/*rasG*$^-$ cells attain elongated shapes and are able to move directionally towards a cAMP secreting micropipette (fig.4.4 and fig.4.10A) albeit without forming stream as the wt cells do (fig.4.10B). The fact that introduction of cAR1 restores directional sensing is expected since *carA* (the cAR1 gene) is among the genes whose expression is virtually absent in the *rasC*$^-$/*rasG*$^-$ cells [5] and a functional cAR1 molecule is required for the activation of genes leading to aggregation [50].

In wt cells that are polarized in a cAMP gradient we reported before that the mobility of cAR1 is polarized and characterized by an increased size of the fast fraction by $\Delta\alpha$ 0.23 at the leading edge of the cell [17]. We speculated that this increased mobile fraction would lead to an initial amplification of the external signal towards downstream effectors. Further we found that polarization in cAR1 mobility was in-

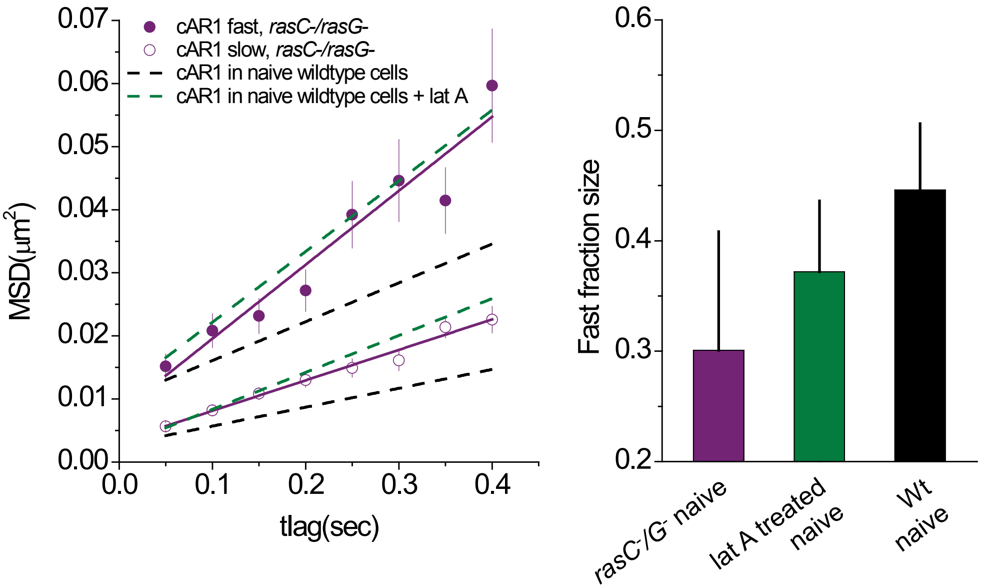

Figure 4.2: cAR1 mobility is elevated in *rasC⁻/rasG⁻* cells. The *rasC⁻/rasG⁻* cells have very amorphous shapes, much more so as wt cells (not shown). The membrane shows thick knob like structures as well as very long (>10 µM) and thin filopodia. The filopodia are found all over the glass slide and often appear to extend from the back of moving cells. When we compare the MSD *vs* time lag behavior of cAR1 in the *rasC⁻/rasG⁻* cells (purple circles/line) to that of cAR1 in naïve wt cells (black dotted line) a twofold increased mobility is observed in both fractions. The fast fraction increases its diffusion constant from D_1 = 0.015 ± 0.002 $\mu m^2/s$ toD_1 = 0.028 ± 0.007 $\mu m^2/s$ whereas the slow fraction goes from D_2 = 0.007 ± 0.001 $\mu m^2/s$ to D_2 = 0.012 ± 0.001 $\mu m^2/s$ in the absence of RasC and RasG. The cAR1 molecules in this mutant show the same behavior as cAR1 in lat A treated wt cells (D_1 = 0.028 ± 0.006 $\mu m^2/s$ and D_2 = 0.015 ± 0.002 $\mu m^2/s$). The fast fraction sizes do not differ significantly (α in equation 4.1).

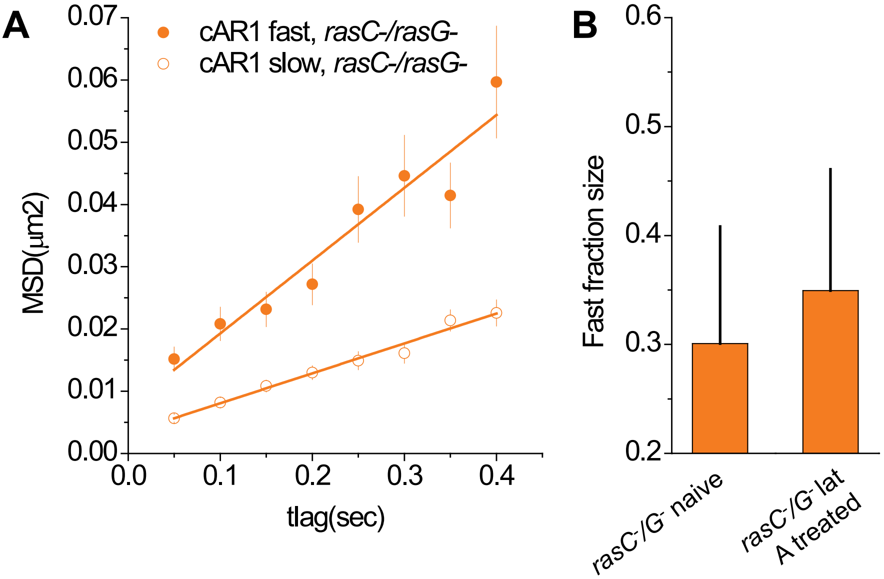

Figure 4.3: F-actin does not obstruct cAR1 diffusion in *rasC*$^-$/*rasG*$^-$ cells. The mobility of cAR1 in lat A treated *rasC*$^-$/*rasG*$^-$ cells was compared to untreated cells by means of keeping the MSDs equal for each time lag and comparing the globally fitted fast fraction sizes. In contrast to wt cells which undergo lat A treatment, in *rasC*$^-$/*rasG*$^-$ cells, the mobility does not increase significantly.

dependent of F-actin breakdown (chapter 3) together suggesting that F-actin plays a role in cAR1 mobility, but does not influence the development of cellular polarity.

Given the results on cAR1 mobility in *rasC$^-$/rasG$^-$* cells shown above, which suggest that the F-actin cortex in those cells is heavily compromised, we would predict that a polarized mobility behavior would evolve in *rasC$^-$/rasG$^-$* cells since we showed that this polarization was F-actin independent. Surprisingly, we did not observe any difference between the anterior and the posterior regarding cAR1 mobility in *rasC$^-$/rasG$^-$* (fig.4.4 and fig.4.9). The mobility as characterized by $D_1 = 0.029 \pm 0.002$ μm^2/s, $D_2 = 0.010 \pm 0.001$ μm^2/s, and $\alpha_{\text{anterior}} = 0.34 \pm 0.25$ *vs* $\alpha_{\text{posterior}} = 0.33 \pm 0.25$ is not different from the mobility measured in naïve *rasC$^-$/rasG$^-$* or lat A treated wt cells. Apparently, the cortex rearrangements resulting in higher anterior cAR1 mobility that take place in polarized wt cells do not take place in *rasC$^-$/rasG$^-$* cells, that includes the F-actin independent interactions reported before (chapter 3).

4.3.3 G$\beta\gamma$ in the RasC/RasG knockout does not immobilize upon cAMP stimulation

In parallel to the polarized cAR1 mobility we have reported before on a cAMP, anterior specific and F-actin dependent immobilization of the G$\beta\gamma$ subunit of the G protein upon activation of cAR1. We hypothesized that this immobilization may be important for downstream signaling by G$\beta\gamma$ and might help the cell in forming a persistent leading edge using a G$\beta\gamma$ - F actin feedback loop. We were curious to see whether the abolishing of RasG and RasC signaling would also abolish this interaction loop.

Before cAMP stimulation the mobility of G$\beta\gamma$ in *rasC$^-$/rasG$^-$* (fig.4.5, yellow dots) was indistinguishable from that in wt cells (black dotted line) characterized by $D_1 = 0.11 \pm 0.01$ μm^2/s, $D_2 = 0.013 \pm 0.005$ μm^2/s, and $\alpha = 0.67 \pm 0.06$. It is worth noting that the slow fraction of G$\beta\gamma$ still shows the same diffusivity as a fraction of the cAR1 molecules (fig.4.5B and fig.4.1, bottom right) suggesting that part of the receptors are precoupled to the G protein prior to stimulation. Upon activation, in contrast to wt cells, no change in mobility of G$\beta\gamma$ was observed. In the presence of cAMP the diffusion is characterized by $D_1 = 0.12 \pm 0.01$ μm^2/s, $D_2 = 0.015 \pm 0.006$ μm^2/s, and $\alpha = 0.73 \pm 0.08$.

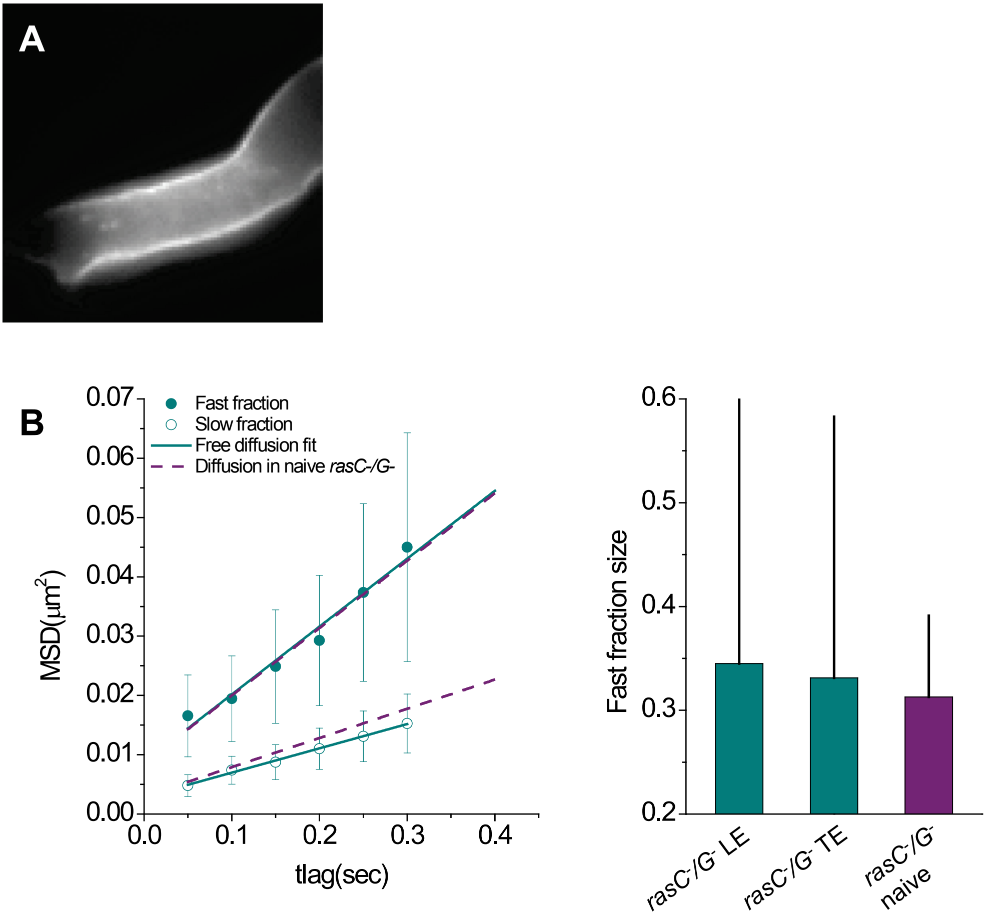

Figure 4.4: The increased mobility of cAR1 and the anterior mobility shift during chemotaxis are lost in the *rasC*$^-$/*rasG*$^-$ cells. **(A)** The *rasC*$^-$/*rasG*$^-$ × cAR1-eYFP cells were subjected to a chemotactic needle assay. As suggested earlier, introduction of a functional cAR1 rescues the chemotaxis defects of the *rasC*$^-$/*rasG*$^-$ cells [5]. The cells polarized (poorly) and crawled directionally to the needle (fig.4.10A). The mobility at the anterior was compared to the posterior, again by leaving the fast fraction size as the only parameter that defines the overall mobility difference between the two datasets. There is no difference in cAR1 mobility between the leading and trailing edge. Moreover, the diffusion of the fitted slow and fast fractions were found to be $D_1 = 0.029 \pm 0.002$ µm^2/s and $D_2 = 0.010 \pm 0.002$ µm^2/s which does not differ from the mobility in naïve *rasC*$^-$/*rasG*$^-$ and the lat A treated wt cells.

Not surprisingly the F-actin dependent microdomains which obstructed the diffusion of the fast fraction disappeared (fig.4.5C). Also the complete immobilization of the slow fraction of G$\beta\gamma$ did not appear (fig.4.5D) which is readily explained by the disrupted F-actin cortex in *rasC$^-$/rasG$^-$*. More importantly however was the disappearance of the characteristic increase in slow fraction size observed in wt cells (fig.4.5E) that characterized cellular polarity independent of F-actin (chapter 2) which suggests that this event is not a direct result of Gβ activation as suggested earlier but of something downstream of RasC and RasG and upstream of F-actin.

4.4 Discussion

Previously we have shown that the mobility characteristics of both the G protein coupled receptor cAR1 and its associated G protein heterotrimer, Gα2$\beta\gamma$, are influenced by F-actin. We hypothesized that this interaction plays a role in an F-actin/cAR1/G protein feedback mechanism that might rely on the temporal enclosement or slowdown of the proteins into signaling domains, a process which has been heavily discussed in literature [55]. Since F-actin organization depends highly on the Ras family of small GTPases, specifically RasC and RasG, we investigated cAR1 and G$\beta\gamma$ dynamics in a *rasC$^-$/rasG$^-$ D. discoideum* cell line in order to unravel correlations between protein mobility and biological function.

The *rasC$^-$/rasG$^-$ D. discoideum* cell line was shown before to be virtually deficient in chemotactic signaling [5]. In a chemotaxis needle assay these cells, when transformed with functional cAR1, did move towards the needle albeit at heavily reduced efficiency (fig.4.10A) as compared to wt cells (fig.4.10B) and without forming streams. As briefly touched upon in the results section, this is probably explained by the fact that we introduce a functional cAR1. It was shown that cAR1 is vital to the expression of proteins important for development [50]. Our results suggest that the lack of directed cell movement may be the direct result of the absence of cAR1 expression in the *rasC$^-$/rasG$^-$* cells as Bolourani et al. also suggested [5].

We show here that the mobility of cAR1 in naïve RasC/RasG knockout cells is similar to that in naïve wt cells treated with lat A. When *rasC$^-$/rasG$^-$* cells experience a cAMP gradient, however, they do not show any polarized behavior in terms of

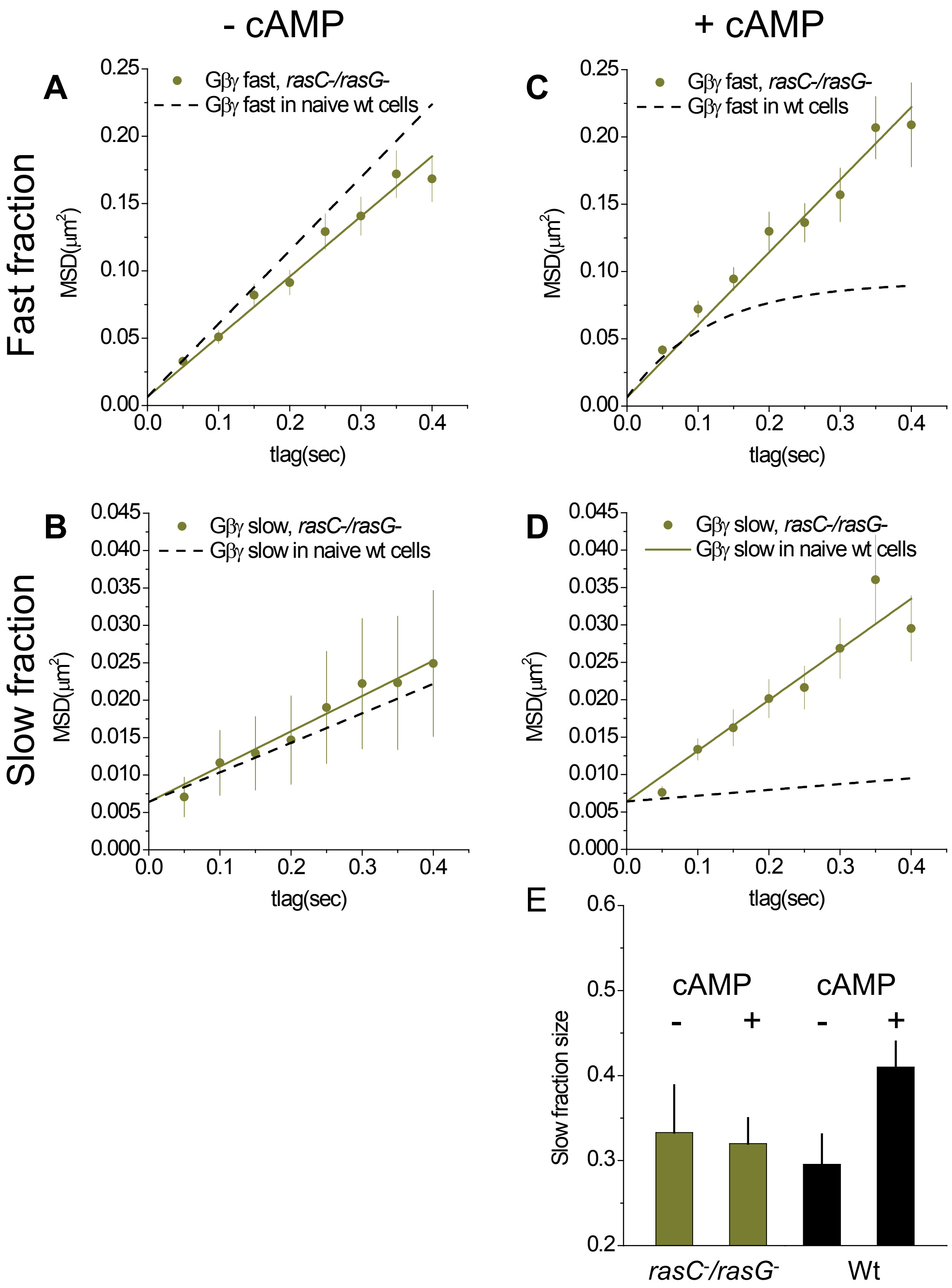
- cAMP
+ cAMP
Fast fraction
Slow fraction
A
Gβγ fast, rasC-/rasG-
Gβγ fast in naive wt cells
MSD(μm²)
tlag(sec)
0.00
0.05
0.10
0.15
0.20
0.25
0.0
0.1
0.2
0.3
0.4
C
Gβγ fast, rasC-/rasG-
Gβγ fast in wt cells
B
Gβγ slow, rasC-/rasG-
Gβγ slow in naive wt cells
0.000
0.005
0.010
0.015
0.020
0.025
0.030
0.035
0.040
0.045
D
Gβγ slow, rasC-/rasG-
Gβγ slow in naive wt cells
E
Slow fraction size
0.2
0.3
0.4
0.5
0.6
cAMP
-
+
cAMP
-
+
rasC-/rasG-
Wt

Figure 4.5: Gβγ does not immobilize and membrane micro domains do not form upon global cAMP stimulation of the *rasC⁻/rasG⁻* cells. **(A)** In naïve *rasC⁻/rasG⁻* cells the mobility of the fast fraction of Gβγ (yellow points) resembles that in naïve wt cells (black dotted line). **(B)** This is also true for the slow fraction. **(C)** Upon addition of 10 μM cAMP to wt cells F-actin dependent confined diffusion is observed (black dotted line), an effect which doesn't take place in the *rasC⁻/rasG⁻* cells (yellow points). **(D)** The slow fraction in wt cells immobilizes (black dotted line), an effect which requires F-actin polymerization and intact RasC/RasG signaling (yellow points). **(E)** The characteristic increase in slow fraction size was observed upon global cAMP stimulation of wt cells (black bars). This effect was shown to be F-actin independent (chapter 3), the effect is lost in the RasC/RasG knockout cell line (yellow bars).

cAR1 and Gβγ mobility. In contrast, wt cells which were treated by lat A to break down the cytoskeleton still exhibit polarized cAR1 mobility (chapter 3). Likewise, the immobilization of Gβγ upon cAMP activation (chapter 2) which was found to be cAMP, cAR1, Gα2 and F-actin dependent, does not occur in *rasC$^-$/rasG$^-$* cells.

The close resemblance of cAR1 mobility in *rasC$^-$/rasG$^-$* to that found in naïve wt cells upon treatment with lat A (fig.4.2; chapter 3) can be indicative of either i; reduced F-actin polymerization in the absence of RasC and RasG, ii; RasC and RasG directly mediate cAR1 binding to F-actin, or iii; RasC and RasG are required for the interaction of F-actin with the membrane. Given the fact that the *rasG$^-$* cells have similar amounts of F-actin [88] and *rasC$^-$* only shows deficiencies in downregulating actin polymerization at the back of a cAMP wave [95], hypothesis i seems unlikely. We can't disprove the second hypothesis (ii) here, although a direct interaction between cAR1 and the Ras proteins seems unlikely, such an interaction would facilitate rapid activation of Ras by precoupled G-proteins. Given the fact that the RasG/RasC knockout phenotype includes countless F-actin related deficiencies hypothesis iii seems most probable as the interpretation of our results. Probably RasC and RasG are important regulators for the local membrane organization that is predicted for proper functioning of the complex signaling networks in cells [55].

The fact that we don't find any effect on the mobility of cAR1 upon lat A treatment of the *rasC$^-$/rasG$^-$* cells compared to a significant effect in wt cells ($\Delta\alpha = 6\%$ *vs* $\Delta\alpha = 37\%$, respectively) further supports the hypothesis that RasC and RasG play a role in the F-actin - membrane interaction. This interaction can be either direct, e.g.: RasC or RasG actively couples F-actin to the membrane, or indirect, e.g.: in the absence of RasC or RasG F-actin organizes in such a way that a tight interaction with the membrane is disturbed. Since Ras proteins are upstream of myosin II regulation both at the cells anterior and posterior [53] and myosin is a principal F-actin regulator, this is a likely explanation.

The most striking finding in *rasC$^-$/rasG$^-$* cells is the loss of polarized mobility of cAR1 in a gradient of cAMP. In an earlier paper we attributed the polarized mobility of cAR1 to differential cortex - membrane interactions although other factors also contribute (chapter 3). As we show here, the *rasC$^-$/rasG$^-$* mutant has a cortex defect affecting cAR1 mobility. Because RasC and RasG are important regulators of F-actin dynamics, we expected to see the same result as in lat A treated wt cells namely, prevalence of the polarized mobility regarding cAR1. However, the mobility between the anterior and posterior of *rasC*$^-$*/rasG*$^-$ cells in a cAMP gradient did not differ indicating that factors that influence the cortex, membrane or cortex - membrane interactions other then F-actin influence cAR1 mobility, as we already suggested. These factors are downstream of RasC/RasG and involved in gradient sensing. Possible candidates are signaling membrane lipids (PI(3,4,5)P_3/PI(4,5)P_2) and/or cortex components other then F-actin. Our speculation of differential cortex - membrane interactions was backed by the fact that lat A treatment globally increased cAR1 mobility (chapter 3). Furthermore, micropipette aspiration experiments that locally probe the elastic properties of the membrane showed a smaller elastic constant of the anterior membrane as compared to the posterior membrane [64]. It was shown that leading edge specific breakdown of the cortex is part of an alternative method of amoeboid movement [101]. Hence, it seems that the *rasC*$^-$*/rasG*$^-$ cells are not capable of modulating cortex strength in a spatial manner that might be needed for proper cellular signaling and locomotion. This further suggests that *rasC*$^-$*/rasG*$^-$ will be deficient in discriminating anterior and posterior with regard to the cortex which might well be the cause of their inefficient random and directed movement.

The latter hypothesis was confirmed by experiments on G$\beta\gamma$ mobility. The fact that we do not observe immobilization of G$\beta\gamma$ in *rasC*$^-$*/rasG*$^-$ came as a surprise. The *rasC*$^-$*/rasG*$^-$ cells are certainly not deprived of F-actin [88] but only show aberrant mechanical properties [95]. The fact that G$\beta\gamma$ does not immobilize upon activation suggests either a physical difference between the F-actin in *rasC*$^-$*/rasG*$^-$ and that in wt cells or lack of a so far not identified G$\beta\gamma$ - F-actin binding factor which could be either RasC or RasG. If this were to be the case, we are able to explain leading edge specific G$\beta\gamma$ immobilization a as result of the local Ras activation [47, 79].

In conclusion our findings support the fact that RasC and RasG are important for actin dynamics but also suggest a function in regulating F-actin - membrane interactions. RasC and RasG appear to play a role in organizing the local membrane structure such that activation remains localized and pseudopods are stabilized (fig.4.6). The former are concluded from our finding that Ras seems to be important for the G$\beta\gamma$ - F-actin binding we observed earlier, and thus for the suggested leading edge specific feedback mechanism. This hypothesis is supported by the fact that RasC/RasG knockout cells show reduced random movement [5]. The deficiency in proper membrane organization may finally lead to a deficiency in keeping activation localized, a hypothesis which will have to be tested in further experiments. We have shown that even though Ras is a downstream effector of cAR1 and the G protein, due to its influence on F-actin it indirectly alters the behavior of the two. Our results point towards a feedback mechanism between F-actin and the GPCR signaling involving Ras, the results might be applicable to a wide range of GPCR - G protein systems.

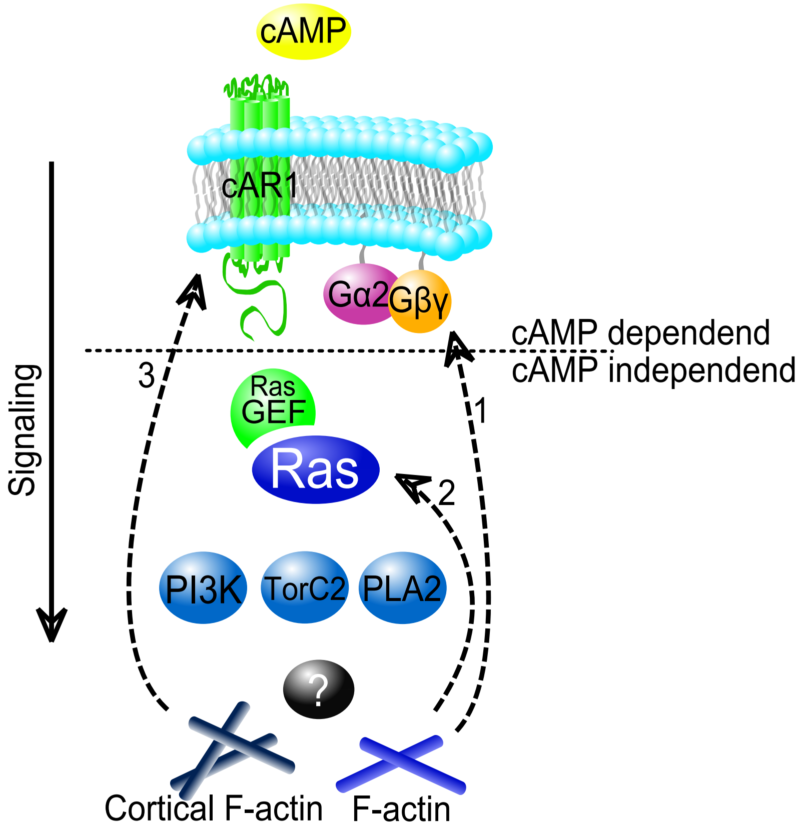
cAMP
cAR1
Gα2
Gβγ
cAMP dependend
cAMP independend
Signaling
3
1
2
Ras GEF
Ras
PI3K
TorC2
PLA2
?
Cortical F-actin
F-actin

Figure 4.6: A model incorporating the results. Upon addition of cAMP to the cells, cAR1 is activated. The G protein heterotrimer splits into its $\alpha 2$ and $\beta\gamma$ subunit. RasGEFs are stimulated by the G protein and in turn function as on switches for the Ras family of small G proteins. Ras proteins then activate several downstream effectors for which it is currently unknown how they exactly lead to actin polymerization. This model incorporates several feedback mechanisms: 1; G$\beta\gamma$ immobilizes in a cAMP, cAR1, G$\alpha 2$, RasC/RasG and F-actin dependent manner. This immobilization also takes place specifically at the leading edge of a chemotaxing cell. We hypothesize that this specific F-actin - G$\beta\gamma$ interaction may function as an enhancer for G protein signaling and thus plays a role as a maintainer/amplifier of polarized chemotactic signaling. The F-actin independent but RasC/RasG dependent increase in slow fraction size upon activation however plays a part in gradient sensing. 2; A cAR1/G protein independent feedback mechanism has been suggested to exist between F-actin and members of the Ras family [80]. This mechanism helps to control stochastic changes in the cytoskeleton by stabilizing forming pseudopods, possibly the cause for reduced motility of the *rasC*$^-$*/rasG*$^-$ cells. 3; We have reported before that the diffusion speed of cAR1 is dominated by F-actin interactions (chapter 3) and that differential membrane cortex interactions may be responsible for the fact that cAR1 mobility is higher at the leading edge with respect to the trailing edge. We have shown in this paper that the regulation of cAR1 mobility by F-actin is Ras dependent but it does not require a functional G protein (chapter 3). Maintaining polarized cortex - membrane interactions however requires G protein and Ras signaling, consistent with idea that the Ras/PI3K/F-actin feedback mechanism does not require GPCR input whereas directed motion does.

Supplemental information

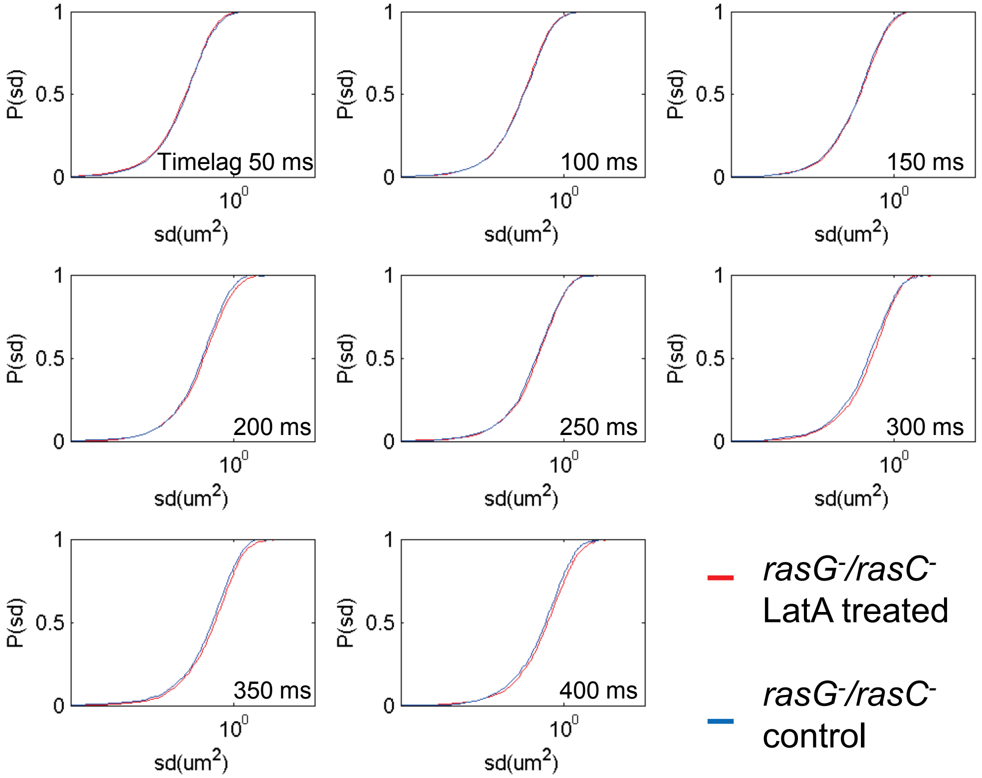

Figure 4.7: The mobility of cAR1 is equal in naïve and lat A treated in *rasC*$^{-}$/*rasG*$^{-}$ cells.

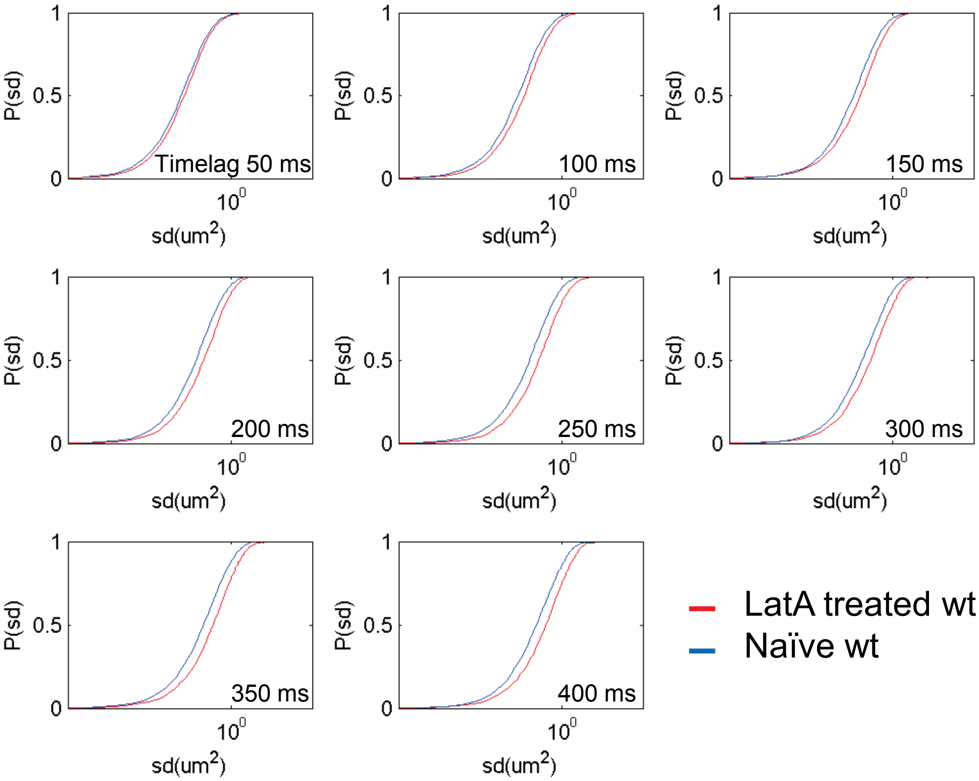

Figure 4.8: The mobility of cAR1 in wt cells is dramatically increased upon lat A treatment.

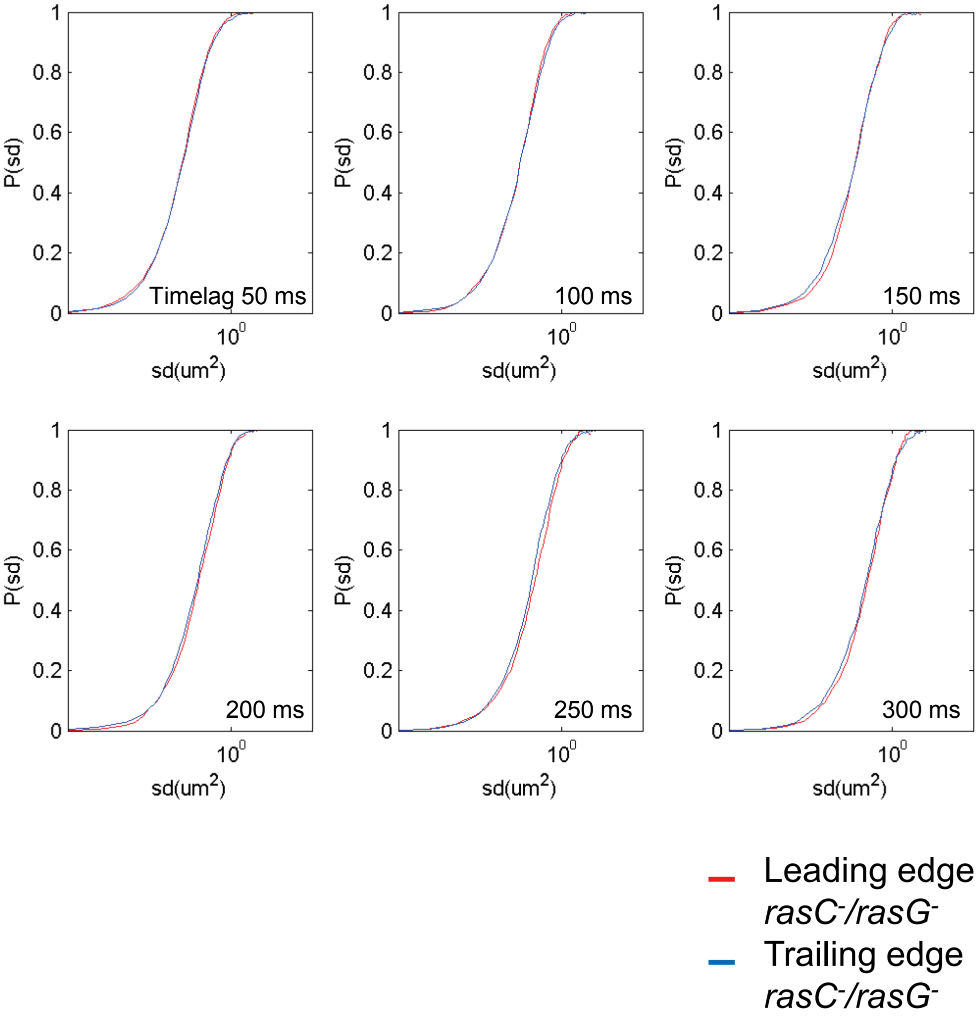

Figure 4.9: the mobility of cAR1 in chemotaxing *rasC*$^-$/*rasG*$^-$ is not polarized.

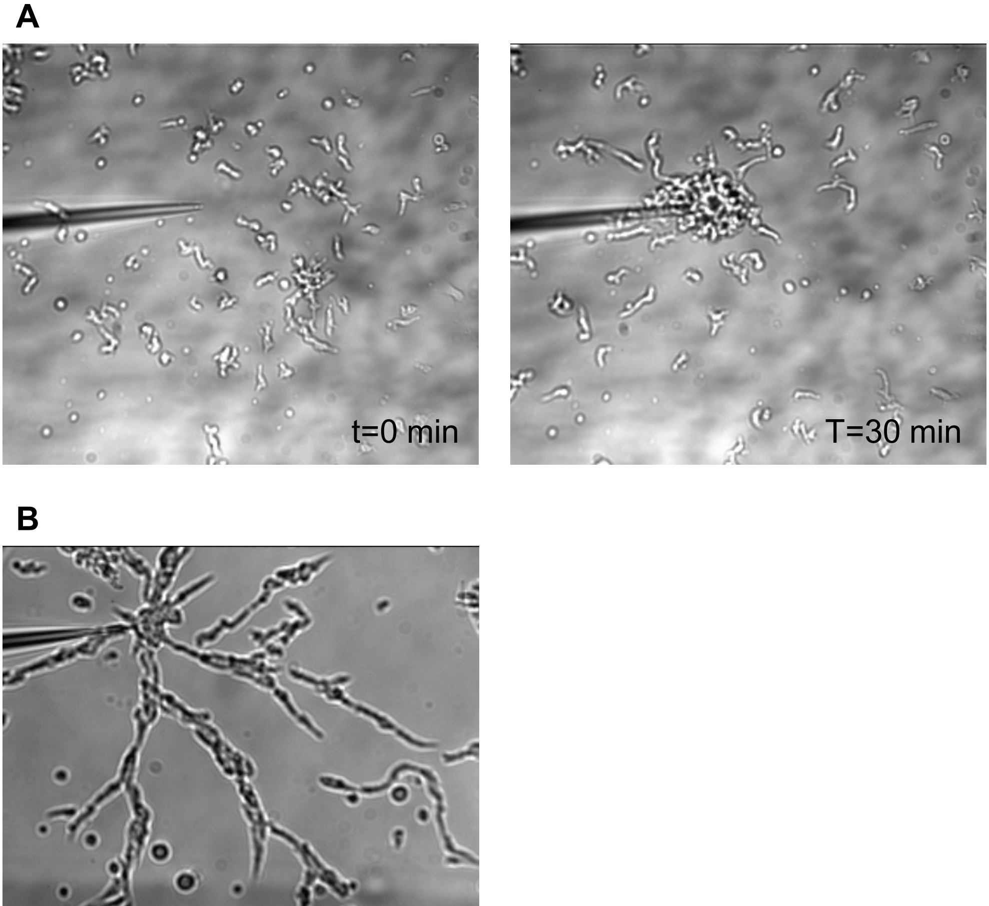
A
t=0 min
T=30 min
B
T=20 min

Figure 4.10: *rasC*$^{-}$/*rasG*$^{-}$ cells show directional movement upon expression of cAR1.

Bibliography

[1] N. Andrew and R. H. Insall. Chemotaxis in shallow gradients is mediated independently of PtdIns 3-kinase by biased choices between random protrusions. *Nat Cell Biol*, 9(2):193–200, 2007.

[2] N. L. Andrews, K. A. Lidke, J. R. Pfeiffer, A. R. Burns, B. S. Wilsona, J. M. Oliver, and D. S. Lidke. Actin restricts fcϵri diffusion and facilitates antigen-induced receptor immobilization. *Nat Cell Biol*, 10(8):955–963, 2008.

[3] Y. Asano, A. Nagasaki, and T. Q. Uyeda. Correlated waves of actin filaments and PIP3 in Dictyostelium cells. *Cell Motil.Cytoskeleton*, 65(12):923–934, 2008.

[4] H. C. Berg. *Random walks in biology*. Humana Press, 1993.

[5] P. Bolourani, G. B. Spiegelman, and G. Weeks. Delineation of the roles played by RasG and RasC in camp-dependent signal transduction during the early development of Dictyostelium discoideum. *Mol Biol Cell*, 17(10):4543–4550, 2006.

[6] L. Bosgraaf and P. J. V. Haastert. Navigation of chemotactic cells by parallel signaling to pseudopod persistence and orientation. *PLoS.One.*, 4(8):e6842, 2009.

[7] H. R. Bourne, D. A. Sanders, and F. McCormick. The GTPase superfamily: conserved structure and molecular mechanism. *Nature*, 349(6305):117–127, 1991.

[8] C. Bouzigues, M. Morel, A. Triller, and M. Dahan. Asymmetric redistribution of GABA receptors during GABA gradient sensing by nerve growth cones analyzed by single quantum dot imaging. *Proc.Natl.Acad.Sci U.S.A*, 104(27):11251–11256, 2007.

[9] M. J. Caterina, J. L. Milne, and P. N. Devreotes. Mutation of the third intracellular loop of the camp receptor, cAR1, of Dictyostelium yields mutants impaired in multiple signaling pathways. *J Biol Chem.*, 269(2):1523–32, 1994.

[10] S. Chandrasekhar. Stochastic problems in physics and astronomy. *Rev.Mod.Phys.*, 15:1–89, 1943.

[11] L. Chen, M. Iijima, M. Tang, M. Landree, Y. Huang, Y. Xiong, P. Iglesias, and P. Devreotes. PLA2 and PI3K/PTEN pathways act in parallel to mediate chemotaxis. *Dev.Cell*, 12(4):603–614, 2007.

[12] L. Chen, C. Janetopoulos, Y. E. Huang, M. Iijima, J. Borleis, , and P. N. Devreotes. Two phases of actin polymerization display different dependencies on PI(3,4,5)P3 accumulation and have unique roles during chemotaxis. *Mol Biol Cell*, 14(12):5028–5037, 2003.

[13] M. Y. Chen, P. N. Devreotes, and R. E. Gundersen. Serine 113 is the site of receptor-mediated phosphorylation of the Dictyostelium G protein α-subunit Gα2. *J Biol Chem.*, 269(19):20925–30, 1994.

[14] J. Colicelli. Human RAS superfamily proteins and related GTPases. *Sci STKE.*, 2004(250):RE13, 2004.

[15] F. I. Comer and C. A. Parent. PI 3-kinases and PTEN: how opposites chemoattract. *Cell*, 109(5):541–544, 2002.

[16] E. L. de Hostos, B. Bradtke, F. Lottspeich, R. Guggenheim, and G. Gerisch. Coronin, an actin binding protein of Dictyostelium discoideum localized to cell surface projections, has sequence similarities to G protein β subunits. *EMBO J*, 10(13):4097–4104, 1991.

[17] S. de Keijzer, A. Sergé, F. van Hemert, P. H. M. Lommerse, G. E. M. Lamers, H. P. Spaink, T. Schmidt, , and B. E. Snaar-Jagalska. A spatially restricted increase in receptor mobility is involved in directional sensing during Dictyostelium discoideum chemotaxis. *J Cell Sci*, 121(10):1750–1757, 2008.

[18] T. Dertinger, V. Pacheco, I. von der Hocht, R. Hartmann, I. Gregor, and J. Enderlein. Two-focus fluorescence correlation spectroscopy: a new tool for accurate and absolute diffusion measurements. *Chemphyschem.*, 8(3):433–443, 2007.

[19] P. N. Devreotes and T. L. Steck. Cyclic 3',5' AMP relay in Dictyostelium discoideum. II. Requirements for the initiation and termination of the response. *J Cell Biol*, 80(2):300–309, 1979.

[20] L. Eichinger, J. A. Pachebat, G. Glöckner, M. A. Rajandream, R. Sucgang, M. Berriman, J. Song, R. Olsen, K. Szafranski, Q. Xu, B. Tunggal, S. Kummerfeld, M. Madera, B. A. Konfortov, F. Rivero, A. T. Bankier, R. Lehmann, N. Hamlin, R. Davies, P. Gaudet, P. Fey, K. Pilcher, G. Chen, D. Saunders, E. Sodergren, P. Davis, A. Kerhornou, X. Nie, N. Hall, C. Anjard, L. Hemphill, N. Bason, P. Farbrother, B. Desany, E. Just, T. Morio, R. Rost, C. Churcher, J. Cooper, S. Haydock, N. van Driessche, A. Cronin, I. Goodhead, D. Muzny, T. Mourier, A. Pain, M. Lu, D. Harper, R. Lindsay, H. Hauser, K. James, M. Quiles, M. M. Babu, T. Saito, C. Buchrieser, A. Wardroper, M. Felder, M. Thangavelu, D. Johnson, A. Knights, H. Loulseged, K. Mungall, K. Oliver, C. Price, M. A. Quail, H. Urushihara, J. Hernandez, E. Rabbinowitsch, D. Steffen, M. Sanders, J. Ma, Y. Kohara, S. Sharp, M. Simmonds, S. Spiegler, A. Tivey, S. Sugano, B. White, D. Walker, J. Woodward, T. Winckler, Y. Tanaka, G. Shaulsky, M. Schleicher, G. Weinstock, A. Rosenthal, E. C. Cox, R. L. Chisholm, R. Gibbs, W. F. Loomis, M. Platzer, R. R. Kay, J. Williams, P. H. Dear, A. A. Noegel, B. Barrell, and A. Kuspa. The genome of the social amoeba Dictyostelium discoideum. *Nature*, 435(7038):43–57, 2005.

[21] L. Eichinger and F. Rivero. *Dictyostelium discoideum Protocols*. Humana Press, 2006.

[22] C. A. Elzie, J. Colby, M. A. Sammons, and C. Janetopoulos. Dynamic localization of G proteins in Dictyostelium discoideum. *J Cell Sci*, 122(Pt 15):2597–2603, 2009.

[23] C. J. L. et al. Loss of the Dictyostelium RasC protein alters vegetative cell size, motility and endocytosis. *Exp.Cell Res.*, 306(1):47–55, 2005.

[24] P. Fey, P. Gaudet, T. Curk, B. Zupan, E. M. Just, S. Basu, S. N. Merchant, Y. A. Bushmanova, G. Shaulsky, W. A. Kibbe, and R. L. Chisholm. dictyBase - a Dictyostelium bioinformatics resource update. *Nucl. Acids Res.*, 37(suppl1):515–519, 2009.

[25] T. Fischer, L. Lu, H. T. Haigler, and R. Langen. Annexin B12 is a sensor of membrane curvature and undergoes major curvature-dependent structural changes. *Journal of Biological Chemistry*, 282(13):9996–10004, 2007.

[26] J. Franca-Koh and P. N. Devreotes. Moving forward: mechanisms of chemoattractant gradient sensing. *Physiology.(Bethesda.)*, 19:300–308, 2004.

[27] J. Franca-Koh, Y. Kamimura, and P. Devreotes. Navigating signaling networks: chemotaxis in Dictyostelium discoideum. *Current Opinion in Genetics & Development*, 16(4):333–338, 2006.

[28] L. Frigeri and J. R. Apgar. The role of actin microfilaments in the down-regulation of the degranulation response in RBL-2H3 mast cells. *The Journal of Immunology*, 162(4):2243–2250, 1999.

[29] T. Fujiwara, K. Ritchie, H. Murakoshi, K. Jacobson, and A. Kusumi. Phospholipids undergo hop diffusion in compartmentalized cell membrane. *J Cell Biol*, 157(6):1071–1081, 2002.

[30] S. Funamoto, R. Meili, S. Lee, L. Parry, and R. A. Firtel. Spatial and temporal regulation of 3-phosphoinositides by PI 3-kinase and PTEN mediates chemotaxis. *Cell*, 109(5):611–623, 2002.

[31] N. J. Galvin, D. Stockhausen, B. L. Meyers-Hutchins, and W. A. Frazier. Association of the cyclic AMP chemotaxis receptor with the detergent-insoluble cytoskeleton of Dictyostelium discoideum. *J Cell Biol*, 98(2):584–595, 1984.

[32] A. Gamba, A. de Candia, S. D. Talia, A. Coniglio, F. Bussolino, and G. Serini. Diffusion-limited phase separation in eukaryotic chemotaxis. *Proc.Natl.Acad.Sci U.S.A*, 102(47):16927–16932, 2005.

[33] K. D. Girard, S. C. Kuo, and D. N. Robinson. Dictyostelium myosin II mechanochemistry promotes active behavior of the cortex on long time scales. *Proc.Natl.Acad.Sci U.S.A*, 103(7):2103–2108, 2006.

[34] P. J. V. Haastert, J. D. Bishop, and R. H. Gomer. The cell density factor CMF regulates the chemoattractant receptor cAR1 in Dictyostelium. *J Cell Biol*, 134(6):1543–1549, 1996.

[35] P. J. V. Haastert, I. Keizer-Gunnink, and A. Kortholt. Essential role of PI3-kinase and phospholipase A2 in Dictyostelium discoideum chemotaxis. *J Cell Biol*, 177(5):809–816, 2007.

[36] G. S. Harms, L. Cognet, P. H. Lommerse, G. A. Blab, and T. Schmidt. Autofluorescent proteins in single-molecule research: applications to live cell imaging microscopy. *Biophys.J*, 80(5):2396–2408, 2001.

[37] D. Hereld and P. N. Devreotes. The cAMP receptor family of Dictyostelium. *Int.Rev Cytol.*, 137B:35–47, 1992.

[38] O. Hoeller and R. R. Kay. Chemotaxis in the absence of PIP3 gradients. *Curr.Biol*, 17(9):813–817, 2007.

[39] L. Holtzer, T. Meckel, and T. Schmidt. Nanometric three-dimensional tracking of individual quantum dots in cells. *Applied Physics Letters*, 90(5):053902, Jan 2007.

[40] M. Iijima and P. Devreotes. Tumor suppressor PTEN mediates sensing of chemoattractant gradients. *Cell*, 109(5):599–610, 2002.

[41] M. Iijima, Y. E. Huang, H. R. Luo, F. Vazquez, and P. N. Devreotes. Novel mechanism of PTEN regulation by its phosphatidylinositol 4,5-bisphosphate binding motif is critical for chemotaxis. *J Biol Chem.*, 279(16):16606–16613, 2004.

[42] T. Inoue and T. Meyer. Synthetic activation of endogenous PI3K and Rac identifies an AND-gate switch for cell polarization and migration. *PLoS.One.*, 3(8):e3068, 2008.

[43] V.-P. Jaakola, M. T. Griffith, M. A. Hanson, V. Cherezov, E. Y. T. Chien, J. R. Lane, A. P. IJzerman, and R. C. Stevens. The 2.6 angstrom crystal structure of a human A2A adenosine receptor bound to an antagonist. *Science*, 322(5905):1211–1217, 2008.

[44] C. Janetopoulos, T. Jin, and P. Devreotes. Receptor-mediated activation of heterotrimeric G-proteins in living cells. *Science*, 291(5512):2408–2411, 2001.

[45] P. M. Janssens and P. J. V. Haastert. Molecular basis of transmembrane signal transduction in Dictyostelium discoideum. *Microbiol.Rev*, 51(4):396–418, 1987.

[46] T. Jin, N. Zhang, Y. Long, C. A. Parent, and P. N. Devreotes. Localization of the G protein complex in living cells during chemotaxis. *Science*, 287(5455):1034–1036, 2000.

[47] H. Kae, C. J. Lim, G. B. Spiegelman, and G. Weeks. Chemoattractant-induced Ras activation during Dictyostelium aggregation. *EMBO Rep.*, 5(6):602–606, 2004.

[48] Y. Kamimura, Yoichiro; Xiong, P. A. Iglesias, O. Hoeller, P. Bolourani, and P. N. Devreotes. PIP3-independent activation of TorC2 and PKB at the cell's leading edge mediates chemotaxis. *Curr.Biol*, 18(14):1034–1043, 2008.

[49] A. R. Kimmel and C. A. Parent. The signal to move: D. discoideum go orienteering. *Science*, 300(5625):1525–1527, 2003.

[50] P. S. Klein, T. J. Sun, C. L. S. 3rd, A. R. Kimmel, R. L. Johnson, and P. N. Devreotes. A chemoattractant receptor controls development in Dictyostelium discoideum. *Science*, 241(4872):1467–1472, 1988.

[51] T. M. Konijn, J. G. van de Meene, J. T. Bonner, and D. S. Barkley. The acrasin activity of adenosine-3',5'-cyclic phosphate. *Proc.Natl.Acad.Sci U.S.A*, 58(3):1152–1154, 1967.

[52] W. J. Koopmans, R. Buning, T. Schmidt, and N. J. van. spFRET using alternating excitation and FCS reveals progressive DNA unwrapping in nucleosomes. *Biophys.J*, 97(1):195–204, 2009.

[53] A. Kortholt and P. J. V. Haastert. Highlighting the role of Ras and Rap during Dictyostelium chemotaxis. *Cell Signal.*, 20(8):1415–1422, 2008.

[54] P. W. Kriebel, V. A. Barr, and C. A. Parent. Adenylyl cyclase localization regulates streaming during chemotaxis. *Cell*, 112(4):549–560, 2003.

[55] A. Kusumi, C. Nakada, K. Ritchie, K. Murase, K. Suzuki, H. Murakoshi, R. S. Kasai, J. Kondo, and T. Fujiwara. Paradigm shift of the plasma membrane concept from the two-dimensional continuum fluid to the partitioned fluid: high-speed single-molecule tracking of membrane molecules. *Annu.Rev Biophys.Biomol.Struct.*, 34:351–378, 2005.

[56] A. Kusumi and Y. Sako. Cell surface organization by the membrane skeleton. *Curr.Opin.Cell Biol*, 8(4):566–574, 1996.

[57] A. Kusumi, Y. Sako, and M. Yamamoto. Confined lateral diffusion of membrane receptors as studied by single particle tracking (nanovid microscopy). effects of calcium-induced differentiation in cultured epithelial cells. *Biophys.J*, 65(5):2021–2040, 1993.

[58] P. D. Langridge and R. R. Kay. Blebbing of Dictyostelium cells in response to chemoattractant. *Exp.Cell Res.*, 312(11):2009–2017, 2006.

[59] H. Levine, D. A. Kessler, and W. J. Rappel. Directional sensing in eukaryotic chemotaxis: a balanced inactivation model. *Proc.Natl.Acad.Sci U.S.A*, 103(26):9761–9766, 2006.

[60] P. Lilly, L. Wu, D. L. Welker, and P. N. Devreotes. A G-protein β-subunit is essential for Dictyostelium development. *Genes & Development*, 7(6):986–995, 1993.

[61] C. J. Lim, G. B. Spiegelman, and G. Weeks. RasC is required for optimal activation of adenylyl cyclase and Akt/PKB during aggregation. *EMBO J*, 20(16):4490–4499, 2001.

[62] C. J. Lim, G. B. Spiegelman, and G. Weeks. RasC is required for optimal activation of adenylyl cyclase and Akt/PKB during aggregation. *EMBO J*, 20(16):4490–4499, 2001.

[63] L. Ma, C. Janetopoulos, L. Yang, P. N. Devreotes, and P. A. Iglesias. Two complementary, local excitation, global inhibition mechanisms acting in parallel can explain the chemoattractant-induced regulation of PI(3,4,5)P3 response in Dictyostelium cells. *Biophys.J*, 87(6):3764–3774, 2004.

[64] R. Merkel, R. Simson, D. A. Simson, M. Hohenadl, A. Boulbitch, E. Wallraff, and E. Sackmann. A micromechanic study of cell polarity and plasma membrane cell body coupling in Dictyostelium. *Biophys.J*, 79(2):707–719, 2000.

[65] Y. Miyanaga, S. Matsuoka, T. Yanagida, and M. Ueda. Stochastic signal inputs for chemotactic response in Dictyostelium cells revealed by single molecule imaging techniques. *Biosystems*, 88(3):251–260, 2007.

[66] N. Morone, T. Fujiwara, K. Murase, R. S. Kasai, H. Ike, S. Yuasa, J. Usukura, and A. Kusumi. Three-dimensional reconstruction of the membrane skeleton at the plasma membrane interface by electron tomography. *J Cell Biol*, 174(6):851–862, 2006.

[67] M. Nobles, A. Benians, and A. Tinker. Heterotrimeric G proteins precouple with G protein-coupled receptors in living cells. *Proc.Natl.Acad.Sci U.S.A*, 102(51):18706–18711, 2005.

[68] K. Okaichi, A. B. Cubitt, G. S. Pitt, and R. A. Firtel. Amino acid substitutions in the Dictyostelium Gα subunit Gα2 produce dominant negative phenotypes and inhibit the activation of adenylyl cyclase, guanylyl cyclase, and phospholipase C. *Mol Biol Cell*, 3(7):735–747, 1992.

[69] K. Palczewski, T. Kumasaka, T. Hori, C. A. Behnke, H. Motoshima, B. A. Fox, I. L. Trong, D. C. Teller, T. Okada, R. E. Stenkamp, M. Yamamoto, and M. Miyano. Crystal structure of Rhodopsin: A G protein-coupled receptor. *Science*, 289(5480):739–745, 2000.

[70] C. A. Parent, B. J. Blacklock, W. M. Froehlich, D. B. Murphy, and P. N. Devreotes. G protein signaling events are activated at the leading edge of chemotactic cells. *Cell*, 95(1):81–91, 1998.

[71] T. Pawson and J. D. Scott. Signaling through scaffold, anchoring, and adaptor proteins. *Science*, 278(5346):2075–2080, 1997.

[72] T. D. Pollard. Regulation of actin filament assembly by Arp2/3 complex and formins. *Annu.Rev Biophys.Biomol.Struct.*, 36:451–477, 2007.

[73] A. Ponti, M. Machacek, S. L. Gupton, C. M. Waterman-Storer, and G. Danuser. Two distinct actin networks drive the protrusion of migrating cells. *Science*, 305(5691):1782–1786, 2004.

[74] M. Postma, J. Roelofs, J. Goedhart, T. W. Gadella, A. J. Visser, and P. J. Van Haastert. Uniform cAMP Stimulation of Dictyostelium Cells Induces Localized Patches of Signal Transduction and Pseudopodia. *Mol. Biol. Cell*, 14(12):5019–5027, 2003.

[75] M. Postma and P. J. Van Haastert. A diffusion-translocation model for gradient sensing by chemotactic cells. *Biophysical Journal*, 2001.

[76] E. O. Potma, W. P. de Boeij, L. Bosgraaf, J. Roelofs, P. J. van Haastert, and D. A. Wiersma. Reduced protein diffusion rate by cytoskeleton in vegetative and polarized Dictyostelium cells. *Biophys.J*, 81(4):2010–2019, 2001.

[77] S. G. F. Rasmussen, H.-J. Choi1, D. M. Rosenbaum, T. S. Kobilka, F. S. Thian, P. C. Edwards, M. Burghammer, V. R. P. Ratnala1, R. Sanishvili, R. F. Fischetti, G. F. X. Schertler, W. I. Weis, and B. K. Kobilka. Crystal structure of the human [bgr]2 adrenergic g-protein-coupled receptor. *Nature*, 450(7168):383–387, 2007.

[78] D. S. Rhoads, S. M. Nadkarni, L. Song, C. Voeltz, E. Bodenschatz, and J.-L. Guan. Using microfluidic channel networks to generate gradients for studying cell migration. *Methods Mol Biol*, 294:347–357, 2005.

[79] A. T. Sasaki, C. Chun, K. Takeda, and R. A. Firtel. Localized Ras signaling at the leading edge regulates PI3K, cell polarity, and directional cell movement. *J Cell Biol*, 167(3):505–518, 2004.

[80] A. T. Sasaki, C. Janetopoulos, S. Lee, P. G. Charest, K. Takeda, L. W. Sundheimer, R. Meili, P. N. Devreotes, and R. A. Firtel. G protein-independent Ras/PI3K/F-actin circuit regulates basic cell motility. *J Cell Biol*, 178(2):185–191, 2007.

[81] T. Schmidt, G. J. Schütz, W. Baumgartner, H. J. Gruber, and H. Schindler. Imaging of single molecule diffusion. *Proc.Natl.Acad.Sci U.S.A*, 93(7):2926–2929, 1996.

[82] G. J. Schütz, H. Schindler, and T. Schmidt. Single-molecule microscopy on model membranes reveals anomalous diffusion. *Biophys.J*, 73(2):1073–1080, 1997.

[83] S. Semrau and T. Schmidt. Particle image correlation spectroscopy (PICS): retrieving nanometer-scale correlations from high-density single-molecule position data. *Biophys.J*, 92(2):613–621, 2007.

[84] L. Song, S. M. Nadkarni, H. U. Bödeker, C. Beta, A. Bae, C. Franck, W.-J. Rappel, W. F. Loomis, and E. Bodenschatz. Dictyostelium discoideum chemotaxis: threshold for directed motion. *Eur.J Cell Biol*, 85(9-10):981–989, 2006.

[85] B. L. Sprague, R. L. Pego, D. A. Stavreva, and J. G. McNally. Analysis of binding reactions by fluorescence recovery after photobleaching. *Biophys.J*, 86(6):3473–3495, 2004.

[86] K. Suzuki, K. Ritchie, E. Kajikawa, T. Fujiwara, and A. Kusumi. Rapid hop diffusion of a G-protein-coupled receptor in the plasma membrane as revealed by single-molecule techniques. *Biophys.J*, 88(5):3659–3680, 2005.

[87] M. Tsujioka, K. Yoshida, A. Nagasaki, S. Yonemura, A. Muller-Taubenberger, and T. Q. P. Uyeda. Overlapping functions of the two talin homologues in Dictyostelium. *Eukaryot.Cell*, 7(5):906–916, 2008.

[88] R. I. Tuxworth, J. L. Cheetham, L. M. Machesky, G. B. Spiegelmann, G. Weeks, and R. H. Insall. Dictyostelium RasG is required for normal motility and cytokinesis, but not growth. *J Cell Biol*, 138(3):605–614, 1997.

[89] K. S. Uchida, T. Kitanishi-Yumura, and S. Yumura. Myosin II contributes to the posterior contraction and the anterior extension during the retraction phase in migrating Dictyostelium cells. *J Cell Sci*, 116(Pt 1):51–60, 2003.

[90] M. Ueda, Y. Sako, T. Tanaka, P. Devreotes, and T. Yanagida. Single-molecule analysis of chemotactic signaling in Dictyostelium cells. *Science*, 294(5543):864–867, 2001.

[91] D. M. Veltman, I. Keizer-Gunnik, and P. J. V. Haastert. Four key signaling pathways mediating chemotaxis in Dictyostelium discoideum. *J Cell Biol*, 180(4):747–753, 2008.

[92] G. H. Wadhams and J. P. Armitage. Making sense of it all: bacterial chemotaxis. *Nat Rev Mol Cell Biol*, 5(12):1024–1037, 2004.

[93] D. J. Watts and J. M. Ashworth. Growth of myxameobae of the cellular slime mould Dictyostelium discoideum in axenic culture. *Biochem.J*, 119(2):171–174, 1970.

[94] I. Weisswange, T. Bretschneider, and K. I. Anderson. The leading edge is a lipid diffusion barrier. *J Cell Sci*, 118(19):4375–4380, 2005.

[95] D. Wessels, R. Brincks, S. Kuhl, V. Stepanovic, K. J. Daniels, G. Weeks, C. J. Lim, G. Spiegelman, D. Fuller, N. Iranfar, W. F. Loomis, and D. R. Soll. RasC plays a role in transduction of temporal gradient information in the cyclic-AMP wave of Dictyostelium discoideum. *Eukaryotic Cell*, 3(3):646–662, 2004.

[96] D. Wessels, N. A. Schroeder, E. Voss, A. L. Hall, J. Condeelis, and D. R. Soll. cAMP-mediated inhibition of intracellular particle movement and actin reorganization in Dictyostelium. *J Cell Biol*, 109(6 Pt 1):2841–2851, 1989.

[97] N. Wettschureck and S. Offermanns. Mammalian G proteins and their cell type specific functions. *Physiological Reviews*, 85(4):1159–1204, 2005.

[98] S. Wieser, M. Moertelmaier, E. Fuertbauer, H. Stockinger, and G. J. Schütz. (un)confined diffusion of CD59 in the plasma membrane determined by high-resolution single molecule microscopy. *Biophys.J*, 92(10):3719–3728, 2007.

[99] L. Wu, R. Valkema, P. J. V. Haastert, and P. N. Devreotes. The G protein β subunit is essential for multiple responses to chemoattractants in Dictyostelium. *J Cell Biol*, 129(6):1667–1675, 1995.

[100] X. Xu, M. Meier-Schellersheim, X. Jiao, L. E. Nelson, and T. Jin. Quantitative imaging of single live cells reveals spatiotemporal dynamics of multistep signaling events of chemoattractant gradient sensing in Dictyostelium. *Mol Biol Cell*, 16(2):676–688, 2005.

[101] K. Yoshida and T. Soldati. Dissection of amoeboid movement into two mechanically distinct modes. *J Cell Sci*, 119(Pt 18):3833–3844, 2006.

[102] N. Zhang, Y. Long, and P. N. Devreotes. Gγ in Dictyostelium: Its role in localization of g$\beta\gamma$ to the membrane is required for chemotaxis in shallow gradients. *Mol Biol Cell*, 12(10):3204–3213, 2001.

[103] S. Zhang, P. G. Charest, and R. A. Firtel. Spatiotemporal regulation of Ras activity provides directional sensing. *Curr.Biol*, 18(20):1587–1593, 2008.

Samenvatting

Cellen zijn de fundamentele eenheid van alle organismen die we met het blote oog kunnen zien. Ze bestaan in allerlei vormen en kunnen alle functies vervullen die mensen nodig hebben om te leven. In het menselijk lichaam bestaan bijvoorbeeld cellen die maagzuur maken en cellen die de electrische signalen doorgeven die je uiteindelijk in staat stellen te denken. De meesten menselijke cellen zijn tussen de 10 en 100 µm in doorsnee (een haar is ongeveer 60 µm, een µm is 1 duizendste mm), een organisme zoals een mens bestaat dus uit miljarden cellen.

Binnen het lichaam vormen cellen samen eenheden die specifieke taken vervullen, dit noemen we organen. Zo zuiveren de nieren het bloed, slaan de hersenen informatie op en voorzien de longen het geheel van zuurstof. Maar niet alle functies zijn vastgelegd in grote, zichtbare organen.

Het imuunsysteem bijvoorbeeld omvat een aantal organen en een groot aantal losse cellen die door het lichaam stromen en kruipen op zoek naar dingen die er niet thuis horen. Een voorbeeld van zulke losse cellen zijn de witte bloedcellen. Witte bloedcellen worden constant met het bloed mee gevoerd totdat ze op een plaats komen waar een infectie is. Deze infectie kan bijvoorbeeld komen doordat er bacteriën in een wond gekomen zijn. Bacteriën zijn eveneens cellen maar dan zo'n 10 tot 100 keer kleiner dan onze lichaamscellen. Ze gedijen goed in de warme vochtige omgeving die het menselijk lichaam biedt, meestal ten koste van de lichaamscellen van de gastheer. Doordat bacteriën een andere stofwisseling hebben dan de mens scheiden ze stoffen uit die normaal gesproken niet voorkomen binnen het menselijk lichaam. Juist deze stoffen zijn voor witte bloedcellen een signaal om uit het bloed te kruipen richting de plaats van infectie. Daar aangekomen zullen ze de bacteriën opnemen (endocyteren) en verteren. Tegelijkertijd vind er nog een scala aan processen plaats die de effectiviteit van het immuunsysteem verhogen en leiden tot het verdelgen van de schadelijke bacteriën door het hele lichaam.

Over dit proces van bacteriën localiseren en verdelgen is al veel bekend, bijvoorbeeld welke stoffen bacteriën uitscheiden die hun aanwezigheid verraden. Er is veel minder bekend over de precieze mechanismen die de witte bloedcellen in staat stellen in de richting van de infectie te kruipen. Hoe bepaalt een cel de juiste richting? Als hij deze richting heeft bepaald, hoe zorgt hij dan dat hij ook daadwerkelijk begint te bewegen? Om dit soort vragen te beantwoorden moeten we nog verder inzoomen en kijken naar de opbouw van de individuele cellen.

Een cel is eigenlijk een zeer goed georganiseerde micro-machine. Eiwitten (ongeveer 1 nm groot, ook wel proteïnen genoemd), waarvan de vorm en functie vastligt in het DNA, vormen de werkzame deeltjes. Wat alle cellen echter gemeen hebben is het hebben van een celmembraan. Het celmembraan is een vlies van phospholipiden wat ervoor zorgt dat de cel bij elkaar blijft en zijn eiwitten en structuur behoudt. Om toch met de buitenwereld te kunnen communiceren en signalen te detecteren heeft de cel eiwitten die door het membraan gaan (transmembrane eiwitten). Sommige van deze eiwitten, zogenaamde receptors, kunnen stoffen die buiten de cel aanwezig zijn binden om vervolgens binnen de cel (in het cytosol) een signaal door te geven. In het cytosol kunnen vervolgens allerlei reacties plaatsvinden die vele eiwitten omvatten en resulteren in een bepaalde actie. In witte bloedcellen resulteert de detectie van bacteriespecifieke stoffen in het kruipen in de richting van de bacteriën. Dit proces van gerichte celbeweging in een concentratiegradiënt van een chemische verbinding (de chemoattractant) wordt chemotaxis genoemd.

Een voorwaarde voor chemotaxis is dat de cel kan bepalen waar de chemoattractant vandaan komt. Dit proces heet "directionele detectie" en de evolutie heeft cellen uitgerust met een hele batterij aan mechanismen om dit te bewerkstelligen. Het detecteren van de richting van een chemoattractant gradiënt begint altijd met het binden van de chemoattractant aan een receptor. Doordat de chemoattractant een hogere concentratie heeft op de plaats waar het gemaakt wordt dan ver weg van deze "bron" zullen aan de kant van de cel die het dichtstbij de chemoattractantbron ligt meer receptoren geactiveerd worden dan aan de kant die verder weg is. Dit zorgt voor

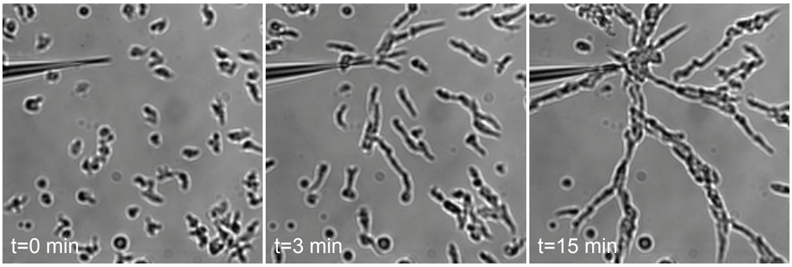

Figure 5.11: ***D. discoideum*** **cellen chemotaxen naar een pipette waaruit cAMP komt.** Hierbij vormen ze stromen omdat ze aan de achterkant zelf ook cAMP produceren en uitscheiden.

een verschil in receptor activatieniveau. De interne eiwitorganisatie van de cel ontvangt het gradiëntsignaal van de receptor, versterkt dit en zorgt ervoor dat de cel een duidelijke voor- en achterkant ontwikkelt, dit wordt polarisatie genoemd. De gepolariseerde eiwitconfiguratie binnen de cel zorgt ervoor dat het celskelet (cytoskelet) groeit in de richting van de chemoattractantbron, aan de voorkant van de cel terwijl aan de achterkant andere eiwitten het membraan meetrekken. Het resultaat is een beweging van enkele µm per minuut. Het doel van dit promotieonderzoek is de dynamica van de chemoattractant receptor en de eiwitten waarmee deze een directe interactie heeft, te begrijpen en te beschrijven.

Omdat menselijke cellen heel slecht overleven buiten het lichaam en enorm veeleisend zijn qua voeding, temperatuur en zuurtegraad, gebruiken we de amoebe *Dictyostelium discoideum* voor dit onderzoek. *D. discoideum* vertoont ook chemotaxis op een manier die vergelijkbaar is met die van witte bloedcellen. Het voordeel is dat *D. discoideum* cellen snel groeien bij kamertemperatuur en geen last hebben van de handelingen die nodig zijn om ze geschikt te maken voor het bekijken met de microscoop. Ze chemotaxen naar cyclisch adenosine mono-fosfaat (cAMP), een simpele, goedkope chemische verbinding. Door een verdunning van cAMP langzaam uit een pipette te pompen ontstaat er een concentratiegradiënt om de pipette die de *D. discoideum* cellen kunnen detecteren. Zoals te zien in figuur 5.11 bewegen de cellen richting de cAMP bron.

D. discoideum maakt voor de detectie van cAMP gebruik van de receptor genaamd "cAMP receptor 1" (cAR1). Dit is een G eiwit gekoppelde recepor (GPCR), wat betekent dat hij het cAMP signaal via een G ewit doorgeeft. Het G eiwit vormt het begin van een signaalcascade die uiteindelijk resulteert in chemotaxis. Veel eiwitten die deel uitmaken van de signaalcascade zijn al geïdentificeerd en men heeft een redelijk goed idee van welke eiwitten een interactie met elkaar hebben. Wat nog allerminst duidelijk is is wat de rol is van de dynamica van deze eiwitten. De eiwitten waar dit proefschrift zich op concentreert zijn de GPCR cAR1 en het hiermee geassocieerde G eiwit Gα2$\beta\gamma$.

In dit proefschrift maken we gebruik van de techniek "single molecule microscopy" (SMM). SMM stelt ons in staat om de beweging van individuele eiwtten in het membraan te bekijken en te beschrijven. Een voorwaarde is dat we de eiwitten labellen met een fluorescerend label, in dit geval een eiwit afkomstig uit de kwal *Aequoria victoria*; yellow fluorescent protein (YFP). Met behulp van genetische technieken kunnen we individuele componenten van het systeem dat we onderzoeken (cAR1, Gα2 en G$\beta\gamma$) koppelen aan YFP om ze vervolgens zichtbaar te maken met behulp van een laser gekoppeld aan een microscoop met een zeer gevoelige CCD-camera. Door de van individuele YFP eiwitten afkomstige, diffractie gelimiteerde lichtsignalen te beschrijven met een tweedimensionale Gaussische kromme kunnen we de positie hiervan (en dus van het eraan gekoppelde eiwit) bepalen met een positionele accuraatheid die alleen afhankelijk is van de signaal/ruis-verhouding. In theorie kan dit met vrijwel oneindige nauwkeurigheid maar in de praktijk betekent dit dat we stappen van ongeveer 40 nm kunnen waarnemen. Door met geschikte snelheid "snapshots" te maken van de moleculaire posities krijgen we een idee van de snelheid waarmee de eiwitten bewegen. Uit deze snapshots halen we informatie over de diffusie van de eiwitten en tevens over de onderliggende structuur van het celmembraan.

In dit proefschift onderzoeken we de beweging van cAR1, Gα2 en G$\beta\gamma$ in *D. discoideum* cellen. Dit doen we in rustende cellen, cellen die behandeld zijn met actine (een cytoskelet component) polymerisatie inhiberende chemicaliën (latrunculine A) en in chemotaxende cellen. Uit onze resultaten blijkt dat het feit dat een eiwit een homogene verdeling over het celmembraan vertoont, niets zegt over de verdeling van zijn dynamische eigenschappen. Zo beschrijven wij in hoofdstuk 2 nauwkeurig de bewegingen van individuele G eiwit *subunits*. De Gα2 en de G$\beta\gamma$ subunits blijken in rustende cellen precies met dezelfde snelheid en op dezelfde manier te bewegen, een sterke aanwijzing dat ze aan elkaar zijn gekoppeld, iets wat andere groepen ook bevestigen. In de afwezigheid van activatie (van cAMP) blijken Gα2 en G$\beta\gamma$ te bestaan in twee fracties, een snelle (D = 0.15 $\mu m^2/s$) en een 10× langzamere fractie (D = 0.015 $\mu m^2/s$). Deze laatste fractie beweegt met dezelfde snelheid als een deel van de cAR1 moleculen (zie hoofdstuk 3). Wanneer cAR1 door middel van toevoeging van cAMP aan het celmedium wordt gestimuleerd om het G eiwit te activeren, beginnen de twee subunits zich verschillend te gedragen. De snelle fractie blijft bestaan maar de bewegingen geven aan dat zich in het membraan domeinen hebben gevormd waaruit de eiwitten niet kunnen ontsnappen. De langzame fractie van de G$\beta\gamma$ subunit wordt compleet immobiel, een sterke aanwijzing dat het ergens aan bindt. Deze immobilisatie en de vorming van de domeinen blijken allebei het resultaat te zijn van cytoskeletgroei. In chemotaxende cellen blijken de waargenomen effecten zich te beperken tot de voorkant van de cel. De domeinen spelen waarschijnlijk een rol in het lokaal houden van de activatie van meerdere signaalmoleculen, de immobilisatie zou kunnen duiden op een feedbackmechanisme wat bijdraagt aan de chemotaxis efficiëntie.

In hoofdstuk 3 onderzochten we in detail de beweging van cAR1. Die beweging blijkt ook sterk af te hangen van het actine cytoskelet maar op een andere manier als de G eiwit subunits. In rustende cellen beweegt cAR1 relatief langzaam. Wanneer we actine polymerisatie wederom inhiberen worden de cellen rond en neemt de mobiliteit van cAR1 ook met factor 2 toe. Eenzelfde mobiliteitstoename vonden we ook in chemotaxende cellen, waarbij de receptoren aan de voorkant nog sneller bewogen dan aan de achterkant. Dit verklaren wij met behulp van de resultaten van een andere groep die concludeerden dat de binding tussen het cytoskelet en het membraan veel minder sterk is in de voorkant van een chemotaxende cel. Het feit dat zelfs na behandeling met Latrunculine A de receptoren aan de voorkant nog steeds sneller zijn dan aan de achterkant geeft aan dat er ook nog andere factoren zijn die de diffusieconstante van cAR1 beïnvloeden, dit kunnen bijvoorbeeld signaallipiden zijn. De afwezigheid van de G eiwit subunits heeft geen gevolgen voor de diffusie van cAR1 echter, in cellen zonder de Gα2 subunit vinden in een cAMP gradiënt geen veranderingen plaatst wat betreft de mobiliteit van cAR1. Een logisch gevolg van het feit dat deze cellen de gradiënt niet kunnen waarnemen wanneer we aanvaarden dat slechts het binden van cAMP geen invloed heeft op de mobiliteit.

In hoofdstuk 4 keken we naar de invloed van de kleine G eiwitten RasC en RasG op het gedrag van cAR1 en G$\beta\gamma$. Deze eiwitten liggen stroomafwaarts van het GPCR / G eiwitsysteem, echter ze zijn van groot belang voor de regulering van het cytoskelet. Omdat het cytoskelet op verschillende manieren de diffusie van cAR1 en G$\beta\gamma$ beïnvloedt onderzoeken we hier eigenlijk een feedback regulering. Eén van de conclusies in dit hoofdstuk is dat wanneer we een functioneel cAR1 molecuul in het systeem brengen de cellen wederom kunnen chemotaxen. De groep die de cellen gemaakt heeft toonde al aan dat de expressie van het cAR1 gen *cara* verwaarloosbaar was maar of alleen dit feit de reden was voor het niet vertonen van chemotaxis was nog onduidelijk. Het blijkt dat de *rasC*$^-$*/rasG*$^-$ cellen geen van de hiervoor beschreven effecten van het cytoskelet op cAR1 en G$\beta\gamma$ vertonen. Het feit dat er geen immobilisatie en domeinvorming plaatsvind na stimulatie en het feit dat de cAR1 mobiliteit homogeen is in chemotaxende cellen duidt erop dat de gebruikte knockouts hun cytoskelet niet goed op een ruimtelijke manier kunnen reguleren.

Dit proefschrift voegt kwantitatieve informatie toe aan de reeds bekende GPCR / G eiwit interactie. Zonder deze informatie is het onmogelijk om een volledig begrip te verkrijgen van de door ruis overspoelde processen die leiden tot chemotaxis. Een volledig begrip van chemotaxis brengt een beter begrip van processen zoals wondgenezing, embryogenese, axonsturing en het immuunsysteem met zich mee.

List of publications

de Keijzer, S., Sergé, A., van Hemert,F., Lommerse, P.H.M., Lamers, G.E.M., Spaink, H.P., Schmidt, T., and Snaar-Jagalska, B.E. (2008). **A spatially restricted increase in receptor mobility is involved in directional sensing during Dictyostelium discoideum chemotaxis.** J. Cell Sci. 121, 1750-1757.

Sergé, A., de Keijzer, S., van Hemert, F., Hickman, M.H., Hereld, D., Spaink, H.P., Schmidt, T., Snaar-Jagalska, B.E. **Quantification of GPCR internalization by counting individual receptors in living cells .** Submitted.

van Hemert, F., Lazova, M.D., Snaar-Jagalska, B.E., Schmidt, T. **Mobility of G proteins is heterogeneous and polarized during chemotaxis.** Submitted.

van Hemert, F., Snaar-Jagalska, B.E., Schmidt, T. **Chemotaxis: A mechanistic perspective.** Integrative Biology. In preparation.

van Hemert, F., Snaar-Jagalska, B.E., Schmidt, T. **Leading edge specific attenuation of cortex / membrane interactions leads to polarized GPCR mobility.** In preparation.

van Hemert, F., Snaar-Jagalska, B.E., Schmidt, T. **RasC and RasG regulate membrane / cytoskeleton interactions which organize the polarized behavior of cAR1 and G$\beta\gamma$ in D. discoideum.** In preparation.

Curriculum Vitae

Freek van Hemert werd geboren op 31 maart 1982 te Oostburg, Nederland. In 1999 rondde hij zijn Havo af om in hetzelfde jaar te starten met zijn studie biologie en medisch laboratoriumonderzoek aan de Hogeschool Rotterdam. Tijdens deze studie heeft hij twee keer vijf maanden stage gelopen, eerst bij DSM, waar hij zocht naar DNA in eiwitmonsters teneinde aan te tonen dat een concurrerend bedrijf inbreuk maakte op patenten. De tweede stage was in de klinische geneticagroep onder dr. Mark Nellist aan het Erasmus Medisch Centrum. Hier werd de eiwitinteractie van Tuberine en 14-3-3 eiwitten gekarakteriseerd; fouten in deze interactie spelen een belangrijke rol in de aandoening Tubereuze Sclerose.

In 2003, na het verkrijgen van de titel Bachelor of Applied science (B.As.) begon Freek aan zijn master Molecular and Cellular Biology aan de Universiteit Leiden. Zijn afstudeeronderzoek vond plaats in de fysica van levensprocessengroep van prof.dr. Thomas Schmidt onder begeleiding van dr. B. Ewa Snaar-Jagalska en dr. Sandra de Keijzer. Het onderzoek omvatte het met behulp van single molecule fluorescentie microscopie karakteriseren van de bewegingen van individuele receptoren *in vivo*. De titel Master of Science (M.Sc.) werd cum laude gehaald. Freek bleef als AIO betaald door het Cyttron-project in de biofysicagroep om het initiële werk te verdiepen en om ook te kijken naar het gedrag van het G eiwit onder verschillende omstandigheden. Tijdens deze periode was hij ook lid van de instituutsraad. Zijn wetenschappelijke werk werd gepresenteerd op meerdere internationale conferenties, waaronder de prestigieuze Gordon research conferenties over "Single Molecule Biology" en "Gradient Sensing and Directed Cell Movement".